Dust and its Effects on Measures of Galaxy Properties

by

Brian M. Devour

A dissertation submitted in partial fulfillment
of the requirements for the degree of
Doctor of Philosophy
(Astronomy and Astrophysics)
in the University of Michigan
2017

Doctoral Committee:

Professor Eric F. Bell, Chair
Professor Nuria P. Calvet
Professor Timothy A. McKay
Associate Professor Chris J. Miller

Brian M. Devour

bdevour@umich.edu

ORCID iD: 0000-0002-9424-3454

ACKNOWLEDGMENTS

This thesis, and the work it represents, would not have been possible without the support of many people. I can't thank all of them without this section becoming a minor book in its own right, but I also can't let this go by without at least trying to thank some of the people who have made important contributions.

First, I absolutely must thank my advisor Eric Bell. Scientifically, for the endless fount of ideas and uncanny ability as a sounding board, but also personally for being an all-around great dude. For being eternally patient with and supportive of my faults and encouraging of my successes. For sharing my love of teaching and joy in passing on to students the wonder we see in the universe. For seeing nothing wrong with fiddling with legos and geeking out about star wars, and just for being a great guy to talk with about anything and nothing. You've made my time here not only more successful, but more fun as well.

I also need to thank Chris Miller, my advisor for my first two years here, for starting me out right, for understanding my uncertainty over my future before I did, and for helping me figure out what to do about it.

There are also a number of other people within the astronomy community here at Michigan that deserve thanks. My thesis committee, consisting of Nuria Calvet and Timothy McKay in addition to Eric Bell and Chris Miller, have given me a great deal of useful advice and encouragement to help make this thesis the best it could be. The faculty, staff, and grad students of the astronomy department in general deserve recognition not only for their scientific acumen and dedication to astronomy, but also for making this department a genuinely welcoming and supportive place to spend seven years of my life. In particular, I

would like to thank my fellow grads Dan Gifford, Jessica Herrington, and Matt Miller, for their companionship and support along the way – they won't stop us now!

The Astronomy department staff deserves thanks for all of the hard work they put in to keep us from tripping over our own feet while our heads are stuck in the stars. We'd be lost without you. I especially want to thank Shannon Murphy for her dedication to, and indefatigable efforts to support, the teaching of astronomy. You are an inspiration to all of us who aspire to pass on our love of the universe.

In the world outside academia, I want to thank the residents of Paragon City and the Rogue Isles, for letting me be a hero with you; the 'mech jocks of the Inner Sphere and the Clan Homeworlds, for sharing my love of stompy robots; and the capsuleers of New Eden and Anoikis, o7 to all you magnificent nutcases. Thanks for helping me stay sane throughout this long, crazy journey.

And finally, and most importantly of all, I have to thank my family for the truly incalculable amount of love and support they have given me over the years. For my brother Stephen, who puts up with my endless natterings on every topic imaginable, for my sister Alegra, who has never stopped calling me her rocket scientist, and for my Mom and Dad, Rose and Michael, who taught me to think for myself and who for some inexplicable reason never hesitated to support their awkward son and his weird obsession with space with all their hearts and love. For my aunts and uncles and cousins and grandparents, who make every family occasion an exercise in silliness and laughter and shared joy (and way too much food!). You're all far more awesome than I could ever have possibly deserved, and I love you all for it.

TABLE OF CONTENTS

LIST OF TABLES

Table

LIST OF FIGURES

Figure

ABSTRACT

Dust in galaxies affects our measurements of galactic properties and gives insight into a range of physical processes. Robust measurements of the effects of dust attenuation on galaxy luminosities, structures, and other properties would be valuable, particularly as a function of intrinsic galaxy properties, but remain largely out of reach due to a lack of reliable dust- and inclination-independent measures of galaxy properties with which to select samples. We use dust-penetrated infrared measurements to construct new dust- and inclination-independent measurements of galaxy properties, including a new inclination-independent metric of galaxy structure. We quantify the inclination dependence of galaxy luminosities and face-on colors as a function of inclination-independent measurements of galaxy stellar mass, specific star formation rate (sSFR), size, and concentration. Relative attenuation – defined as the difference between edge-on and face-on luminosity – increases strongly with sSFR, is strongest for intermediate mass galaxies, and varies in complex and non-monotonic ways with galaxy structure. Face-on galaxy color reddens with decreasing sSFR and with increasing mass, and reddens quite strongly with decreasing galaxy size. Simple scaling relation-based models in which dust optical depth scales only with gas density and metallicity, coupled with published radiative transfer simulations, reproduce the observed patterns in relative attenuation and face-on color with startling accuracy. The insights offered by these models allow us to explain these complex patterns in terms of relatively simple physical properties. We also quantify how dust and inclination affect a range of traditional optical galaxy property measurements such as size, concentration, SFR, and metallicity, finding that almost all of them suffer from significant biases with dust and inclination. We conclude that dust- and inclination-independent metrics are critical for understanding dust properties and attenua-

tion, that optical measurements of galaxy structures and other properties are strongly biased by dust and inclination, that while dust attenuation is complex it primarily varies with sSFR and size, and that simple scaling relation models can reproduce observations well and give important insight into the drivers of the seemingly complex variation of attenuation with galaxy parameters.

CHAPTER I

Introduction

1.1 Introduction

Dust is an important component of galaxies, affecting observations of properties such as luminosity and stellar mass, color and star formation rate, size, and morphology. The dust content of a galaxy also traces its gas content and gives insight into star formation rates and dynamics, gas temperatures, metallicities, and other properties. In other words, dust is intimately tied with many of the most basic observations we can make and the most elementary properties we can measure for galaxies. As such, understanding the dust content of galaxies and how it affects our observations is an important task.

However, this task has often been less than straightforward. It is difficult to disentangle intrinsic variation in properties from variation due to dust, and this is complicated by the fact that the effects of dust also vary with viewing angle even for otherwise identical galaxies. This is further complicated by the fact that some types of observations, mostly structural measurements, can also vary with inclination even in the absence of dust! As such, when we measure the distribution of a given property among the galaxy population, it is not initially clear what variation is intrinsic, what is due to dust, and what is due to further variation of dust effects with inclination (or to non-dust inclination effects). Further, it is a natural question to ask how dust effects vary with galaxy properties, for example 'how does dust content vary with luminosity?' However, if the property in question (e.g. luminosity) is itself

one that is affected by dust and/or inclination, then one again cannot untangle the intrinsic from the dust-induced variation. Attempting to correct the parameterizing property to avoid this issue instead leads one down the arguably circular path of requiring dust/inclination corrections in order to study dust/inclination effects and derive those corrections.

In this thesis we develop a comprehensive set of techniques to measure dust attenuation and the effects of dust and inclination on galaxy property measurements that avoids these complications. We develop a set of dust- and inclination-independent infrared measurements that enable us to classify galaxies according to their intrinsic properties in an unbiased manner. This then allows us to reliably isolate samples of galaxies which are identical except for their inclination, enabling us to directly *exploit* the inclination dependence of dust attenuation in these samples (a technique known as the inclination test) to quantify dust and inclination effects as a function of galaxy properties.

In this introductory chapter we present necessary background information for the techniques and methods used in the remainder of this thesis. In §1.2 we discuss in more detail the challenges presented by dust attenuation and the physical properties tied to galaxy dust content. In §1.3 we more fully explain the properties, advantages, and drawbacks of the inclination test method. In §1.4 we briefly review the multi-wavelength surveys we use for our work. As a significant part of our work revolves around the development of a new set of structural measurements, in §1.5 we review the types of structural measurements and their properties. Finally, in §1.6 we outline our overall plan for the remainder of the thesis.

1.2 Dust

Dust is an integral component of a very wide range of galaxy observations, both as a contaminant that must be corrected for and as an object of study in its own right that can inform on physical processes and properties of galaxies. Here we review the basic properties of dust and some of these effects.

Physically, dust is believed to be composed of small particles of silicate and carbona-

ceous materials in the sub-micron size range (Whittet, 2003). The presence of dust grains within galaxies alters our view of those galaxies by both absorbing (removing) and scattering (redirecting) light. Both of these processes remove light that would otherwise reach us from objects behind the intervening dust grains; scattering can additionally *add* some light by redirecting light traveling in other directions into our line of sight. Collectively, the removal of light from our line of sight is referred to as *attenuation*, though in many cases 'absorption' is colloquially used interchangeably.

For light along a given line of sight, the total attenuation can be expressed as

$$I_\lambda = I_{0,\lambda} \mathrm{e}^{-\tau_\lambda}, \tag{1.1}$$

where I_λ is the observed intensity at a given wavelength λ, $I_{0,\lambda}$ is the un-attenuated intrinsic intensity, and τ_λ is the dust optical depth. The optical depth is expressed as

$$\tau_\lambda = N_\mathrm{d} C_{\mathrm{ext},\lambda}, \tag{1.2}$$

where N_d is the integrated dust column number density along that line of sight and $C_{\mathrm{ext},\lambda}$ is the characteristic extinction cross section of the dust per particle at that wavelength (also referred to as the opacity). Alternatively, the optical depth can also be expressed in terms of mass as

$$\tau_\lambda = \Sigma_\mathrm{d} \kappa_{\mathrm{ext},\lambda}, \tag{1.3}$$

where Σ_d is the dust mass surface or column density and $\kappa_{\mathrm{ext},\lambda}$ is the characteristic dust extinction opacity at that wavelength per unit mass.

As the notation of wavelength may suggest, the extinction cross section, and therefore overall dust attenuation, is not the same for all wavelengths of light. In general, longer wavelengths of light suffer from less attenuation than shorter wavelengths; additionally there are many smaller-scale features of the attenuation curve that arise from the detailed physical

properties of the dust grains. (Both measured and modeled attenuation curves have been produced many times; see, e.g. Cardelli et al. 1989; Li & Draine 2001; Draine & Li 2007; Conroy 2010.) Figure 1 shows an example attenuation curve from Li & Draine (2001)[1]; while specifics of course vary from work to work, the overall features visible in this example remain relatively constant. The large overall drop in extinction with wavelength can be easily seen, with the opacity dropping by roughly an order of magnitude between optical and near-IR wavelengths and by several more orders of magnitude into the mid- and far-IR. This comparative lack of extinction in the IR is a critical component of our analysis in this work. One can also see various characteristic features such as the '2175Å bump' and mid-IR silicate and PAH features near 10μm.

Additionally, not only will the optical depth for a galaxy vary with wavelength due to varying dust opacity, even at a single wavelength the optical depth will also be affected by variations in total dust column density with viewing angle. For disk galaxies, a face-on viewing angle will result in relatively short sightlines vertically through the disk's dust distribution, while an edge-on viewing angle will entail long sightlines through the entire width of the dust disk. Thus, even for identical galaxies, an edge-on view will result in a much higher column density of dust than a face-on view, and so much higher overall attenuation. This variation in attenuation even among identical galaxies further highlights the importance of understanding the dust content of galaxies.

The most obvious measurement that is affected by dust attenuation is luminosity – galaxies simply appear dimmer than they otherwise would in the absence of dust attenuation. Additionally, the frequency dependence of opacity causes galaxies to be more attenuated at shorter wavelengths than at longer wavelengths. Thus, dust attenuation not only affects the luminosity of galaxies at a given wavelength, but also affects the ratios between galaxy brightnesses at different wavelengths - in other words, it affects their colors, biasing them

[1]Reproduced by permission of the AAS from Fig. 16 of *Infrared Emission from Interstellar Dust. II. The Diffuse Interstellar Medium* by Li & Draine, 2001, *The Astrophysical Journal*, Vol. 554, 778 (Li & Draine, 2001)

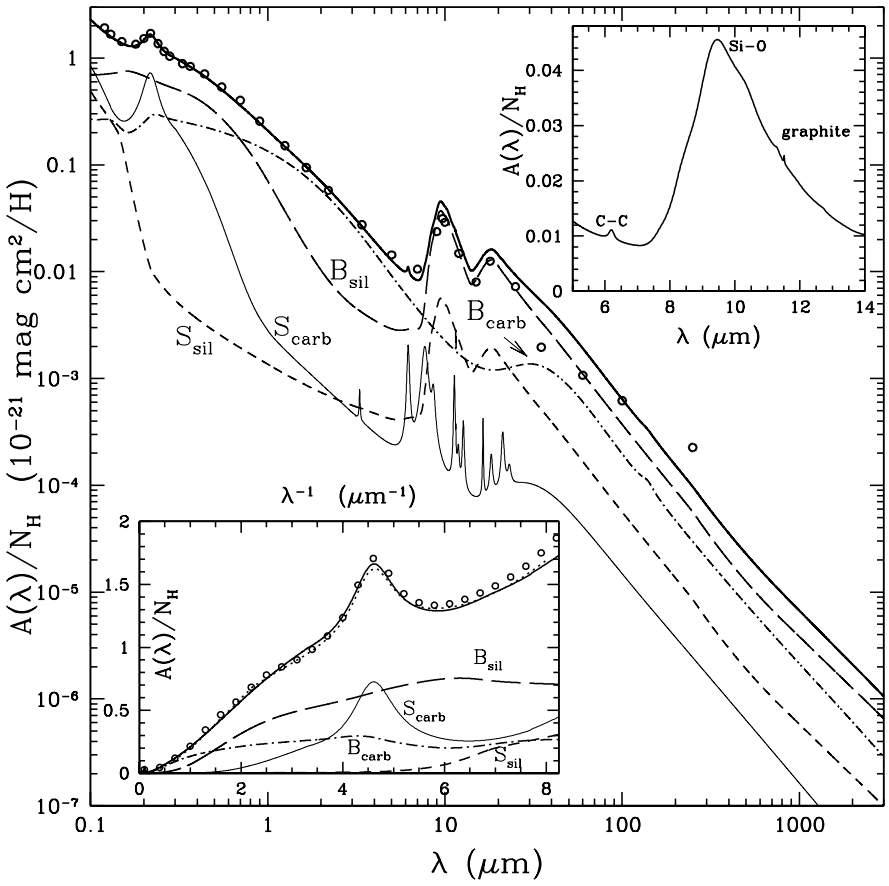

Figure 1.1: Attenuation curve from Li & Draine (2001). Dark solid line is the final calculated extinction for their model, circles are observed average extinction, and the other lines show the relative contributions from various components of their model. Upper inset zooms in on the ~10μm region; lower inset replots the curve versus λ^{-1} instead of λ. Figure © AAS. Reproduced with permission.

towards longer wavelengths (redder colors).

The effects of dust attenuation and reddening are far-ranging, affecting a wide variety of observations and the deductions we can make from them regarding galaxy properties.

Dust attenuation can introduce uncertainty in estimates of stellar M/L ratios, although the degree to which this occurs is uncertain (Gallazzi & Bell, 2009). Dust corrections to stellar masses are especially important for the baryonic form of the Tully-Fisher relation (Tully & Fisher, 1977), as the rotation velocities used in the T-F relation are easiest to measure in the edge-on galaxies that will have the highest attenuation. Dust attenuation also must be accounted for in measurements of the evolution of the galaxy stellar mass function (Muzzin et al., 2013) and luminosity function (Finkelstein et al., 2015) over the history of the universe.

In the use of color-magnitude diagrams to classify galaxies into star-forming (blue) and quiescent (red), reddening in dusty star-forming disk galaxies (especially edge-on) can cause them to appear similar in color to the quiescent galaxies. For example, Masters et al. (2010) found at least 0.5 mag of reddening in optical colors for some edge-on disk galaxies; as they show, this is more that sufficient to shift them into the region of the color-magnitude diagram supposedly reserved for quiescent elliptical galaxies. Dust attenuation and reddening can also affect luminosity- and spectral line-based measurements of star formation rate, particularly since more actively star-forming galaxies are likely to have more gas, and therefore, more dust. Dust corrections are thus required for UV luminosity-based star formation rates (e.g. Erb et al. 2006; Salim et al. 2007) and optical line-based star formation rates (e.g. Rosa-González et al. 2002; Dopita et al. 2003) alike; these corrections can be on the order of 50-100% or more. Corrections of these sorts to star formation rates are critical for understanding the star formation history of the universe, especially as different methods and surveys must often be combined to measure star formation over wide ranges of redshifts (see, e.g., Madau et al. 1996; Rosa-González et al. 2002). Figure 2 shows an example of these corrections

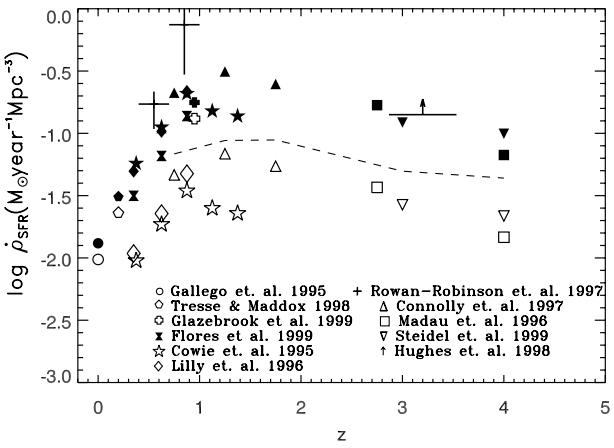

Figure 1.2: Star formation rate density history of the universe, from Rosa-González et al. (2002). Solid symbols denote dust-corrected star formation rates, while open symbols are the un-corrected measurements. Different symbol shapes denote different sources of star formation rate measurements; the dashed line shows a sub-mm based (i.e. likely dust independent) lower limit.

applied to the star formation history of the universe, from Rosa-González et al. (2002)[2]. One can see that the dust-corrected star formation rates (solid symbols) are not only significantly higher than the un-corrected rates, but also that they trace out a much more coherent, less scattered curve.

Attenuation and reddening also can affect estimates of galaxy metallicity through differential attenuation of emission-line diagnostics (e.g. Dopita et al. 2006). The required emission line dust corrections are often derived from the Balmer decrement and applied as a foreground screen. However, dust does not solely lie in the foreground; rather, HII regions are often embedded within dense dust clouds, and therefore these corrections are not necessarily accurate (this has been discussed by e.g. Bell et al. 2002; Caplan & Deharveng 1986). And indeed, in chapter 5 of this thesis we show that metallicities do suffer from dust-induced biases.

As galaxies are not one-dimensional point sources like stars, dust attenuation also affects

[2]Reproduced from Fig. 9 of *An Empirical Calibration of Star Formation Rate Estimators* by Rosa-Gonzalez, Terlevich, & Terlevich, 2002, *Monthly Notices of the Royal Astronomical Society*, Vol 332, 283 (Rosa-González et al., 2002)

the projected distribution of their light on the sky. Dust and stars are not evenly distributed throughout galaxies, and the amount of attenuation suffered by starlight depends sensitively on the star-dust geometry. Thus, different portions of galaxies will suffer from different amounts of attenuation, and therefore measurements that rely on the relative distribution of galaxy light can be affected.

This can affect a variety of types of galaxy structural measurements, but this question has not been widely researched. Some work has been done using radiative transfer simulations to predict the effects of dust on structural measurements; for example, Pastrav et al. (2013a,b) find that in their simulations disk effective radii, Sérsic indices, and bulge-to-disk ratios all tend to be underestimated due to dust and projection effects. It is difficult, however, to study these effects observationally, as it demands the ability to match galaxies of intrinsically similar structural parameters in order to isolate the effects of varying dust contents or inclinations.

And yet, galaxy structural measurements are important for understanding the evolution of structure in our universe. The growth of bulges (quantified using bulge to disk ratio) is related to the onset of quiescence (Lang et al., 2014b), the size distributions of galaxies are related to their formation and merger histories (van der Wel et al., 2014a), and galaxy structure is strongly correlated with star formation rate (Wuyts et al., 2011), as just some examples of the importance of structural measurements. As such, it would be very useful to be able to measure structural parameters in dust- and inclination-independent ways, and to quantify the variation in existing structural measurements caused by dust and inclination, tasks which we undertake in chapters 3 and 5 of this thesis.

In addition to the effects of dust attenuation on other measurements, direct observations of the dust itself and its properties can also give insight into physical processes within and properties of galaxies. Dust takes part in star formation processes and contributes to chemical evolution, and its physical properties and lifecycle offer insight into the properties of the stellar envelopes, clouds, and supernova ejecta where it may be formed or destroyed.

Dust is a important cooling agent for the collapse of star-forming clouds, particularly in low-metallicity cases. Notably, this has been invoked as a likely mechanism to allow for the formation of the first low-mass stars in the early universe (Klessen et al., 2012; Schneider et al., 2012; Hopkins & Conroy, 2017). Dust grains are also the primary catalyst for the formation of molecular hydrogen, which cannot efficiently form in a gaseous phase but can form through the meeting of two hydrogen atoms on a grain surface (e.g. Gould & Salpeter 1963; Katz et al. 1999; Perets et al. 2007). Other chemical evolution in molecular clouds also depends on dust grains; similar grain-surface processes can result in the creation of more complex molecules as well (e.g. Garrod et al. 2008), and heavy elements also freeze out onto the surfaces of dust grains (e.g. Bergin & Tafalla 2007), altering the abundances within the clouds. Measuring dust abundances is thus important for understanding star formation processes.

Another important method of investigating dust properties is through detailed observations of the shape of the dust attenuation/emission curves, as the strength, shape, and position of the various spectral features depends sensitively on the composition and mixtures of the dust grains and the distribution of grain sizes. The complex shapes of these curves results in equally complex dust grain models (see, e.g., Li & Draine 2001; Draine & Li 2007). Dust has traditionally been thought to be formed primarily in the envelopes and outflows from AGB stars and planetary nebulae, with the differences between oxygen-enriched and carbon-enriched stars accounting for the distinction between silicate and carbonaceous dust grains (Whittet, 2003). However, with the high dust destruction rates expected due to supernova shock waves, it has been calculated that average dust lifetimes should be too short to explain the overall dust abundances observed (Temim et al., 2015). Production in molecular clouds or the supernova remnants themselves has been postulated to explain this shortfall (Temim et al., 2015), but the overall dust lifecycle is still somewhat uncertain. Thus, it is important to understand the physical properties and distributions of the dust grains, as this may offer insight into their formation conditions.

A major tool that is used to aid in investigations of all of these dust effects are dust radiative transfer simulations. The effects of dust are subtle and often counter-intuitive, and the overall effects on light from the complex distributions of stars and dust in galaxies are not easily analytically solved – simple slab and screen models can work, but do not capture the full details. As such, radiative transfer simulations are very important for our understanding of dust effects on galaxies.

Radiative transfer simulations have been commonly used to study a variety of questions related to dust effects on galaxy properties – general predictions of attenuation and reddening (e.g. Bruzual A. et al. 1988; de Jong 1996b; Tuffs et al. 2004), the fraction of light absorbed by dust in starburst galaxies (Jonsson et al., 2006), the additional influence of scattering effects (Witt & Gordon, 2000), dust heating and energy balance (Popescu et al., 2000), and the variation in attenuation with galaxy properties (Ferrara et al., 1999).

Of particular relevance to our work, radiative transfer simulations also highlight the strong influence of inclination and geometric effects on dust attenuation. For example, Tuffs et al. (2004) simulate attenuation for multi-component galaxies containing both thin and thick disks as well as bulges at a variety of inclinations and optical depths. Their work shows that both the overall attenuation and the variation of the attenuation with inclination are strongly different for these geometrically distinct components. The absolute attenuation of the bulge is larger than that of the thick disk, yet the *variation* of attenuation with inclination is weaker for the bulge; meanwhile for the *thin* disk both the absolute attenuation and the variation with inclination are much larger than for either the thick disk or the bulge. This model does not include any variation in stellar population colors; all of these differences are driven solely by the varying geometry of these populations relative to the dust.

1.3 The inclination test

It is clear that the ability to measure dust effects and quantify dust attenuation is useful for informing a wide range of measurements about galaxies. In this thesis, the primary

tool we use to carry this out is the inclination test method; here we discuss the nature, advantages, and limitations of this method in more detail.

The inclination test method is conceptually quite simple – one merely assembles a sample of disk galaxies that one believes to be intrinsically similar but which are observed at a variety of viewing angles, and then measures how the observed luminosities (or other properties) of this sample change as a function of inclination. Since the galaxies are believed to have the same intrinsic properties, any variation in the observed properties must, therefore, represent some systematic error in the measurement in question. For the most part we attribute these variations to the effects of dust, though in the case of structural measurements there can also be purely geometric projection effects that contribute as well. These variations can be used both to attempt to correct the measurements in question as well as to understand the properties of the dust that causes them.

This technique has a number of important advantages. First, it is a non-parametric technique – it does not require making any assumptions about the dust or light distributions of the galaxies. Therefore, it cannot be confused by *mistaken* assumptions, and its results are equally applicable to any models one may wish to use.

Second, not only is the technique simple, it does not require extremely high resolution imagery, complex analysis, or uncommon superpositions of galaxies. It is therefore ideally suited to take advantage of the modern advent of large survey catalogs to provide statistical studies of very large samples of galaxies.

As well, while this technique has traditionally been applied to luminosity in order to measure the relative attenuation of galaxy light, there is no reason why it cannot be applied to essentially any observable property of a galaxy – not only luminosity or color, but also sizes, structures, spectral lines, and quantities derived from these such as stellar masses, metallicities, or star formation rates. The inclination test is therefore a 'broad spectrum' technique that can be used to quantify the effects of dust and inclination on a wide variety of galaxy properties using one simple methodology.

There are, of course, also challenges to the use of this method. The greatest is that the method only works if the samples of 'intrinsically similar' galaxies are actually similar. One could in principle tolerate some spread in galaxy properties within a sample; at some loss in accuracy, of course, but not to the point of rendering the results meaningless. However, many metrics that one might use to select these samples can themselves suffer from inclination dependence (whether dust-induced or otherwise). This leads not only to spread in galaxy properties within a sample, but *inclination-dependent* spread in properties, which compromises the basic assumption of the method in that the galaxies viewed edge-on are in fact *not* intrinsically similar, on average, to the ones viewed face on. For example, if observed optical luminosity is used to select similar galaxies, then the (more heavily dust extincted) edge-on galaxies will in fact be drawn from an intrinsically more luminous population than the face on ones, even though their observed optical luminosities are identical.

As such, when employing this method one must take great care to avoid inclination-dependent selection biases. Historically this has been difficult, and several studies have been compromised by these effects (e.g., Valentijn 1994 showed that inclination tests of diameter can fail if sample completeness is not carefully considered). The difficulty, of course, is that all optical measurements will be subject in greater or lesser degree to the very dust effects that we wish to study, and optical measurements have historically made up the majority of the data available. However, in recent years large *infrared* surveys such as 2MASS (Skrutskie et al., 2006), UKIDSS (Lawrence et al., 2007), and WISE (Wright et al., 2010) have made comprehensive catalogs of dust-independent galaxy properties available. It is therefore now possible to select samples of truly intrinsically similar galaxies across a wide range of galaxy masses, star formation rates, sizes, and morphologies for the first time. The development of inclination-independent galaxy selection metrics from these data sets that can be used to reliably select samples of truly identical galaxies is a major part of the work in this thesis.

Another important limitation of the inclination test is that it only measures the *difference* in properties between the edge-on and face-on cases; i.e. in most cases it cannot probe any

further difference that may exist between the face-on and *dust-free* cases. However, we know that galaxies still suffer from dust attenuation even when viewed from face-on orientations; thus, the technique can explore the differential dust attenuation between edge-on and face-on, but cannot measure the *total* attenuation without resort to models. Similarly, one generally cannot measure any effects that the face-on dust attenuation may have on other galaxy properties (such as structural measurements) relative to the dust-free case. It is, however, possible to work around the edges of this limitation in some cases if one can put constraints on the controlling factors of galaxy properties when observed face-on. We explore one such extension of this technique in chapter 4, where we exploit the expected dependence of *intrinsic* galaxy face-on color on stellar mass and specific star formation rate to interpret the variation in *observed* face-on color with galaxy structure as variation in the face-on total attenuation. This measurement is only weakly model dependent, but one may not always be able to constrain the controlling factors of observations of face-on properties in order to make this sort of measurement.

A more subtle limitation is that spread or variation in the intrinsic vertical structures of galaxies can cause issues even if the selection is completely inclination-independent, because such variations will alter the relationship between observed axial ratio (which is taken as a proxy for inclination) and true inclination. For example, within a sample that exhibits some spread in intrinsic thickness, the thinner elements of the population will not have the same axial ratios as the thicker members at a given inclination, potentially altering the measured variation in properties with axial ratio. This can also cause issues in comparing different samples to each other; for example, if one sample of disk galaxies has larger bulges (and thus thicker edge-on axial ratios) than another, even if the two samples actually have an identical variation in properties with *inclination*, the bulgier sample will appear to have a steeper variation in properties with *axial ratio* simply because its range of axial ratios between face-on and edge-on will be smaller. Essentially, when using this method one must take care to avoid biases in the mapping between axial ratio and inclination, by controlling

for vertical variation within samples as much as possible and by carefully choosing axis ratio measurements to avoid influences from bulges and other distorting effects.

1.4 Surveys

The advent of large, homogeneous multi-wavelength surveys is a major enabling factor for the work we do in this thesis. The very large sample sizes possible with modern surveys, combined with the natural scalability of the inclination test method to such large samples, enables truly comprehensive statistical studies even with relatively fine binning across a wide range of galaxy properties. Even more importantly, the advent of large *infrared* surveys allows for the selection of these samples to be done in the inclination-independent manner necessary for the inclination test method to function. In this section we briefly review the development of these surveys, including the ones we use for our work in this thesis.

Galaxies exhibit a very wide range of observable properties – in some senses more even than stars, as galaxies are extended objects while stars are point sources. Galaxy observations, therefore, possess an additional spatial dimension from which to draw information about their properties; their extended nature also complicates measurements of some properties (such as total flux) that they do have in common with stars. As such, in order to understand galaxies, it is extremely important to obtain observations of large numbers of these objects. Large catalogs of galaxy properties also allow us to discover phenomenon that are emergent properties of the overall distributions of galaxies rather than of individual objects – analogous to e.g. the stellar main sequence or other features of the classical HR diagram – such as the fundamental plane relationship between elliptical galaxy sizes-surface brightnesses-velocity dispersions (Djorgovski & Davis, 1987), or the 'red sequence' of quiescent galaxies and 'blue cloud' of star-forming galaxies (also known as the star forming main sequence, Noeske et al. 2007) evident in galaxy color-magnitude diagrams, or the inhomogeneous distributions of galaxies in space that trace the large scale structure of the universe.

The advent of large, homogeneous surveys of galaxies has, therefore, been a great boon to the study of galaxies. This began with the first large surveys using photographic plates in the mid 20th century; one notable example was the first Palomar Observatory Sky Survey (POSS-I). This survey covered roughly 2/3 of the sky in two optical bands (one red and one blue), and resulted in early galaxy catalogs such as the Uppsala General Catalog (UGC, Nilson 1973) and Morphological Catalog of Galaxies (MCG, Vorontsov-Vel'Yaminov & Arkhipova 1962). Further variations on this theme followed, including the follow-on second Palomar Observatory Sky Survey (POSS-II, Reid et al. 1991), and the southern sky equivalent ESO/SERC Southern Sky Survey (Holmberg et al., 1974). Complementary to these, significant catalogs of galaxy redshifts were compiled through spectroscopic surveys such as the Center for Astrophysics (CfA) redshift surveys (Huchra et al., 1983), and others. These surveys resulted in catalogs containing properties of tens or hundreds of thousands of galaxies by the early 1990s, but the true revolution in galaxy surveys came with the advent of the first large, fully digital photometric and spectroscopic surveys – foremost being the Sloan Digital Sky Survey (SDSS, Eisenstein et al. 2011). Begun in 1998, the SDSS has observed roughly 1/3 of the sky in 5 optical wavelengths (ugriz) covering the full visible spectrum, and as of DR13 in 2015 has cataloged more than 900 million sources (including more than 200 million galaxies) and more than 4 million spectra (including 2.4 million galaxies). It is little exaggeration to say that SDSS revolutionized many areas of astronomy – never before was there any catalog containing such a wealth of data on so many objects. In many ways SDSS ushered in the era of survey astronomy, where significant numbers of major astronomical projects and discoveries can be made solely from the use of survey data rather than dedicated observing campaigns. While there have been more modern surveys since, the SDSS is still one of the foremost examples and remains commonly used today. Our work is no different in this respect, as we use SDSS catalog data as the reference optical (dust-affected) galaxy property measurements to compare with our infrared (dust-independent) measurements.

The majority of early surveys were conducted in optical wavelengths. However, while it was once thought that galaxies were largely transparent (e.g. Holmberg 1958, 1975), it is now understood that many galaxies are partially to completely optically thick depending on area and viewing angle (e.g. Disney et al. 1989; Valentijn 1990). As such, many optical survey quantities are heavily affected by dust reddening and extinction. While in some senses this is a useful thing from the perspective of measuring dust effects (as one cannot, of course, quantify dust effects without dust-affected measurements), it means that one cannot necessarily trust these measurements for other purposes. Additionally, even merely exploring dust effects using these measurements is not possible without knowledge of the true intrinsic properties. As such, it is necessary to conduct surveys at other wavelengths than only optical.

In particular, surveys in the infrared are highly valuable. Near-infrared observations allow for the most dust-free view of galaxies available, being long-wavelength enough to avoid most dust *attenuation* yet short-wavelength enough to avoid most dust *emission*. Meanwhile, mid- and far-infrared observations probe dust emission at varying temperatures, providing measures both of dust content and star formation activity. However, observations at these wavelengths have several challenges relative to optical observations. For one, the Earth's atmosphere is opaque (or at least less than transparent) at many wavelengths in the infrared regime, mainly due to water vapor. This restricts ground-based infrared observations to limited wavelength windows, and even in these windows one must find the highest, driest locations possible to limit atmospheric effects. (These location incentives are also present for optical observations, of course, but to an even greater extent in the infrared.) As with many other non-optical observations, some infrared bands are accessible only to space-based instruments. Second, infrared observations are vulnerable to thermal noise from the instruments themselves, as they are attempting to detect radiation of similar wavelengths to that given off by objects at room temperature. Thus, infrared detectors must generally be cooled in some manner, particularly for longer wavelength observations. This is a particular concern for spacecraft, and coolant supply is often the principal limitation on their useful

lifespans. Finally, due to the basic physics involved, infrared observations are inherently lower resolution than optical ones due to the longer wavelengths. This limits the resolution obtainable from a given practically achievable telescope diameter, which is, again, a particular concern for space-based instruments. As such, while observing in the infrared is not as difficult as observing in e.g. x-rays or gamma rays, when compared to optical observations infrared observations do tend to be lower resolution, lower signal-to-noise and/or sensitivity, less comprehensive in wavelength coverage, and all-around a bit harder to do.

Thus, it is unsurprising that the implementation of infrared surveys has lagged slightly behind that of optical surveys. The Two Micron All Sky Survey (2MASS, Skrutskie et al. 2006) was the first major large-scale infrared survey; carried out from 1997-2001, it surveyed the entire sky at three wavelengths from 1.2 – 2.2μm. Even though it was contemporary to the SDSS and covers a much wider sky area, it observed no more objects ($\sim$300 million vs $\sim$290 million in SDSS as of the completion of the main survey area in DR6) due to its lower sensitivity, and its resolution is significantly lower. Nevertheless, the survey made important contributions to observations of brown dwarfs, low mass stars, and areas of the sky obscured by dust in the Milky Way. The United Kingdom Infrared Telescope (UKIRT) Infrared Deep Sky Survey (UKIDSS, Lawrence et al. 2007), begun in 2005, succeeded 2MASS and is in some ways the infrared counterpart to the SDSS. Observing at four wavelengths between 1.0–2.2μm, this survey covers roughly half ($\sim$4000 square degrees) of the regions of the northern sky covered in the original SDSS surveys, and is significantly more sensitive and higher resolution than 2MASS. Of particular relevance to our work, we use the K-band images from this survey to create the inclination-independent structural measurements discussed in chapters 2 and 3 of this thesis. The last major infrared survey we discuss here is that carried out by the Wide-field Infrared Survey Explorer (WISE, Wright et al. 2010) satellite, which surveyed the entire sky in four wavelengths from 3.4 – 22μm between its launch in late 2009 and the exhaustion of onboard coolant in late 2010. While WISE's observations are of low resolution ($\sim$6 arcsec in the W1–W3 bands and 12 arcsec in W4)

due to its small aperture and long wavelengths of operation, its location above the Earth's atmosphere gives it superb sensitivity and wavelength coverage. In particular, its longer wavelength observations allow it to probe emission from hot and warm dust, unlike shorter-wavelength ground-based observations. For our work, WISE 3.4μm observations are used as a nearly dust attenuation-independent measurement of stellar mass, while WISE 12μm observations probe hot dust emission and therefore serve as a tracer of star formation activity.

1.5 Structural measurements

A major part of our thesis work is the development of new inclination-independent structural measurements from dust-penetrated infrared survey images. These are not simply inclination-independent parameters taken from survey catalog data, but a new photometric technique that we have developed, implemented, and applied to the actual imaging data. In many ways this has been the most challenging part of the project, both in terms of technical complexity as well as designing solutions to the various practical and conceptual problems encountered along the way. In order to provide context for our efforts in this area, we briefly review here the general concept and some of the properties of the various types of structural measurements.

A galaxy structural measurement is simply a metric, numeric or otherwise, that attempts to quantify the physical distribution of mass and/or light within a galaxy. As discussed in §1.2, the structure of galaxies correlates with many interesting properties of galaxies, notably star formation activity and assembly history, and so is well worth studying. There are many challenges to this task, both practical and conceptual, and many different structural measurements have been developed over the years, each approaching these challenges in their own way.

An important point is that a structural *measurement* is not the same thing as the actual physical structure of a galaxy. The structure of a galaxy is defined by the physical, 3-dimensional distribution of light/mass; to hypothetically fully describe this structure one

would need to somehow measure the density $\rho(\mathbf{x})$ for every point $\mathbf{x}$ within a galaxy. This is not, and indeed in practical terms cannot, be done. We do not directly observe the 3-d density distribution of a galaxy. Rather, we observe the *2-dimensional* light distribution projected onto the plane of the sky, and moreover we observe this distribution convolved with modifications due to viewing angle, dust, physics (e.g. diffraction or lensing), the atmosphere, instrumental limitations, etc. From these observations one may attempt to reconstruct what one *believes* the 3-d density distribution to be through modeling, or to assign a numerical or other parameter to quantify the structure or classify it in some way, but one may not directly measure this distribution. Additionally, the mapping from intrinsic 3-d density distribution to what we actually observe is not one-to-one – a given galaxy may be projected into many different possible observed 2-d brightness distributions, and therefore our structural measurements are similarly not necessarily unique. As such, it is important to keep in mind that all structural measurements represent different, imperfect attempts to quantify the true underlying physical structure, and they will all have their own advantages and drawbacks.

Structural measurements fall into (roughly) three categories: visual classifications, parametric measurements, and non-parametric measurements.

Visual classification is the oldest set of methods, dating back to, for example, observations of the morphology of the so-called 'spiral nebulae' before the existence of other galaxies was even known. Requiring no more than a set of eyes and a telescope or image, this method evolved from simple descriptive impressions of shape through the systematic Hubble 'tuning fork' diagram (Hubble, 1926) and other similar/related classification systems such as that of de Vaucouleurs (de Vaucouleurs, 1959). These systems classify galaxies based on their visual appearance into groups such as elliptical, spiral, barred spiral, lenticular, irregular, etc. The systems of gradations and sub-classifications vary, but generally distinguish among ellipticals by shape (degree of flattening) and spirals by size of bulge and prominence and tightness of wrapping of arms.

While useful as an overall organizational scheme, purely morphological visual classification systems suffer from a number of issues. Most obvious is that they are subjective; even if the majority of observers were to agree on the classification of a galaxy, the assignment into one class or sub-class or another can ultimately be somewhat arbitrary, and the sources and effects of biases in classification are difficult or impossible to determine. Additionally, there is not necessarily a strict correlation between the most prominent visual differences between galaxies and the most physically meaningful and informative differences in their intrinsic properties. The qualitative, rather than quantitative, nature of such classification systems also limits their potential for robust analysis. These systems definitely remain useful as a means of organizing our thoughts about galaxies, and can provide useful supplements to more quantitative analysis (for example, the use of Galaxy Zoo visual morphological classifications to explore the type discriminating potential of quantitative measures such as concentration and f_{DeV} in Masters et al. 2010), but ultimately they cannot serve alone.

The first type of quantitative structural measurements, parametric measurements attempt to fit the observed light distribution with some type of functional form or model, with the parameters of the fit then serving as structural measurements. One of the earliest examples was the use of the de Vaucouleurs profile to fit the surface brightness profile of massive elliptical galaxies (de Vaucouleurs, 1948); this was later expanded and generalized into the Sérsic profile (Sérsic, 1963), which can fit the brightness profile of both elliptical and disk galaxies. These models allow for the use of parameters such as the effective radius to quantify size, and the Sérsic index to quantify the overall light profile shape and degree of central concentration. More sophisticated models may fit multiple profiles simultaneously, e.g. to decompose a galaxy into a bulge and a disk (e.g. Simard et al. 2011), or to model a bar (e.g. de Jong 1996a), or even to fit spiral structure or other features. These can provide parametric measurements of many galaxy properties; size, central concentration, bulge-to-disk ratio, intrinsic shape, viewing angle, total brightness, and many others.

The second type of quantitative structural measurements are the non-parametric mea-

surements. These measurements do not fit a function or model; rather, they merely assign a quantitative measure to the galaxy's structure by applying some given algorithm to the observed light distribution (e.g. fraction of light within some given radius). Unlike parametric measurements, these measurements do not require making any assumptions about the underlying physical distribution of light or mass. The most common types of non-parametric measurements are various measures of galaxy size or the central concentration of the light profile. Concentration measurements in particular have a long history and have been measured in many ways (e.g. Morgan 1958; Doi et al. 1993; Abraham et al. 1994; Blanton et al. 2001); what they all have in common is that they parameterize galaxies by in some way comparing the amount of light concentrated near the center of a galaxy's light profile to the total amount of light. Many radius measurements are non-parametric as well (e.g. isophotal radii), even if they are not commonly thought of as such – a particularly notable modern example is the Petrosian radius measurement, which defines a size based on the ratio of surface brightness at a given radius to the average surface brightness within that radius (Blanton et al., 2001); variations of this technique are commonly used in a wide variety of modern surveys. More recently, concentration has been combined with non-parametric measurements of asymmetry and clumpiness in the CAS system (e.g. Conselice 2003).

Parametric and non-parametric measurements each have their own advantages and drawbacks. Parametric fits often give multiple measurements at once – namely, the various parameters of the fit, e.g. scale length and Sérsic index for a Sérsic fit – while non-parametric measurements do not. Parametric measurements also often degrade more gracefully than non-parametric ones for low signal-to-noise or mildly contaminated images. A parametric measurement's fit will become more uncertain in such cases, with a consequent increase in the uncertainty of the measured parameters, but a non-parametric fit will often acquire significant biases as portions of the brightness distribution become effectively undetectable, or be thrown wildly off by the presence of a contaminating object. On the other hand, parametric fits rely sensitively on their assumptions about the true underlying distribution of light or

mass, and are vulnerable to various subtle (and not-so-subtle!) biases if these assumptions are not correct. This is the major reason why non-parametric fits are valuable, as they are not subject to these issues – parametric measurements are in a sense a blend of observation and theory, while non-parametric measurements are pure empirical observations. Ultimately, both types of measurement are useful, and are often complementary. For example, the SDSS catalog contains both a non-parametric concentration parameter (expressed as ratios of different Petrosian radii) and the parametric $f_{\rm DeV}$ parameter (a ratio of model fit likelihoods), which both probe the shape of a galaxy's light profile but do so in different ways; when used in concert, the two parameters together can better distinguish between spiral and elliptical galaxies than either parameter can manage alone (e.g. Strateva et al. 2001).

The structural measurements that we develop fall into the non-parametric category, being, conceptually, variants on the concepts of half-light radius and concentration modified to avoid biases due to inclination effects. One of the major advantages of our use of the inclination test method is that this technique is also non-parametric and therefore not vulnerable to systematics due to uncertain model effects; thus, we continue this in our structural measurements in order to avoid compromising the benefits offered by this approach. The non-parametric approach also allows us to maintain tight control over the exact algorithms that translate brightness distributions into structural parameters, which is necessary for our objective of ensuring that these measurements are by construction blind to geometric projection effects caused by varying inclinations.

1.6 Thesis outline

The objective of this thesis is to make use of new, inclination-independent measures of galaxy properties in concert with the inclination test to quantify dust attenuation and the effects of dust and inclination on galaxy property measurements, particularly as a function of intrinsic galaxy properties. In particular, we wish to address the following questions:

- How can we best construct inclination-independent galaxy property and structural measurements from the infrared survey catalog data and imagery available to us, and what can the properties and advantages of these measurements tell us about the limitations of existing measurements?

- How does dust attenuation vary as a function of inclination-independent parameterizations of galaxy mass, star formation rate, size, and central concentration, particularly as these four properties have never been simultaneously explored in the same study before?

- How can we explain the patterns we see in these observations, and what do they tell us about the controlling physical processes behind the dust attenuation we observe?

- How do dust and inclination effect other measurements of galaxy properties, specifically traditional structural measurements as well as measures of mass, star formation activity and metallicity?

Towards this end, in chapter 2 of this thesis we develop inclination-independent infrared measurements of galaxy stellar mass and specific star formation rate, and use them in conjunction with the inclination test to measure the dust attenuation of galaxies as a function of these properties. This chapter also introduces the scaling relation-based physical model we use to attempt to explain our observations.

Chapter 3 covers the development of our new inclination-independent 'linear' infrared structural measurements as a complement to our existing metrics, and examines the properties, distributions, and reliability of these structural measurements in detail.

In chapter 4 we then make use of these measurements to expand the analysis of chapter 2 to measure dust attenuation as a function of the full four-dimensional galaxy property parameter space of stellar mass, specific star formation rate, size, and concentration. We also further develop and expand the scaling relation model introduced in chapter 2, and

make use of the insights offered by this model to develop a unified physical model to explain the patterns we observe in our observations.

In chapter 5 we then extend the use of our inclination-independent metrics and the inclination test to measurements other than dust attenuation, showing that traditional structural metrics, as well as a variety of other optical measurements, suffer from significant inclination biases due to both dust and geometric effects.

Finally, in chapter 6 we wrap up our results and discuss potential future applications for our techniques.

CHAPTER II

Sample selection, and relative attenuation as a function of stellar mass and specific star formation rate

Preface

This chapter was originally published in the *Monthly Notices of the Royal Astronomical Society*, Vol 459, 2054 (Devour & Bell, 2016), under the title *Global dust attenuation in disc galaxies: strong variation with specific star formation and stellar mass, and the importance of sample selection*, coauthored with Eric Bell. Portions of the model assumptions and analysis in §2.6.2 have been superseded by the updated version presented in Chapter 4; in the interest of retaining consistency with the published version I have not modified this portion, but rather have added an explanatory footnote.

Abstract

We study the relative dust attenuation–inclination relation in 78,721 nearby galaxies using the axis ratio dependence of optical–NIR colour, as measured by the Sloan Digital Sky Survey (SDSS), the Two Micron All Sky Survey (2MASS), and the Wide-field Infrared Survey Explorer (*WISE*). In order to avoid to the greatest extent possible attenuation-driven biases, we carefully select galaxies using dust attenuation-independent near- and mid-IR luminosities and colours. Relative u-band attenuation between face-on and edge-on disc galaxies along

the star forming main sequence varies from ∼0.55 mag up to ∼1.55 mag. The strength of the relative attenuation varies strongly with both specific star formation rate and galaxy luminosity (or stellar mass). The dependence of relative attenuation on luminosity is not monotonic, but rather peaks at $M_{3.4\mu\mathrm{m}} \approx -21.5$, corresponding to $M_* \approx 3 \times 10^{10} M_\odot$. This behavior stands seemingly in contrast to some older studies; we show that older works failed to reliably probe to higher luminosities, and were insensitive to the decrease in attenuation with increasing luminosity for the brightest star-forming discs. Back-of-the-envelope scaling relations predict the strong variation of dust optical depth with specific star formation rate and stellar mass. More in-depth comparisons using the scaling relations to model the relative attenuation require the inclusion of star-dust geometry to reproduce the details of these variations (especially at high luminosities), highlighting the importance of these geometrical effects.

2.1 Introduction

The presence of dust strongly affects almost every observable property of gas-rich, star-forming galaxies in the optical, ultraviolet, and some infrared bands. Short-wavelength light from star forming regions is absorbed, heating the dust and effectively reprocessing this light into the infrared (see, e.g., Witt & Gordon 2000; Charlot & Fall 2000; Calzetti 2001 for an overview). Dust not only absorbs but also scatters optical and ultraviolet light, reducing the emitted flux in some directions, while potentially even boosting it in others (e.g. de Jong 1996b). The exact interplay of absorption and scattering depends sensitively on the relative geometry of stars and dust. This geometry is generally quite complex – young stars and star-forming regions are often embedded in dense dust, different stellar populations often have different scale lengths and heights, and the dust distribution can also be highly structured and clumpy (see, e.g., Witt & Gordon 2000; Holwerda et al. 2007; Schechtman-Rook et al. 2012; Liu et al. 2013). As such, the total attenuation due to dust along any given line of sight – defined as the sum total of the removal of light due to absorption and the scattering of

light both into and out of the line of sight – is difficult to *a priori* predict (see, e.g., Bruzual A. et al. 1988; Witt & Gordon 2000; Jonsson et al. 2006; Steinacker et al. 2013).

The magnitude of dust attenuation and its effects on our inferences about galactic properties can be large. Averaged over the present-day galaxy population, roughly one third of all emitted starlight is absorbed by dust and reprocessed into the infrared (Soifer & Neugebauer, 1991; Driver et al., 2012). Almost all optically measured quantities of dust-rich disc galaxies are strongly affected by this dust attenuation – examples of affected measurements include optical luminosities and colours (e.g. Tully et al. 1998; Maller et al. 2009; Masters et al. 2010), surface brightness profiles (e.g. Byun et al. 1994; de Jong 1996b), and structural measurements such as half-light radii, bulge-to-total (B/T) ratios, or Sérsic indexes (Pastrav et al., 2013a). These dust effects influence scaling relations such as the Tully-Fisher relation (e.g. Tully et al. 1998), colour-magnitude relations (Cho & Park, 2009), and stellar mass estimates (e.g. Bell & de Jong 2001; Maller et al. 2009).

One possible approach to understand the impacts of dust on these measurements and scaling relations would be to model the effects of dust on the light from a galaxy using analytical prescriptions or numerical simulations (e.g. Bruzual A. et al. 1988; Disney et al. 1989; de Jong 1996b; Popescu et al. 2000; Tuffs et al. 2004; Jonsson et al. 2006; Steinacker et al. 2013). However, the attenuation from dust depends sensitively on the absorption and scattering properties of dust grains, the distribution and substructure of dust within a galaxy, and the distribution of stars, including the varying distributions of different populations of stars (e.g. younger and older) with different spectra (e.g. Witt & Gordon 2000). This complexity means that modeling the dust attenuation, even in a simplified form, is a non-trivial task. Moreover, even for relatively sophisticated simulations, it is difficult to know for certain whether the dust properties, dust and star distributions, and other elements of the models actually match the physical properties of galaxies in the real universe. Overall, the distributions of stars and dust are not well characterized enough to yield robust predictions, so the predictions of these models remain useful, but primarily in a qualitative sense.

Accordingly, it is important to directly measure the effects of dust on the light distributions of galaxies. Historically, many methods have been used to explore the question of dust attenuation in disc galaxies. One method relies on observations of pairs of large disc galaxies that appear to overlap on the sky (e.g. Berlind et al. 1997; Keel et al. 2014). By measuring the change in the appearance of the two galaxies in the regions where they overlap and comparing it to their non-overlapping regions, using the assumption of symmetry one can measure the dust distribution in the foreground galaxy. Another method uses counts of distant background galaxies observed through the discs of large, nearby, face-on disc galaxies (e.g. Holwerda et al. 2005); such methods can be applied at very large distances from galaxies to reveal low-level extremely extended dust envelopes (e.g. Ménard et al. 2010). Both of these methods are capable of giving fairly detailed insight into the dust distributions of their target galaxies – in particular, they have established radial gradients in dust optical depth and that spiral arms are considerably richer in dust than inter-arm regions (e.g. White et al. 2000; Holwerda et al. 2005) – but are limited in terms of sample size.

The most statistically powerful method is to measure the dust-induced inclination dependence of parameters such as galaxy luminosities, colours, and structures (e.g. Valentijn 1990; Tully et al. 1998; Maller et al. 2009; Masters et al. 2010). Because it does not rely on chance alignments, large sample sizes spanning a range of galaxy properties are possible with modern sky surveys. As a consequence, it is well suited for measuring how dust attenuation varies among the galaxy population as a function of observable galaxy properties. This method addresses only the observed relative attenuation difference between edge-on and face-on galaxies. On one hand, this means that this methodology cannot correct galaxy properties to their 'intrinsic' dust-free values without invoking models. On the other hand, this means that these measurements are robust and model-independent; they can be used to provide a useful check of more model-dependent dust correction methods that require assumptions about the stellar populations and attenuation curves of target galaxies.

This technique has been employed many times in the past, with varying results. Optically-

selected samples have proven challenging to analyze; the quantities used to select samples suffer from dust attenuation, and early results were contradictory (Valentijn 1990; Huizinga & van Albada 1992; Giovanelli et al. 1994). Subsequent samples selected in the (nearly attenuation-independent) near-infrared (e.g. Tully et al. 1998) concluded that dust attenuation varies strongly with luminosity and is almost negligible for faint galaxies; this broad trend is now well-established (e.g. Maller et al. 2009; although Masters et al. 2010 argue that attenuation decreases again somewhat towards the brightest luminosities). Dust attenuation appears to vary with other galaxy parameters, such as surface brightness (e.g. de Jong & Lacey 2000) or morphology (e.g. Masters et al. 2010). Most such studies have chosen different samples, analysis methods, or parameters of interest, and these differences have made it difficult to develop a comprehensive overall picture of how dust content and dust attenuation (which are *not* necessarily the same thing, as we explore later) vary among the diverse galaxy population.

For example, (as explored later in this chapter) Tully et al. (1998) and Maller et al. (2009) both measure attenuation in terms of change in optical-K band colour with axis ratio for galaxies of similar K band luminosity. Despite this similarity, and despite the fact that both parametrize variations in attenuation in terms of absolute magnitude, they recover differing results, both in predicting significantly different levels of attenuation for galaxies of similar luminosity, and more broadly in disagreeing on the strength of the luminosity dependence of attenuation by factors of 2–3. It is difficult to pin down the physical significance of these disagreements, however, due to the differences between the studies – are they related to Tully et al.'s parametrization in terms of BRI magnitudes versus Maller et al.'s use of K? Is part of the variation in attenuation being expressed in Maller et al.'s additional parameter of Sérsic index?

In general, this lack of uniformity between different works makes it difficult to discern which parameters are most important in controlling dust attenuation. The broad outlines are visible, but the quantitative details are not. Many studies have focused on galaxy

luminosity as the primary source of variation in attenuation. Yet other parameters such as star formation rate (e.g. Wild et al. 2011) or surface density (e.g. de Jong & Lacey 2000) can be argued to be equally (if not more) fundamental, but comparison between current studies does not allow for a conclusive resolution of such questions. What is needed is an effort that addresses this by measuring the variation in dust attenuation as a function of many parameters simultaneously, using the same methodology and uniformly selected samples. This chapter represents the first part of such a study, exploring the variation in optical attenuation in the SDSS bands *ugriz* as a function of *WISE* parameters (scaling with stellar mass and star formation rate). In chapters 3 and 4 we will expand this by adding measurements of galaxy size, surface density, and structure to create a more comprehensive catalog of variation in attenuation with galaxy properties.

In addition to measuring the dependence of attenuation on stellar mass and star formation rate, our work focuses on the question of selecting samples in a uniform, unbiased manner. Since we cannot actually observe the same galaxy from multiple angles, measuring the inclination dependence of dust attenuation requires creating ensembles of galaxies which we believe to be essentially identical, save for their viewing angles. With such ensembles in hand, one can then study how the observable properties of these samples vary as a function of inclination to robustly measure the relative attenuation from edge-on to face-on orientation. Properly assembling these samples is the key challenge of this method, as any inclination-dependent variation in inherent properties among the members of the sample will bias the resulting attenuation measurements.

This is now possible thanks to advances in wide-area near- and mid-IR surveys, for example, the Two Micron All-Sky Survey (2MASS; Skrutskie et al. 2006), the near-IR Large Area Survey from the UKIRT Infrared Deep Sky Survey (UKIDSS-LAS; Lawrence et al. 2007), and especially the all-sky mid-IR coverage from 3.4μm to 22μm provided by the Wide-field Infrared Survey Explorer (*WISE*; Wright et al. 2010). Near-IR wavebands such as K or 3.4μm provide measurements of total stellar luminosity (and stellar mass to within factors of

two; Bell & de Jong 2001; Cluver et al. 2014; Meidt et al. 2014) and are well-resolved enough to measure galaxy structures. Mid-IR bands such as 12μm or 22μm measure hot and warm dust emission that correlates with star formation activity. Accordingly, these surveys allow us to probe important physical parameters of galaxies in a manner which is not affected by dust attenuation.

It is an important point that the analysis presented in this chapter does not, and is not intended to, correct galaxy properties to their intrinsic, dust-unaffected states. Rather, this analysis corrects for the *additional* effects of inclination – in effect, it attempts to correct all galaxies to their *face-on* states, rather than their *dust-free* states. For the purposes of classifying galaxies into different categories or comparing them to each other, this correction is usually sufficient – for these purposes, the intrinsic dust-free properties are not relevant, and the simpler analysis offers less scope for the introduction of systematic error. This restriction also means that the technique requires no assumptions about the intrinsic physical properties of the galaxy such as dust attenuation curves, star/dust geometry, stellar populations, etc. Correcting face-on to dust-free introduces the possibility of model-dependent variation; for this chapter we do not attempt this, instead leaving that task to the more complex study presented in chapter 4.

The plan of this chapter is as follows. In §2.2 we discuss and carefully select the most appropriate catalog SDSS and WISE flux measurements, and critically examine available axis ratio measurements. We explain how we frame our sample selection in terms of *WISE* 3.4μm luminosities ($M_{3.4\mu\mathrm{m}}$) and 12μm–3.4μm colour ([12]–[3.4]), construct a sample which is independent of inclination, and discuss the demographics of our sample in the *WISE* color–luminosity plane in §2.3. Our analysis method and measurements of relative attenuation as a function of inclination are presented in §2.4, and we compare these results in detail with two important previous works in §2.5. In §2.6 we compare our results more briefly with some other notable previous works and explore the implications of a simple scaling relation model of our results. We conclude in §2.7. All magnitudes throughout are presented in the AB

system (Oke & Gunn, 1983), all logarithms are base-10, and where necessary we assume a cosmology of $\Omega_M = 0.3$, $\Omega_\Lambda = 0.7$, and $H_0 = 70$ km s^{-1} Mpc^{-1}.

2.2 Data

Our goal is to measure the difference between edge-on and face-on attenuation in the optical SDSS *ugriz* passbands as a function of parameters drawn from longer-wavelength datasets (*WISE* and 2MASS) that scale with stellar mass and dust-enshrouded star formation rate. Accordingly, we choose for analysis a sample of galaxies drawn from the Sloan Digital Sky Survey (SDSS) DR10 (Eisenstein et al. 2011, Ahn et al. 2014), cross-matched with data from the Wide-field Infrared Survey Explorer (*WISE*) All-Sky Data Release (Wright et al., 2010). We use axis ratio measurements derived from the SDSS bulge/disc decompositions of Simard et al. (2011) (hereafter S11) as the best available measurements of galaxy inclination, and for some of our sample diagnostics we make use of data from the the 2-Micron All Sky Survey Extended Source Catalog (2MASS XSC; Skrutskie et al. 2006). After all cross-matching and cuts, we have a sample of approximately 80,000 galaxies of all types with reliable axis ratios, SDSS optical photometry, and *WISE* dust- and inclination-independent NIR-MIR photometry.

As noted below, basic catalog measurements often suffer from issues which make them less ideal for our purposes. Nonetheless, we use these catalog measurements whenever possible rather than derived quantities for two main reasons – first, to avoid any hidden dust-dependent systematic errors in more complex model-derived quantities, and second, to enable easy use of our work by others.

2.2.1 Photometric catalog data

Our initial sample selection is from the SDSS, drawing from the Galaxy view of the `PhotoPrimary` table and selecting objects with clean photometry as defined by the flag CLEAN = 1 and associated spectral data in the `SpecObj` table. The SDSS provides the

optical magnitudes we use to probe dust attenuation, but the reason to start with this base sample is that the SDSS is the source of the spectroscopic redshifts we use to calculate absolute magnitudes. The only SDSS-based selection criteria applied to this inital sample is a limit of $m_r \leq 17.7$ mag, to ensure clean spectral data. (We are cognizant that optical selection limits may introduce biases, and as described in §2.3.2 we use an additional redshift selection in our analysis which controls for this effect.) There is also roughly 6 per cent incompleteness in the SDSS spectroscopic sample due to fiber collisions (Strauss et al., 2002), but as this selection is geometric rather than dependent on galaxy properties it will not introduce any biases in our sample. This returns a sample of 513,597 galaxies, which, after later cross-matching with *WISE*, results in a final sample of 78,721 galaxies.

In this subsection we detail the various photometric measurements available in our catalogs, and explain our reasoning for choosing the specific quantities we use. The choice of photometric parameters has a notable quantitative effect on our analysis, though not enough to make a qualitative difference in our final conclusions (see discussion in §2.4.2).

2.2.1.1 WISE

In our sample, we use *WISE* infrared data to provide inclination-independent measures of galaxy properties. We take our initial catalog of SDSS galaxies and cross-match it with *WISE*, treating any *WISE* source falling within 5 arcsec of the centre of an SDSS galaxy as a match. The SDSS-based limit of $m_r \leq 17.7$ noted above is significantly more restrictive than the *WISE* detection limits, and so this cross-match is able to match the vast majority of our sources, with the initial cross-matching resulting in a sample of 509,305 galaxies with SDSS and *WISE* catalog properties. However, as explained below, the number of galaxies with photometry measured in the most useful manner is smaller, at 78,721.

From *WISE*, we extract galaxy apparent magnitudes $m_{\rm w1}$, $m_{\rm w2}$, $m_{\rm w3}$, $m_{\rm w4}$ in the *WISE* W1 (3.4μm), W2 (4.5μm), W3 (12μm), and W4 (22μm) bands. The foreground extinction in these bands is essentially zero, so no extinction corrections are necessary, but K-corrections

are applied using the IDL `kcorrect` package (Blanton & Roweis, 2007). Absolute magnitudes $M_{3.4\mu\mathrm{m}}$, $M_{4.5\mu\mathrm{m}}$, $M_{12\mu\mathrm{m}}$, $M_{22\mu\mathrm{m}}$ are calculated using spectroscopic redshifts from the SDSS `SpecObj` table, and the results are converted to the AB photometric system.

However, there are a variety of different magnitude measurements given in the *WISE* catalog, and not all of them are suitable for our purposes. The primary issue is that most *WISE* photometry is optimized for measuring the brightness of point sources.

Profile fit photometry fits the *WISE* PSF to the observed profile of a source, assuming that the source is unresolved (`wXmpro` in *WISE*, where X is a numeral 1–4 referring to the four *WISE* bands). However, most of the galaxies in our sample have sizes which are similar to or larger than the 6 arcsec FWHM of the W1–3 band *WISE* PSF. Since the profile fit photometry assumes an unresolved source, this results in substantial systematic errors in magnitudes and colours as a function of apparent galaxy size. This is shown in the first panel of Fig. 2.1, where the W1 profile fit magnitudes are compared to the 2MASS extended source J magnitudes (a measurement much less susceptible to this form of error) as a function of 2MASS K band radius.[1] It can be seen that the *WISE* magnitudes are a strong function of radius. Additionally, the *WISE* PSF varies in size in different bands, and the apparent size of the galaxy itself may also vary due to population gradients, giving further scope for systematic error in various difficult-to-predict forms. Therefore, the profile fit photometry is not suitable for our use.

Standard aperture photometry returns the flux within a 'standard' aperture (8.25 arcsec radius for W1–3, 16.5 arcsec radius for W4), corrected for the curve-of-growth of the PSF again assuming an unresolved source (`wXmag` in *WISE*). This type of photometry suffers from many of the same problems as the profile fit photometry. Since the aperture correction assumes an unresolved source while our galaxies are generally resolved, the fluxes will be underestimated, particularly for larger galaxies. Again, this is shown by comparison to

[1] 2MASS radii and extended source magnitudes are measured using properly-scaled elliptical apertures, mitigating these sorts of errors. J-band photometry is chosen because of its high S/N assisting in capturing the outskirts of a galaxy, while K-band radii are measured using the longest wavelength available.

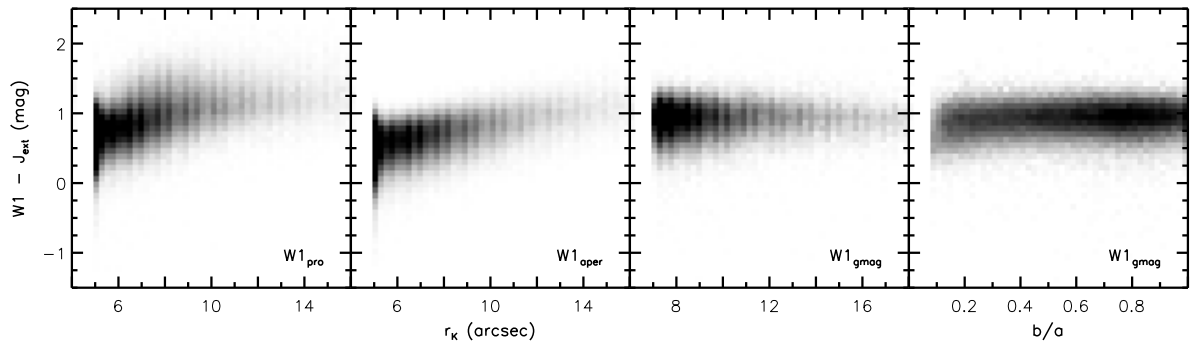

Figure 2.1: Left to right: Panels 1-3: *WISE* W1 profile-fit magnitude, *WISE* W1 standard aperture magnitude, and W1 gmag, all minus 2MASS extended J magnitude, as a function of 2MASS K-band radius. Panel 4: *WISE* W1 gmag minus 2MASS extended J magnitude, as a function of axis ratio.

2MASS extended source J magnitudes in the second panel of Fig. 2.1. The standard aperture colours are also affected by colour gradients due to the aperture preferentially sampling the core rather than the outskirts. The aperture photometry is also vulnerable to contamination to some degree, though to a relatively limited extent due to the fairly small aperture. For these reasons, the standard aperture photometry is also not suitable for our work.

Finally, multi-aperture photometry returns the flux within a series of apertures with radii ranging from 5.5–24.75 arcsec (W1–3) or 11.0–44.0 arcsec (W4), with no further correction (`wXmag_Y` in *WISE*, where Y is a numeral 1–8 referring to the 8 different aperture sizes). The multi-aperture photometry is theoretically not subject to the radius-dependent errors of the previous two varieties, because an appropriately sized aperture can be chosen to correctly capture our extended sources. However, the multi-aperture photometry is significantly more vulnerable to contamination as the size of the aperture increases. Additionally, the multi-aperture photometry uses circular apertures, which further broadens the scope for systematic errors with galaxy size and axis ratio. For these reasons, the multi-aperture photometry is also less than ideal for our purposes.

The most useful *WISE* photometry for galaxy magnitudes is the 2MASS-association-based elliptical aperture photometry (`wXgmag` in *WISE* – referred to henceforth as gmag).

WISE sources are internally cross-matched with the 2MASS XSC, and sources which lie within 2 arcsec of a XSC source are assumed to be that same object. In addition to the standard photometry, these sources are measured using an elliptical aperture whose radius, axis ratio, and position angle are derived from the 2MASS K band 'standard' elliptical aperture for that source. This provides a non-point source magnitude measured in an aperture whose size and shape are scaled appropriately based on non-optical measurements of that source, thus avoiding most of the systematic errors present in the profile-fit, standard aperture, and multi-aperture photometry. This can be seen in the remaining two panels of Fig. 2.1. In the fourth panel we compare the gmags to the 2MASS extended source J magnitudes as a function of radius in the same manner as before, and we find that the gmags do not have any significant dependence on radius, unlike the profile fit and standard aperture photometry. Similarly, in the fourth panel, we see via the same comparison that the gmags also do not show any significant inclination dependence. This is the photometry we use for our work.

The gmags are the best overall magnitude available in the *WISE* catalog, but using these does come with some significant drawbacks, the most obvious of which is sample size. While we have 509,305 galaxies with basic SDSS+*WISE* photometry, only 78,721 of them have gmags measured in both W1 and W3 due to the requirement of cross-matching with 2MASS. The lower sensitivity of 2MASS eliminates some of the faintest galaxies, and more are eliminated due to this photometry's requirement of $r \geq 7$ arcsec in 2MASS K-band. Also, the 2MASS K-band 'standard' aperture that these magnitudes are based on is defined by the 20 mag arcsec^{-2} surface brightness isophote, which does not capture the faint outskirts of a galaxy and thus underestimates the total flux. Therefore, while the colours measured using these magnitudes are quite accurate, the total luminosities may be an underestimate. However, it is important to note that the purpose of our selection criteria is to divide our sample into bins of essentially identical galaxies. For this purpose it does not actually matter whether the luminosities are accurate – merely that, if they are biased, that this bias affects

all galaxies equally and does not depend on the parameters of the galaxies involved. This appears to be the case for these magnitudes, as we find no systematic trend in the gmag measurements with properties such as radius. Therefore, while this choice of photometry does limit our sample size and comes with some caveats, the resulting sample is the only one that is free from all of the various biases described above.[2]

2.2.1.2 SDSS

The SDSS optical catalog data provide the dust-sensitive measurements we use to quantify the dust attenuation in our sample. From the SDSS, we extract the apparent magnitudes m_u, m_g, m_r, m_i, m_z in the 5 SDSS bands. These magnitudes are corrected for foreground Galactic extinction using the extinction values given in the `Extinction_X` (where X $\in$ {u,g,r,i,z} refers to one of the five SDSS bands) columns of the SDSS and are K-corrected using the IDL `kcorrect` package (Blanton & Roweis, 2007). As with *WISE*, galaxy redshifts z are adopted from the `SpecObj` table and are used to calculate the absolute magnitudes M_u, M_g, M_r, M_i, M_z.

As with *WISE*, there are several different magnitudes given in the SDSS catalog, and like *WISE*, many of the most commonly used are not suitable for our purposes.

Petrosian magnitudes (`petroMag_X` in SDSS) are measured in an aperture whose size is defined as the radius at which the local surface brightness in the r band drops to a given fraction of the average surface brightness interior to that radius. While this includes the majority of a galaxy's light, it does not capture the full extended flux of a galaxy, and the extent to which the flux is underestimated depends on light profile shape (larger for light profile shapes with larger wings, such as the de Vaucouleurs profile). Also, since the Petrosian

[2]There is one further set of magnitudes we might choose to use – the SDSS/ *WISE* forced photometry of Lang et al. (2014a). In principle this catalog could combine good extended source photometry with larger sample sizes. In practice, however, in order to avoid selection biases we subject our sample to relatively restrictive volume limits as detailed in §2.3.2, so the sample size advantage of using Lang et al.'s magnitudes is limited. Additionally, since this is a set of model magnitudes based on optically-derived SDSS parameters, there are several potential systematics that we do not yet feel we understand well enough to be comfortable using these magnitudes. This decision may be revisited in our future work.

radius is defined in terms of surface brightness in circular annuli, this raises the possibility of axis ratio-dependent effects. Given that we have a wide range of galaxy morphologies in our sample and that our analysis relies on inclination dependence of galaxy magnitudes, we do not use Petrosian magnitudes.

In addition to the Petrosian magnitude, there are two types of model magnitude. The standard model magnitudes (`modelMag_X` in SDSS) are based on fitting the light profile of each galaxy in the r band with both an exponential and a de Vaucouleurs profile, choosing the better profile fit, and extrapolating that profile fit in each band (appropriately scaled) to estimate the galaxy's total flux. This model magnitude is good for tasks that require accurate measurement of SDSS colours, since the use of the r-band fit means that flux is measured in an equivalent way in all bands. However, this magnitude has the limitation that it is derived solely from the better fitting of the exponential *or* the de Vaucouleurs fits, even if the galaxy is actually best fit by a combination. This leads to inconsistent results when applied to galaxies which have intermediate light profiles (bulgy spirals or discy ellipticals). This can cause systematic errors in SDSS–NIR colours with morphology, as well as leading to discontinuities in magnitude measurements for the population of galaxies which are almost equally well fit by either profile. Since our work includes galaxies with a wide range of morphologies and we are most concerned with the stability of SDSS–NIR colours rather than intra-SDSS colours, we also do not use standard modelMags.

Rather, we use the composite model magnitudes (`cModelMag_X` in SDSS). These magnitudes are based on the same exponential and de Vaucouleurs fits to each galaxy's light profile, but gives a magnitude based on the linear combination of the two that best fits the galaxy's profile rather than simply using only the better of the two fits. This provides superior photometry for the large number of galaxies which are not well fit by a pure exponential or de Vaucouleurs profile. This fit is also done individually in each band rather than using the r-band fit for all bands, which sacrifices some accuracy for intra-SDSS colour measurements but further improves the quality of the photometry for comparisons to NIR

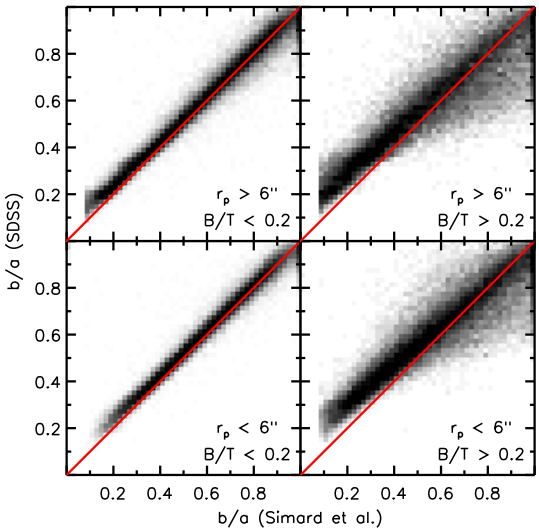

Figure 2.2: Comparison of axis ratio measurements from S11 (horizontal axis) and SDSS (vertical axis) for disc galaxies, divided by B/T ratio and r-band angular size. In each panel the 2-d histogram shows the distribution of galaxies within that bin of B/T and angular size, and deviations from the diagonal 1-to-1 line reflect differences in the axis ratio measurements assigned by these two datasets.

data. Therefore, the composite model magnitudes are the best choice for our work.

2.2.2 Measures of projected axis ratio

We wish to measure the change in observed galaxy properties as a function of disc inclination i. However, inclination i is not an immediately observable property – rather, we observe galaxy axis ratios a/b, measured using isophotal fits or similar methods. The connection between galaxy inclination – the fundamental physical property we wish to exploit – and observed axis ratio depends on a host of other effects, including galaxy morphology differences such as intrinsic asymmetry and bulge size, photometric effects such as surface brightness limits and seeing, and even the very dust attenuation we wish to study. Therefore, the choice of inclination metric is an important one, and indeed has a significant quantitative and qualitative effect on the results (see discussion in §2.4.2).

If our goal is to avoid visual wavelength measurements to reduce the risk of dust-induced

biases, a natural choice of inclination metric would seem to be the 2MASS axis ratios. In the K band, for example, these would be essentially unaffected by dust attenuation. However, the relatively low resolution of 2MASS imagery renders these measurements unsuitable for our purposes. In the online 2MASS documentation, Cutri et al. (2006) caution that the various galaxy shape measurements become unreliable for objects smaller than 10 arcsec, which encompasses roughly 70 per cent of our sample. Additionally, since these are isophotal axis ratios they will suffer from biases due to the presence of bulges, which we would prefer to avoid. And so, despite the desirability of a non-optical inclination metric, we do not use the 2MASS axis ratios.

The SDSS provides axis ratios based on their model magnitude exponential and de Vaucouleurs profile fits. These fits are convolved with the SDSS PSF to account for seeing, but as we show below, this correction is possibly incomplete. Additionally, since they are fit with either a pure exponential or a pure de Vaucouleurs profile, they cannot account for the presence of both a bulge and a disc in the target galaxies, which results in biased axis ratios. Finally, like the standard model magnitudes, the model axis ratios will also be subject to discontinuous behavior for the population of galaxies which are almost equally well fit by either profile. For these reasons, we do not use the SDSS axis ratios.

Rather, for our analysis we adopt the r-band disc inclinations from the two-component Sérsic models (Sérsic, 1963) of Simard et al. (2011) (S11). S11 perform two-dimensional bulge-disc fits to the g and r-band images for galaxies in the SDSS, accounting for the effects of seeing. For our purposes, a key advantage is that for a disc galaxy such a measurement should account for the changes in b/a expected from both the addition of the bulge and the convolution of a thin disc with a (much rounder) PSF; both effects would tend to drive a direct measurement of b/a to larger values, impacting analyses such as ours. Thus, using this measurement should return more accurate disc axis ratios for disc galaxies with significant bulge components.

Of course, these fits and axis ratios do not operate in quite the same way for bulge-

dominated galaxies without significant disc components. As discussed in S11, in such cases the disc component of the bulge-disc model instead fits to the outer, flatter portions of the bulge-dominated galaxy's light profile. In this case the axis ratio returned is obviously no longer a 'disc' axis ratio; however, it is still a reliable measurement of the shape of the outer isophotes. This is fortuitous from our perspective, as it means that this single measurement returns accurate axis ratios for disc-dominated galaxies and reasonable axis ratios for bulge-dominated galaxies. While the brightest bulge-dominated galaxies are usually triaxial in shape, and thus not appropriate targets for our analysis method since their axis ratio distributions do not reflect variations in inclination, this does allow us to probe the inclination dependence for the intermediate populations of bulgy galaxies which tend to be shaped like oblate spheroids (van der Wel et al., 2009a).

Fig. 2.2 shows a comparison between b/a values derived from S11's disc inclinations and those derived from the SDSS models, illustrating the differences between these measurements. This includes disc galaxies only (for our purposes, this is roughly defined as *WISE* $M_{12\mu\mathrm{m}} - M_{3.4\mu\mathrm{m}}$ colour $< \sim 0.5$ – see discussion in §2.3.3), and this sample is divided by angular galaxy size (r-band petrosian radius) as measured by SDSS and bulge/total ratios as measured by S11 (both of these parameterizations are potentially dust, and therefore inclination, dependent, but this division of the sample is purely for illustrative purposes).

In the left column of highly disc-dominated galaxies in Fig. 2.2, as may be expected the correspondence is overall quite good. However, deviations are apparent for both the highest and lowest b/a galaxies. For very high b/a galaxies in the larger radius subsample, there is a slight trend for the SDSS b/a measurements to fall below S11's. This is likely due to inherent asymmetries in the target galaxies, which can cause the measured b/a value to fall short of unity even for a galaxy which is in truth being observed essentially face-on. S11's model fits appear to be less vulnerable to such effects than the SDSS fits, which we speculate is due to the ability of S11's two-component fits to account for the presence of a bar or other non-axisymmetric bulge. This effect is less prominent for the smaller galaxies, likely because

in these cases seeing will tend to blur out weaker asymmetries. At the other end of the scale, there is a small but notable trend for the SDSS b/a measurements to report larger axis ratios than S11 for the most edge-on galaxies. This is likely due to some combination of seeing and bulge effects. For edge-on galaxies whose size on the sky is not greatly larger than the average PSF, their apparent minor axis size will be inflated to a greater relative extent than their major axis size, which will lead to b/a measurements which are biased high if the PSF correction is insufficient. Additionally, as a galaxy becomes more inclined, the relative contribution to the projected axis ratio from any bulge component becomes larger. The SDSS single-component fits cannot account for this, but S11's two-component fits can. The fact that this effect is present at all for this disc-dominated subsample suggests that it may be a seeing effect. However, it is also present for both the large and small galaxies, which suggests a bulge effect. Therefore, it is unclear which of these two effects contributes more to the observed offset in this case.

In the right column of galaxies with more significant bulge components in Fig. 2.2 both of these effects become much stronger. We observe a much stronger trend for the SDSS b/a measurements to be lower than S11's at high b/a. The strengthening of this trend with increasing B/T ratio suggests that it is indeed being driven by bars or other non-axisymmetric central features which S11's two-component fits can account for but the SDSS's single-component fits cannot. This effect is still slightly more prominent for larger galaxies, but unlike for the disc-dominated subsample it is also significant for the smaller galaxies. Similarly, the trend for the SDSS b/a measurements to be larger than S11's for the most edge-on galaxies is also larger than in the disc-dominated sample. The seeing effect discussed above may still be in play, but it is apparent that the significant increase in deviation in this subsample is being driven by the increasing effects of bulges on the SDSS-measured axis ratios of edge-on galaxies. It is also notable that for this larger B/T subsample this effect is significant even at intermediate b/a values – the axis ratios measured by the SDSS are somewhat inflated by the presence of the bulge even for galaxies which are not being viewed

completely edge-on.

The sample considered here focuses only on disc galaxies, but for our purposes the axis ratios of the highest B/T, bulge-dominated galaxies are not especially important, since these spheroid galaxies are typically dust-poor and the fact that they have only weak or nonexistent discs makes them inappropriate targets for our analysis technique. Therefore, the effects noted above are all strong reasons to adopt S11's inclinations rather than the SDSS axis ratios. It is important to note, however, that this does not mean that this is the perfect solution. The use of a model photometric fit always has the potential to introduce model-dependent biases, and this potential increases for more complex models such as S11's. Additionally, as mentioned one would ideally prefer to have NIR-derived inclination measurements rather than optical to avoid any potential dust effects. However, since the inclination measurements of these fits rely most strongly on light from the outskirts of the galaxies (the least dust-affected areas), these effects should not be large enough to compromise our analysis, and regardless these possible systematics are less problematic than the known systematics of the SDSS (and 2MASS) axis ratios. And so while in some senses S11's inclinations are not completely ideal and it is important to remember that there may be issues introduced by the use of this data set, we believe that they represent the best available measurement of inclination for our purposes.

2.3 Sample selection criteria & population demographics

We wish to study attenuation by dust by examining the inclination dependence of the optical luminosities of galaxies as a function of galaxy properties. As discussed previously, the core challenge of any such study is the ability to identify and select samples of galaxies based on intrinsic, dust-independent properties.

In choosing a set of parameters for characterizing the properties of galaxies for a study of dust attenuation, there are a few criteria which we wish to reflect on. Most importantly, the parameters must be as dust and inclination independent as possible – in practice, this

will drive selection passbands to as long wavelengths as circumstances allow. It is useful to adopt a directly-observed parameter (e.g., an observed colour instead of a specific star formation rate) to avoid any hidden dependence of model-derived quantities on dust attenuation. Furthermore, it is very desirable that the properties in question are either observationally or theoretically expected to correlate with dust attenuation, at least broadly. Finally, it is helpful to the community to use properties that are widely available.

2.3.1 WISE absolute magnitudes and colours as valuable galaxy classification parameters

We maintain that *WISE* near and mid-infrared catalog absolute magnitudes and colours satisfy the above criteria. *WISE* probes long-wavelength near and mid-infrared light which suffers from more than an order of magnitude less dust *attenuation* than the optical passbands. Our analysis in §2.2.1.1 illustrated that *WISE* 'gmags' appear to be unaffected by galaxy size and inclination. They are observational quantities, and are readily available for large samples of galaxies. In particular, we choose to sort galaxies as a function of their *WISE* absolute 3.4μm magnitude and 12μm $-$ 3.4μm colours.

We choose to adopt *WISE* 3.4μm absolute magnitude (henceforth referred to as $M_{3.4\mu\mathrm{m}}$) as an observational proxy for stellar mass. Dust attenuation at 3.4μm is small, dust *emission* from PAHs and hot dust is moderate on galaxy-wide scales, and stellar M/L variations are expected to be modest $<$ 0.3dex (Meidt et al. 2012, 2014, Cluver et al. 2014, see also Fig. 2.3 and discussion below). Dust attenuation would *a priori* be expected to correlate with $M_{3.4\mu\mathrm{m}}$ as both gas density and metallicity (which is expected to influence the dust-to-gas ratio) vary as a function of stellar mass (e.g. Tremonti et al. 2004). Indeed, previous works find a correlation between attenuation and K-band luminosity (e.g. Tully et al. 1998, Maller et al. 2009).

In addition to $M_{3.4\mu\mathrm{m}}$ luminosity, we choose also to select galaxies for study using their *WISE* 12μm $-$ 3.4μm colour (henceforth referred to as [12]–[3.4]). Again, the effects of

dust attenuation on [12]–[3.4] colour are small, and this is a purely observational quantity, not dependent on dust attenuation sensitive models for sample classification. The [12]–[3.4] colour is expected to be a good proxy for dust enshrouded specific star formation rate (star formation rate per unit stellar mass; discussed further by Chang et al. 2015). Specific star formation rate is expected *a priori* to correlate with dust attenuation. Star formation rate should scale with gas density (Kennicutt, 1989, 1998) and therefore dust density; indeed, Wild et al. (2011) noted that attenuation curve shape varies strongly as a function of specific star formation rate. As noted above, $M_{3.4\mu\mathrm{m}}$ luminosity correlates very strongly with stellar mass. Meanwhile, 12μm emission arises primarily from PAH molecules, small dust grains, and hot dust (Calzetti, 2013). While a variety of heating mechanisms contribute to 12μm emission, the 12μm luminosity correlates to within a factor of two with the total infrared luminosity, which in turn gives insight into the dust enshrouded star formation rate (Papovich & Bell, 2002; Bell, 2003; Wen et al., 2014; Chang et al., 2015). In practice, 12μm luminosity not only measures dust-enshrouded star formation, but for star-forming galaxies very closely tracks overall star formation rate as well. Wen et al. (2014) compare 12μm luminosity with Balmer-decrement extinction corrected Hα luminosity (an alternate measure of star formation activity) for star-forming galaxies and find a tight relationship between IR and Balmer line brightness; estimating by eye from their fig. 3 suggests an RMS in the relationships of roughly 0.1 dex. Meanwhile, we adopt bins that are a half-magnitude (0.2 dex) wide in [12]–[3.4] – thus, we are not attempting to divide our data more finely than the precision of this estimator. Therefore, we maintain that [12]–[3.4] is a robust and sufficiently effective diagnostic of star formation per unit stellar mass to meet our goals.

Fig. 2.3 shows estimated stellar mass and specific star formation rate for our sample, calculated from *WISE* magnitudes and colors using the 3.4 and 4.6μm-stellar mass relation of Cluver et al. (2014) and the 12μm-star formation rate relation of Wen et al. (2014). The contours show the overall galaxy distribution within the parameter space defined by

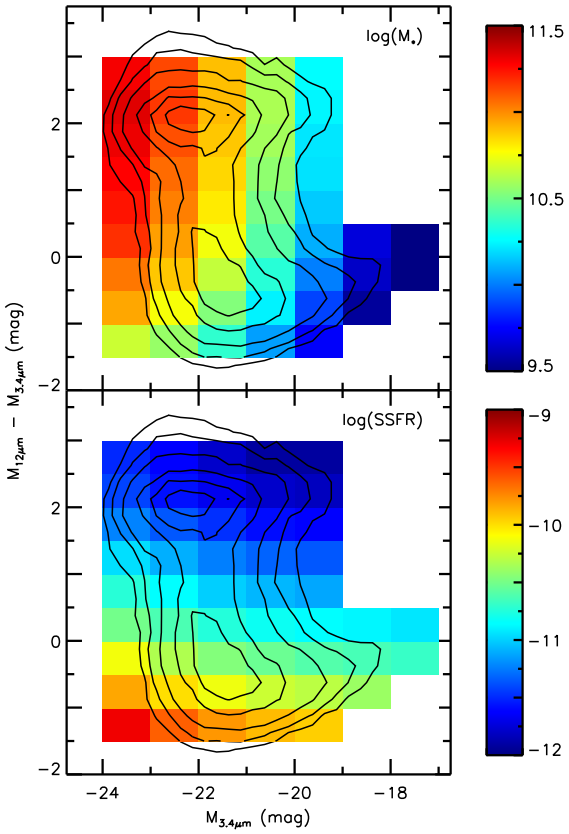

Figure 2.3: Upper panel: stellar mass as a function of $M_{3.4\mu\mathrm{m}}$ luminosity and [12]–[3.4] colour. The color scale shows $\log(M_*)$ in units of $M_\odot$. Lower panel: specific star formation rate as a function of $M_{3.4\mu\mathrm{m}}$ luminosity and [12]–[3.4] colour. The color scale shows $\log(\mathrm{SFR}/M_*)$ in units of yr^{-1}. In both panels, background contours show the distribution of galaxies in this parameter space.

$M_{3.4\mu m}$ luminosity and [12]–[3.4] colour, and the colour coding shows the average stellar mass or specific star formation rate at that location in parameter space. We can see that our interpretation of $M_{3.4\mu m}$ luminosity and [12]–[3.4] colour as proxies for stellar mass and specific star formation rate is, as a whole, reasonably justified. Stellar masses range from $\sim 10^{9.5}$ $M_{\odot}$ at the very dimmest end of the star-forming main sequence to more than 10^{11} $M_{\odot}$ for the brightest quiescent galaxies. There is a tilt due to varying stellar mass-to-light ratios in the 3.4μm band between quiescent and star-forming galaxies (see Cluver et al. 2014), but overall, and in particular when considering galaxies at a fixed [12]–[3.4] color, $M_{3.4\mu m}$ serves as a reasonable proxy for stellar mass. Similarly, specific star formation rate varies from $\sim 10^{-12}$ yr^{-1} for the most quiescent galaxies to more than $10^{-9.5}$ yr^{-1} for the most active galaxies. Again, while the same mass-to-light variations also produce a tilt in the distribution of specific star formation rate, both overall, and particularly when considering galaxies at a fixed $M_{3.4\mu m}$ luminosity, [12]–[3.4] color serves as a reasonable proxy for specific star formation rate.

These *WISE* quantities satisfy our primary criteria in that they are long wavelength, dust attenuation insensitive, and widely-available observed quantities. Furthermore, as reasonable proxies for stellar mass and (dust-enshrouded) specific SFR, we expect them to capture some of the variation in dust attenuation from galaxy to galaxy. Nonetheless, there are doubtless other galactic parameters that should correlate with dust attenuation that one could select by. For example, the surface density of gas and stars should also correlate with attenuation (as argued e.g., by de Jong & Lacey 2000), and bulge-to-total ratio (and more generally morphology) should affect attenuation by varying the star-dust geometry (e.g. Witt & Gordon 2000). Unfortunately, such metrics are widely available only using dust attenuation- and inclination-dependent parameters (i.e., using half-light radii or morphologies from optical SDSS-derived catalogs; e.g. Blanton et al. 2005, S11) or are available for modest samples of very nearby galaxies (i.e., gas densities from HI or CO interferometry). In chapter 3, we will develop long wavelength-derived inclination-independent galaxy structure and morphology

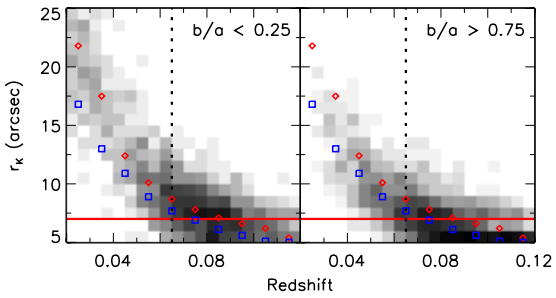

Figure 2.4: Distribution of K-band radius as a function of redshift, for edge-on (left panel) and face-on (right panel) galaxies, in an example bin of parameter space ($-22 < M_{3.4} < -21$, $-1.0 <$ [12]–[3.4] < -0.5). Red diamonds and blue squares show the median of radius in redshift slices for the edge-on and face-on subsamples, respectively. The horizontal red line shows the 7 arcsec selection limit, and the vertical dashed line shows the adopted redshift limit in this bin.

metrics and explore their correlation with dust attenuation; for our purposes in this chapter, we focus on what is immediately available and study the variation of attenuation with *WISE* catalog luminosities and colours.

2.3.2 Inclination independence of selection limits

While our individual subsample selection metrics are independent of inclination, it is important that our overall sample selection limits also have this property. Our initial sample is subject to two potentially problematic selection limits which we consider.

First is the limit of $m_r \leq 17.7$ mag in the SDSS, which is required to ensure clean spectroscopic data. Since this is an optical selection, for dusty disc galaxies this limit will introduce a bias against faint edge-on galaxies within each bin, as these galaxies may drop below the magnitude limit due to attenuation while their intrinsically equally-bright but less attenuated face-on counterparts do not.

Second, due to the required cross-match with 2MASS, the *WISE* gmag photometry is subject to an apparent radius limit of $r \geq 7$ arcsec in the 2MASS K band. This is an isophotal radius, so it is affected by the projected surface brightness of the target galaxy.

Since galaxies are essentially transparent in K band, their surface brightness will increase with inclination as the same amount of light is concentrated in a smaller area on the sky. Thus, for intrinsically identical galaxies, the measured isophotal radius will be increased for galaxies viewed closer to edge-on. This induces a bias which acts in the opposite sense as the SDSS apparent magnitude limit. In this case, edge-on galaxies which otherwise would lie just below the radius limit have their measured radius increased due to their inclination by enough to rise into the sample, while their intrinsically similar face-on counterparts remain below the cutoff.

Both of these biases are potentially problematic. Since our method relies on measuring the inclination dependence of dust-affected optical measurements in a subsample of intrinsically similar galaxies, it is required that the high-inclination and low-inclination components of that subsample are actually representative of the same underlying population. Thus, selection effects that act to include or exclude galaxies based on their inclinations are obviously not desirable, and the fact that we have two different selection limits whose biases act in opposite directions and whose relative sizes are difficult to predict only further increases the potential confusion.

To control for these effects, we introduce a redshift limit within each bin of $M_{3.4\mu\mathrm{m}}$ luminosity and [12]–[3.4] colour in order to preempt these biased selection limits with an unbiased one. Since both apparent brightness and angular size decrease with distance, an appropriately chosen redshift limit ensures that the bin acts as a proper volume-limited subsample by removing (in an unbiased manner) galaxies which lie near to these problematic selection limits.

In practice, we find that the radius limit is generally more significant than the magnitude limit. (That is, as redshift increases, the distribution of isophotal K-band radii of face-on galaxies within a bin approaches 7 arcsec before the distribution of apparent r-band magnitudes of edge-on galaxies approaches 17.7 mag. This radius limit obviously does not correspond to an exact magnitude limit, but of the galaxies with $r \geq 7$ arcsec, 93 per cent

have $m_r \leq 17$ and 79 per cent have $m_r \leq 16.5$.) Thus, within each bin we determine the appropriate limit by finding the redshift at which the fraction of face-on galaxies whose angular sizes fall below the 7 arcsec limit crosses a threshold of 33 per cent – in other words, this is the redshift at which face-on galaxies begin to disproportionately drop out of the sample compared to edge-on galaxies due to the radius limit.

This procedure is illustrated in Fig. 2.4, which shows the distributions of radius with redshift for face-on and edge-on galaxies in a single example bin within our parameter space. It is easy to see that the face-on galaxies are systematically smaller than the edge-on galaxies at a given redshift, illustrating the bias in radius measurements. However, by considering only galaxies whose redshifts are less than the indicated limit we ensure that all galaxies are included equally in the sample regardless of their inclination. (Similarly, one could determine an analogous redshift limit based on finding where the distribution of apparent r-band magnitudes of edge-on galaxies approaches the 17.7 mag limit, but, as noted above, in practice this is not necessary as a separate step since the radius-based redshift limit is smaller than the magnitude-based limit.) Therefore, by taking this redshift cut within each bin, we ensure that the inclination-dependent radius and magnitude selection limits do not introduce biases into our sample.

2.3.3 Sample population demographics

The joint selection on $M_{3.4\mu\mathrm{m}}$ luminosity and [12]–[3.4] colour defines the parameter space for our analysis, and the properties of this parameter space also allow us to divide galaxies based on their morphology and isolate the disc galaxies we are interested in without relying on dust-affected morphology metrics such as SDSS f_{DeV} or concentration. In Fig. 2.5, we show the distribution of our sample with respect to inclination in this parameter space.

The upper panel of Fig. 2.5 shows the distribution of [12]–[3.4] as a function of $M_{3.4\mu\mathrm{m}}$ absolute magnitude for a subsample with nearly round shapes (minor axis to major axis ratio $b/a > 0.75$), corresponding to intrinsically round galaxies and/or low inclination discs. The

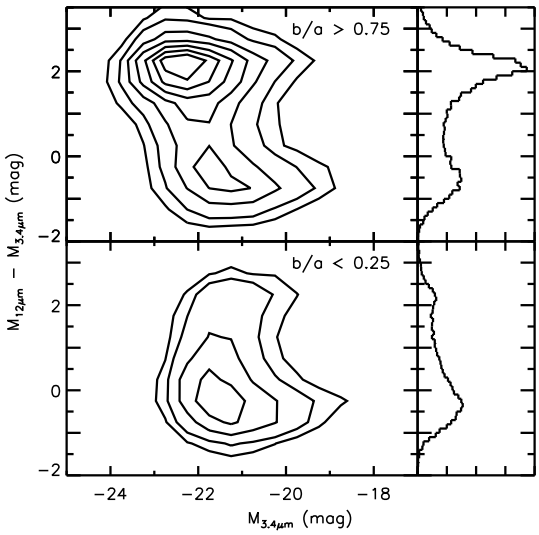

Figure 2.5: Upper left panel: The distribution of galaxies with nearly circular shapes ($b/a > 0.75$) in [12]–[3.4] colour as a function of $M_{3.4\mu\mathrm{m}}$ absolute magnitude. Quiescent galaxies have [12]–[3.4] > 0.5 and relatively round shapes, and the star forming main sequence has [12]–[3.4] ≈ -0.5. Upper right panel: The distribution of [12]–[3.4] colours for the $b/a > 0.75$ subsample. Lower left panel: The distribution of galaxies with flattened shapes ($b/a < 0.25$) in [12]–[3.4] colour as a function of $M_{3.4\mu\mathrm{m}}$ absolute magnitude. Lower right panel: The distribution of [12]–[3.4] colours for the $b/a < 0.25$ subsample.

lower panel shows the corresponding distribution for flattened galaxies with $b/a < 0.25$, corresponding to highly inclined intrinsically flattened galaxies. The lower panel contains almost entirely disc galaxies; these have more negative [12]–[3.4] colours, having large amounts of 12μm emission relative to their 3.4μm emission. These galaxies have high (dust enshrouded) specific star formation rate. These star-forming galaxies cluster along a well-defined track in the $M_{3.4\mu\mathrm{m}}$ vs. [12]–[3.4] parameter space – the 'star forming main sequence' – due to the tight correlation between specific star formation rate and stellar mass (e.g. Salim et al. 2007; Noeske et al. 2007). Meanwhile, in the top panel we can see another prominent population of galaxies at less negative [12]–[3.4] colours. These galaxies have weak 12μm emission and therefore low star formation rates, and are mostly round, quiescent bulge-dominated galaxies. We can also see in the bottom panel a small number of low star formation rate elongated galaxies, which represent less common edge-on quiescent S0 galaxies.

The population of quiescent galaxies varies with axis ratio due to these galaxies' intrinsic round shapes, but these galaxies are not important for our purposes since they are expected to (and indeed do, see §2.4) have little dust attenuation. Meanwhile, the population of star-forming disc galaxies is almost unchanged between the two bins of inclination, with a difference in median [12]–[3.4] colour of ∼0.1 mag. This is in contrast to optical studies such as Tully et al. (1998), who found a difference in median $B - K$ colour of more than more than 1 mag between their highly inclined and low inclination samples. Therefore, these two parameters allow us to classify galaxies according to their stellar mass and specific star formation in an almost completely inclination independent manner.

These populations of quiescent, rounded galaxies and star-forming, flattened galaxies are illustrated visually in Fig. 2.6, which shows SDSS postage stamp images for representative galaxies throughout our parameter space. As in Fig. 2.5, the upper panel shows galaxies with large axis ratios, while the lower panel shows galaxies with small axis ratios. It is apparent that the region with [12]–[3.4] > 0.5 contains mostly bulge-dominated galaxies in the upper panel, though towards the bottom and right of this area some hints of discy features can

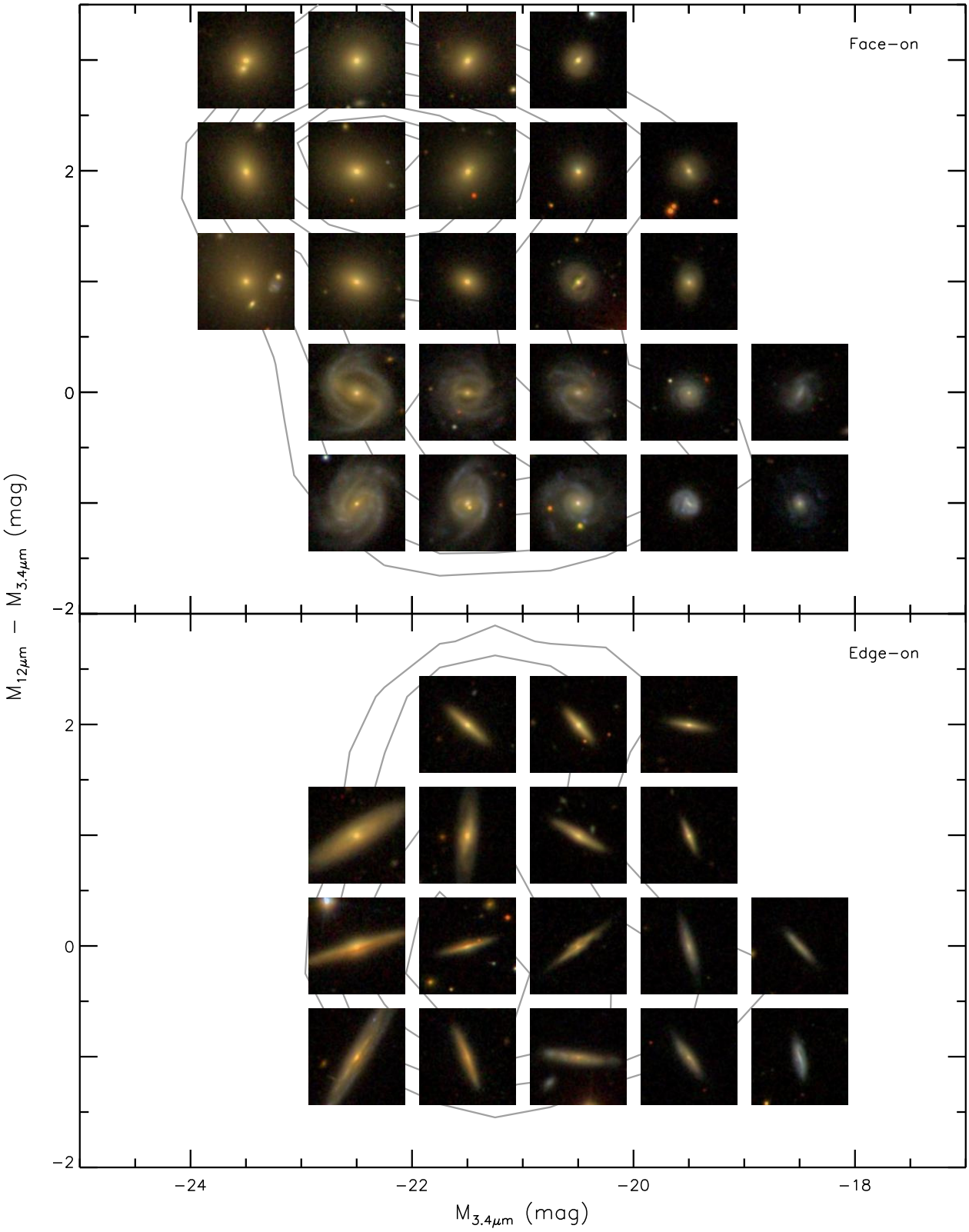

Figure 2.6: Example SDSS postage stamp images for representative face-on (top) and edge-on (bottom) galaxies in our sample, placed according to their positions in our parameter space. All galaxies have $0.0333 < z < 0.05$ for size matching.

be seen. In the lower panel, the upper left-most bins of parameter space are very sparsely populated and so not included, but the remainder of the region [12]–[3.4] > 0.5 appears to contain reddish, mostly featureless discs with unobscured bulges, suggesting S0 or similar galaxies. In both panels, the region [12]–[3.4] < 0.5 is obviously populated by discs. In the upper panel we can see that these discs contain obvious spiral structure, suggesting star-forming galaxies rather than quiescent S0s, and in the lower panel we can see that these discs appear significantly obscured when viewed edge-on (e.g. dust lanes or obscured bulges). Additionally, all of these galaxies were chosen from a restricted redshift range, so the size gradient from large galaxies on the left to small galaxies on the right is real and reflects the luminosity variation among our sample. All of these trends broadly confirm our physical interpretation of the divisions between types of galaxies in different regions of our parameter space.

We further visualize the properties of this selected sample in Fig. 2.7, which shows the distributions of axis ratio and Sérsic index for our sample. We show the distribution of galaxies in the $M_{3.4\mu\mathrm{m}}$ luminosity-[12]–[3.4] plane as background contours. Each overlaid panel shows the distribution of S11 axis ratio b/a (in blue) and S11 Sérsic indexes n (in red) at that location in parameter space (i.e. for subsamples selected to have narrow ranges in $M_{3.4\mu\mathrm{m}}$ luminosity and [12]–[3.4]).

Towards the lower parts of Fig. 2.7 (towards negative [12]–[3.4] corresponding to star-forming galaxies), and on the right hand side even at [12]–[3.4] ≈ 0, our sample has a nearly uniform distribution of b/a – a property of a sample of thin discs viewed from random directions. As outlined previously, this is an important property of our selection procedure: if photometry were inclination-dependent, it would drive galaxies towards preferential axis ratios in given colour bins. Such behavior is not seen for this combination of long-wavelength parameters and selection limits, illustrating that they are close to dust attenuation and inclination-insensitive and are well-suited for selection of samples with which we can study

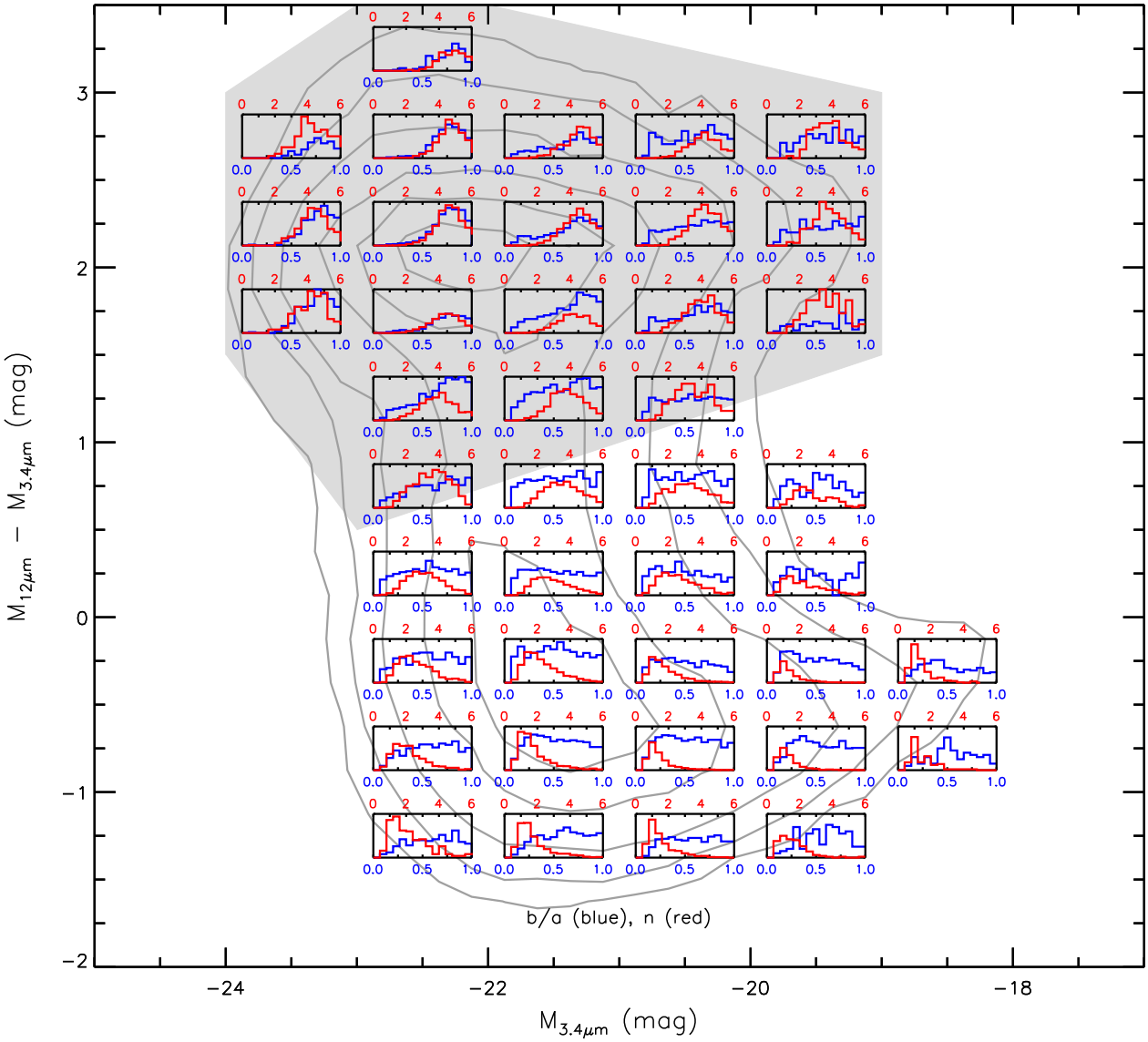

Figure 2.7: Background contours show the distribution of galaxies in $M_{12\mu m} - M_{3.4\mu m}$ vs $M_{3.4\mu m}$ space. The inset panels show the distribution of axis ratios b/a (blue) and Sérsic index n (red) from S11 for galaxies at that location in $M_{12\mu m} - M_{3.4\mu m}$ vs $M_{3.4\mu m}$ space. Grey fill shows approximately the region of parameter space occupied by bulge-dominated galaxies.

the effects of dust attenuation at *shorter* wavelengths.[3]

The upper left part of the distribution in Fig. 2.7, with bright 3.4μm absolute magnitude and [12]–[3.4] ≈ 2 corresponding to luminous quiescent galaxies, shows preferentially larger values of b/a. These galaxies are much rounder than the flattened star-forming population; detailed analysis indicates that these galaxies are likely to be triaxial spheroids (e.g. Tremblay & Merritt 1996, Vincent & Ryden 2005, van der Wel et al. 2009a). These galaxies violate our assumption that axis ratio b/a reflects the inclination of a thin disc. We nonetheless analyze the run of colours with b/a for this sample; if nothing else, it is important to verify that the change in colour with axis ratio is low for this sample of largely dust-free galaxies.

The red histograms show the distribution of Sérsic indices, measured by S11 using single-component Sérsic fits, for these subsamples. This measurement reflects the relative degree of bulge- or disc-dominance of the galaxies in these samples, as extended exponential discs are fit with shallower light profiles (lower Sérsic indices), while more centrally-concentrated bulges are fit with more sharply peaked light profiles (higher Sérsic indices). Consideration of the Sérsic index distributions enriches the picture of the population painted with axis ratios. While the star-forming population ([12]–[3.4] $\lesssim 0$) is indeed disc-dominated overall, showing Sérsic indices in the 1-2 range, at high luminosities bulges are somewhat more prominent than at faint luminosities. Bulges are much more prominent for the quiescent population ([12]–[3.4] $\gtrsim 1$), with most of these galaxies showing Sérsic indices of 3–4 or more; the 3-D shape of these bulges (shown by their axis ratio distribution) is a function of luminosity, mirroring the distinction between fast rotators at low luminosity and slow rotators at high luminosity (Emsellem et al., 2011).

[3]This also can act as a diagnostic of axis ratio parameter – the use of SDSS axis ratios does not give flat b/a distributions regardless of selection.

2.4 Analysis & results

The galaxies which occupy any given location in our $M_{3.4\mu m}$ - [12]–[3.4] parameter space should be close to identical in terms of their stellar populations. As such, they should have equal intrinsic magnitudes M_λ in any optical band λ. The optical luminosity suffers from dust attenuation while the 3.4μm NIR luminosity does not (or, at least, does to a much smaller extent). Since we observe these galaxies at an arbitrary range of viewing angles and this attenuation will be more severe when viewed closer to edge-on, the observed $M_\lambda - M_{3.4\mu m}$ (henceforth noted as [λ]–[3.4]) colour of these galaxies will vary as a function of inclination. If one makes the assumption that the structures of the galaxies in that bin in stellar populations are drawn from a population of flattened discs viewed from random directions (consistent with observed axis ratio distributions, except for luminous non-star forming galaxies; Fig. 2.7), the dependence of [λ]–[3.4] on inclination should correspond directly to a dependence of [λ]–[3.4] on *axis ratio*. It is this dependence which we seek to characterize in this section.

However, the intrinsic (rather than observed) [λ]–[3.4] colour of galaxies also varies as a function of $M_{3.4\mu m}$, both between bins (which does not affect our analysis) and even across an individual bin (which does). Therefore, within each bin we fit the relationship between [λ]–[3.4] colour and $M_{3.4\mu m}$ with a linear relation and remove it. We shear the [λ]–[3.4] - $M_{3.4\mu m}$ distribution around the centre of the $M_{3.4\mu m}$ bin, which removes the $M_{3.4\mu m}$ dependence while preserving the average [λ]–[3.4] colour of the bin (this is not, strictly speaking, necessary, as the normalization of colour is arbitrary in our analysis since we are concerned only with the *variation* of colour with axis ratio, but this facilitates more intuitive comparisons between bins). For each bin, we denote the resulting galaxy colours as [λ]–[3.4]$'$.[4]

As described in §2.3.2, at this stage we impose a redshift cut within each bin to guard against biases due to sample selection limits in apparent magnitude and radius. On average this removes roughly 50–60 per cent of the galaxies in each bin, but while this does result in

[4]This correction is carried out because this is the proper way to conduct this analysis, but its presence (or absence) has only minimal effect on the results (see §2.4.2).

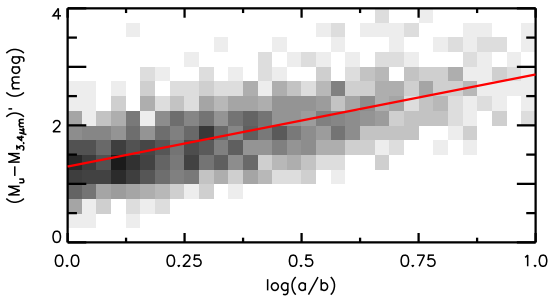

Figure 2.8: Distribution of galaxies as a function of $[u]$-$[3.4]'$ colour and axis ratio for a representative example bin of parameter space located at $-22 \leq M_{3.4\mu\mathrm{m}} \leq -21$ in luminosity and $-1.0 \leq [12] - [3.4] \leq -0.5$. The 2-d histogram shows the galaxy distribution, while the solid line shows the best-fitting linear relation to this distribution. The slope of the line is the attenuation parameter γ for this bin.

somewhat larger statistical errors, as long as the number of galaxies does not drop too low this does not significantly hamper the measurement of the attenuation.

Finally, we quantify the inclination dependence of luminosity in any given bin with the commonly-used parametrization (e.g. Tully et al. 1998, Maller et al. 2009) $A_\lambda = \gamma_\lambda \log(a/b)$, where A_λ is the attenuation relative to face-on in the passband λ, a/b is the ratio of the semi-major to semi-minor axis (inverse of the axial ratio), and γ_λ is the resulting attenuation amplitude parameter in that band. This is done by fitting a linear relationship to the $[\lambda]$–$[3.4]'$ - $\log(a/b)$ distribution of galaxies – the slope of this relationship is the amplitude parameter γ_λ of interest.[5] This procedure is illustrated in Fig. 2.8, which shows the galaxy distribution and fit relationship in SDSS g band for a representative example bin in our parameter space located at $-22 \leq M_{3.4\mu\mathrm{m}} \leq -21$ in luminosity and $-1.0 \leq [12] - [3.4] \leq -0.5$ – this represents star-forming disc galaxies broadly similar to the Milky Way.

The use of a linear fit to parametrize the relationship between A_λ and $\log(a/b)$ has been challenged in the past. For one example, Masters et al. (2010), in studying the variation of NIR colours with axis ratio, suggested that a bilinear or quadratic fit may be more

[5]The total face-on vs. edge-on relative attenuation for a disc galaxy, in mag, is thus $\sim 0.85\gamma$, as the run in $\log(a/b)$ using S11's axis ratios is ~ 0.85 for most disc-dominated bins of parameter space.

appropriate. Indeed, a linear relationship is not required by any physical law, but rather represents the simplest functional form that fits the data to within the scatter. While the true physical form of the relationship may be substantially more complex, the distribution of colours as a function of axis ratio in Figs. 2.8 and 2.9 (see below) show little in the way of systematic deviation from a linear fit that is outside the random or systematic uncertainties. For this reason, we feel comfortable retaining a linear relationship between A_λ and $\log(a/b)$, especially as this enables a far more direct comparison with most previous work.

It is also important to note that this parametrization depends significantly on the range of axis ratios covered by the sample in the chosen set of input measurements. Since γ_λ is the *slope* of the relationship between A_λ and $\log(a/b)$, variations in the axis ratio distribution within a bin between different sets of input axis ratio measurements can alter the resulting slopes even for an identical colour distribution. (We explore this issue further in §2.4.2.) This parametrization is thus in some ways not ideal, but for now we retain it in the interest of comparison with previous work. We may revisit this issue in the future.

We apply this method in bins of $M_{3.4\mu\mathrm{m}}$ luminosity and [12]–[3.4] colour throughout our parameter space. Each bin is 1 magnitude wide in luminosity and 0.5 magnitudes wide in colour, and our parameter space contains sufficient galaxies to populate bins in the area $-24 \leq M_{3.4\mu\mathrm{m}} \leq -18$ in luminosity and $-1.5 \leq [12] - [3.4] \leq 3.5$. (Galaxies can, of course, be found outside these limits, but not in sufficient numbers for reliable analysis.) A schematic outline of our analysis across this parameter space can be found in Fig. 2.9.

Fig. 2.9 shows both the overall distribution of galaxies within the parameter space (background contours), and the $[u]$–$[3.4]'$ vs. $\log(a/b)$ distributions and attenuation fits for the galaxies in each bin (inset panels). The variation in attenuation across our parameter space can be seen in the varying slopes of the attenuation fits in each bin. For each inset panel of Fig. 2.9, the y-intercept of the fit represents the face-on $[u]$–[3.4] colour of the galaxies in that bin. It can be seen that this colour varies with $M_{3.4\mu\mathrm{m}}$ luminosity, becoming redder for brighter galaxies. This has been studied a number of times in the past (e.g., de Jong

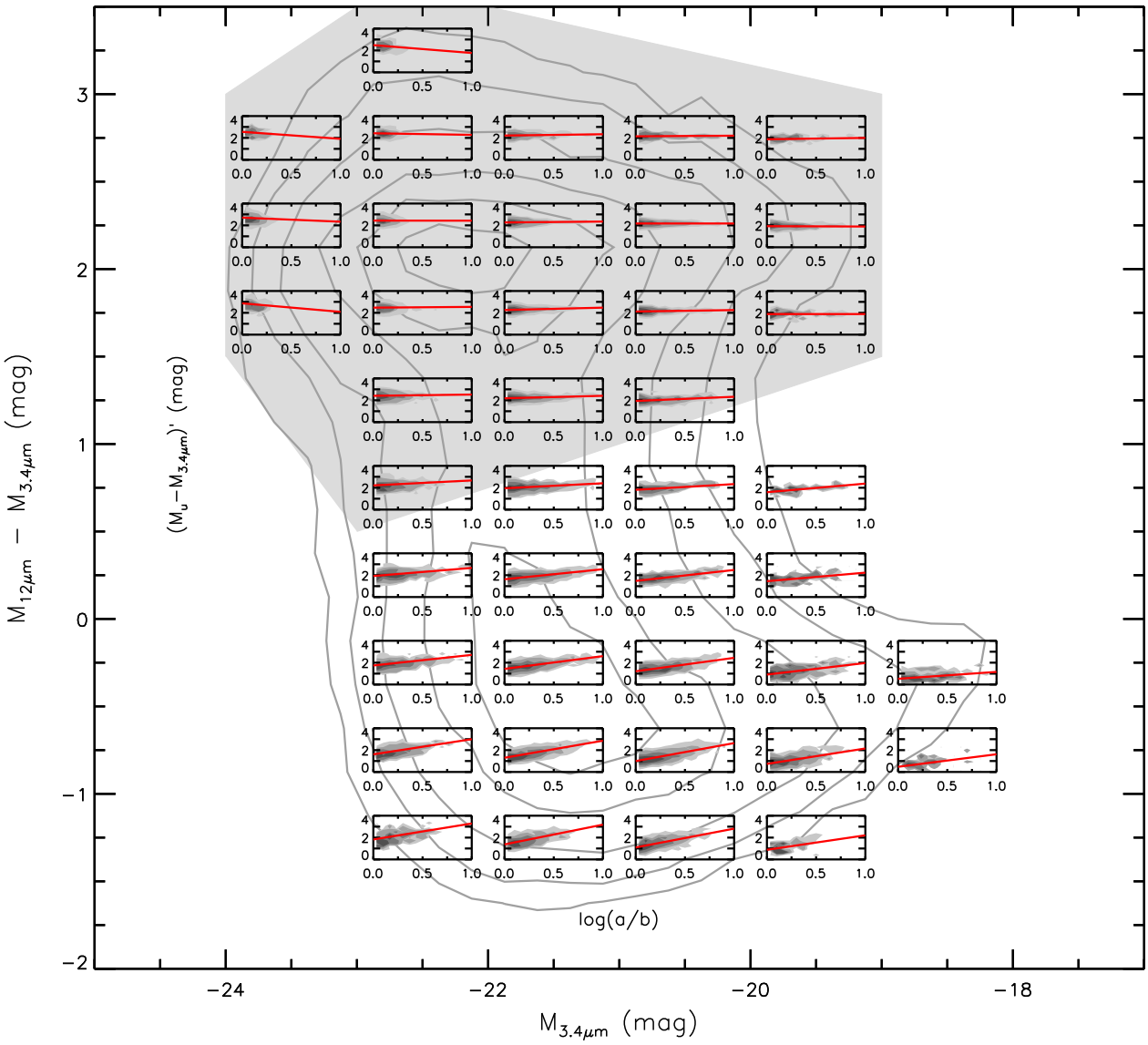

Figure 2.9: Background contours show the distribution of galaxies in [12]–[3.4] vs $M_{3.4\mu\mathrm{m}}$ space. The inset panels show the distribution of $[u]$–$[3.4]'$ colour vs $\log(a/b)$, and the best-fitting line thereof, for galaxies at that location in [12]–[3.4] vs $M_{3.4\mu\mathrm{m}}$ space. The slope of the best-fitting line represents the amplitude of the attenuation at that point in the parameter space. Grey fill shows approximately the region of parameter space occupied by bulge-dominated galaxies.

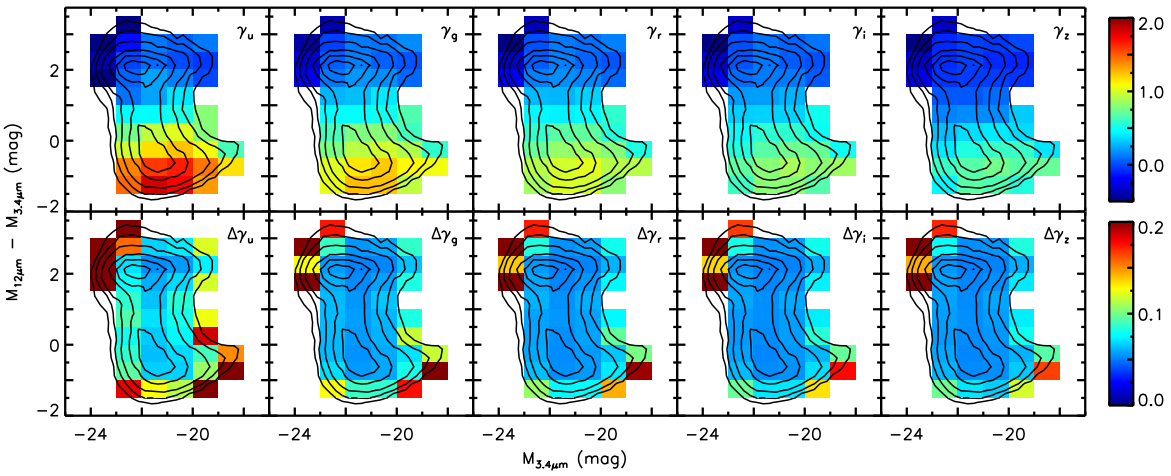

Figure 2.10: Top row: Dust attenuation amplitude parameter γ as a function of $M_{3.4\mu\mathrm{m}}$ luminosity and [12]–[3.4] colour throughout our parameter space, for the 5 SDSS bands u, g, r, i, z. As in Fig. 2.3, contours show the distribution of galaxies within this parameter space. Colours show the value of the attenuation parameter γ for galaxies within each bin, and the colour scale is the same for all bands. Bottom row: Same as top row, except colours show the uncertainties in the attenuation parameter γ.

1996b, Bell & de Jong 2001), and this variation reflects a combination of variations in star formation history, metallicity, and dust content with luminosity.

2.4.1 Attenuation as a function of wavelength and galaxy parameters

Our results for all 5 SDSS bands *u, g, r, i, z* are presented graphically in Fig. 2.10 and numerically in appendix A in Tables A.1–A.5. The colour coding represents the size of the attenuation amplitude parameter γ_λ, with blue colours representing low values (little or no dependence of $[\lambda]$–$[3.4]'$ colour on axis ratio, and so little or no dust attenuation) and red colours representing high values (strong dependence of $[\lambda]$–$[3.4]'$ colour on axis ratio, and so large amounts of dust attenuation). The colour scale is identical throughout, allowing comparison between the bands.

First, and most obviously, the attenuation is stronger in the shorter wavebands. While the amplitude of the attenuation varies with band as expected, the patterns with galaxy

properties within each band are extremely similar. The effects discussed below are easiest to see in the u band in Fig. 2.10 since this band has the strongest attenuation, but these effects apply with very little modification to the other bands as well.

Second, there is a very obvious gradient in attenuation strength with [12]–[3.4] colour. Near the top of the diagram we find quiescent, bulgy galaxies. For many of the most luminous or least negative [12]–[3.4] colour bins, their axis ratio distributions are so narrow (Fig. 2.7) that our method does not produce meaningful results, as these are obviously not discs but rather spheroids and any variation in axis ratio is intrinsic rather than due to random inclination. Therefore, the near-zero (or even negative) values of γ_λ for these bins are not physically meaningful. However, many of the less luminous and/or more negative [12]–[3.4] colour bins in this area have sufficiently broad axis ratio distributions to indicate the presence of flattened discs seen from a variety of viewing angles, and for these we can see that they are consistent with little or no dust attenuation, consistent with our interpretation of these systems as quiescent, with little in the way of cold gas or dust content.

However, as one moves to more negative [12]–[3.4] colours, the attenuation increases strongly towards the star-forming main sequence. This area is populated by star-forming disc-dominated galaxies which have notable dust attenuation. Within this region, there are two major parameters that correlate with attenuation – luminosity and star formation activity.

First, attenuation varies as you move along the star-forming main sequence from faint to bright at a given [12]–[3.4] colour. The dimmest galaxies have the least attenuation, and attenuation increases as you move towards brighter galaxies, similar to the results of previous studies. However, in our case we find that attenuation reaches a maximum for galaxies of intermediate luminosity, and begins to decrease again for the most luminous galaxies. This (seemingly) contradicts many studies which have found a monotonically increasing dependence of attenuation on luminosity (e.g. Tully et al. 1998, Maller et al. 2009). However, these studies generally have not probed to high enough luminosities to match our analysis –

for example, Tully et al. are limited to roughly $K \geq -23.25$ and Maller et al. consider only galaxies with $K \geq -22.75$ (corresponding to $M_{3.4\mu\mathrm{m}} \approx -22.0$ and -21.5), neither of which pass the turnover region we find by enough of a margin to discover this effect (see discussion in §2.5).

Second, as one crosses the star-forming main sequence vertically from the least to the most star-forming galaxies at a given luminosity the attenuation increases, reaching a maximum for the galaxies with the most negative [12]–[3.4] colours at the very bottom edge of the star-forming main sequence. In other words, not only does [12]–[3.4] colour divide star-forming dusty galaxies from quiescent non-dusty ones, but within the star-forming dusty galaxies the dust attenuation is a strong function of specific star formation. Notably, the variation of attenuation with specific star formation rate is comparable in magnitude to, or even stronger than, the variation of attenuation with luminosity.

Finally, in addition to the obvious variations with $M_{3.4\mu\mathrm{m}}$ luminosity and [12]–[3.4] color within a given band and the variations in overall attenuation between bands, there are hints that the location of strongest attenuation shifts slightly fainter along the star-forming main sequence in the longer wavebands. It is difficult to see in Fig. 2.10, but perusal of the numerical data in Tables A.1–A.5 shows that the strongest attenuation in the r, i, and z bands is located at $M_{3.4\mu\mathrm{m}} \approx -20.5$ rather than -21.5, though the differences are slight (especially in the r band, where they are essentially negligible).

2.4.2 Statistical & systematic uncertainties and the effects of varying input measurements

Errors for the attenuation parameters are presented graphically in Fig. 2.10 and numerically in appendix A in Tables A.1–A.5. Statistical errors are calculated by bootstrap resampling, and are generally of order ∼0.04–0.06 in slope, though they increase near the edges of the populated regions of our parameter space where there are fewer galaxies per bin. They vary somewhat with wavelength, being slightly greater in the shorter wavelength u and

g bands and slightly smaller in the longer wavelength r, i, and z bands, but the difference is small.

Systematic errors are somewhat more difficult to quantify. One potential source of error is the various methodological choices we have made in our analysis. In an attempt to quantify this source of error, we have repeated our analysis while varying or omitting some of these refinements. We have experimented with the effects of omitting the K-corrections, omitting the redshift cut within each bin, increasing or decreasing the threshold for the redshift cut, varying the choice of linear fit algorithm, and omitting the shear correction for the $M_{3.4\mu\mathrm{m}}$ – [λ]–[3.4] correlation in each bin. Generally we find that these give variations of approximately the same order as (or slightly smaller than) most of the existing statistical errors, ~0.03–0.05 in slope, and do not depend strongly on location in the parameter space. They vary slightly with wavelength in the same manner as the statistical errors, but again the difference is not large. Therefore, these are conservatively quantified by taking the statistical errors and adding in quadrature an extra slope uncertainty of 0.05, resulting in the final errors.

In addition to the statistical and systematic errors, it is also interesting to study the effects of the choice of input measurements used, namely magnitudes and axis ratios. As might be expected, varying these choices significantly alters the measured attenuation parameters. Notably, the alterations due to varying the input measurements are generally significantly larger than those due to the variations in analysis methods mentioned above, and also often show variations with wavelength and across our parameter space.

As discussed in previous sections, we believe that our choices of the SDSS cmodelmags for optical magnitudes, the *WISE* gmags for IR magnitudes, and the S11 axis ratio measurements represent the best available measurements. Therefore, we do not consider the differences presented here to represent any additional error in our work. Rather, we examine the ways in which varying the input data could alter the results in order to help illuminate why we made the choices we have and show the potential consequences of using possibly biased inputs. These effects are illustrated in Fig. 2.11.

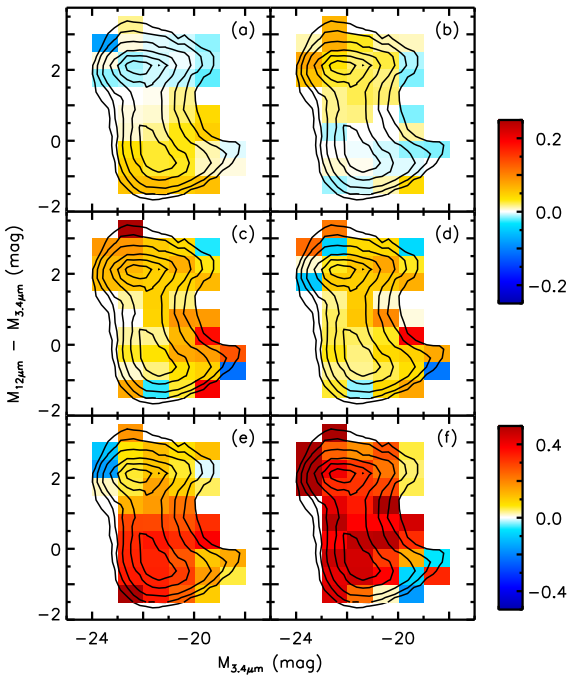

Figure 2.11: Example g-band attenuation measurement differences due to differing choices of input parameters, as a function of $M_{3.4\mu\mathrm{m}}$ luminosity and [12]–[3.4] colour. The colour scale shows the difference between the attenuation measured within a bin using a particular alternate input parameter and that measured using the canonical set of parameters. Background contours show the distribution of galaxies in this parameter space. By panel, the alternate input parameters used are: panel a: SDSS model magnitudes, panel b: SDSS Petrosian magnitudes, panel c: *WISE* profile magnitudes, panel d: *WISE* aperture magnitudes, panel e: SDSS axis ratios, panel f: 2MASS axis ratios. Note that the colour scale in the last two panels covers twice the range as the others.

For optical magnitudes, our other options besides the SDSS cmodelmags were the standard modelmags and the Petrosian magnitudes. Using either of these alternate magnitude measurements significantly alters the measured attenuation values in ways that depend both on location within the parameter space and on passband.

When using the standard modelmags, the most notable deviation within the parameter space is the variation along the star-forming main sequence, with the brightest star-forming galaxies consistently showing an increase in measured attenuation of ~0.05 in slope relative to the dimmer star-forming galaxies. That is, the use of standard modelmags preferentially boosts the measured attenuation of the brightest star-forming galaxies compared to the results derived with the cmodelmags. In addition to this effect, the overall attenuation of the entire star-forming main sequence relative to that derived from the cmodelmags is enhanced for u and g bands and decreased for i and z bands – in other words, the attenuation curve is steeper when measured using the standard model mags. This effect increases the average attenuation parameter difference between the u and z bands by roughly ~0.2. While the exact cause of the size and patterns of variation of these differences is not necessarily apparent without a more detailed analysis, it is notable that since the standard modelmag method fits galaxies with only *either* an exponential or a de Vaucouleurs profile, the bright star-forming galaxies that it assigns higher attenuations to (which contain both strong bulge and disc components) are exactly the ones that the modelmags might be most expected to have trouble with.

Unlike the modelmags, using the Petrosian magnitudes does not cause an increase in variation between different parts of the star-forming main sequence. Rather, the use of the Petrosian magnitudes mostly acts to weaken the divide between the star-forming and quiescent galaxies by increasing the attenuation slope parameters measured for the non-star forming galaxies near the top of our parameter space. This increase is roughly of order ~0.1 in slope, and varies non-monotonically with magnitude with the u and z bands – the bands with the poorest S/N for petrosian magnitudes – being slightly more strongly affected. The

star-forming main sequence, on the other hand, while not showing any particular increase in variation within any given band, does again show a steepened attenuation curve, with the measured attenuation decreasing slightly in the r band and more significantly in the i and z bands. This results in an increase of roughly ~0.05 in the average attenuation difference between the u and z bands, significantly smaller than the similar increase due to the use of the modelmags. Like the variations due to using the modelmags, the exact causes of the details of these variations is not especially apparent without a more detailed analysis, but again, it is notable that the quiescent galaxies (i.e. galaxies with de Vaucouleurs light profiles) which are strongly affected are ones that the Petrosian magnitude measurement method is known to have difficulty measuring.

The other major choice of photometric input measurements we made was to use the 2MASS-derived *WISE* gmags for our NIR photometry, rather than the standard aperture or profile-fit measurements. As noted in §2.2.1.1 these alternatives are not well-suited to measuring extended sources such as our galaxies, and, as with the alternate SDSS photometric measurements, using them results in significant alterations in measured attenuation.

The use of either the standard aperture or profile-fit photometry results in roughly similar variations in measured attenuation. In both cases, measured attenuation increases for quiescent galaxies by roughly ~0.05, in a band-independent manner. For star-forming galaxies, the peak of highest attenuation becomes notably broader (which has the effect of also increasing measured attenuation for most star-forming galaxies by ~0.05) and shifts roughly 1 mag fainter along the star-forming main sequence. Finally, once more the attenuation curve for star-forming galaxies is affected, in both cases becoming shallower by roughly ~0.07 in the average attenuation difference between u and z bands.

Finally, and in many ways most critically, we also chose to use S11's axis ratio measurements instead of those from the SDSS or 2MASS. Axis ratio is the choice of input measurement with by far the largest potential effect on output attenuation measurements. As noted previously, this is largely due to the mechanics of this analysis method, since at-

tenuation is expressed as the slope of the colour-axis ratio relationship. This is a notable drawback of this particular choice of parametrization, since it can create or exaggerate differences between studies even when the analysis techniques and other galaxy properties are similar or identical. One could in principle correct for this by scaling to the range of axial ratios present in the sample, but this has not been commonly done in past studies. Therefore, since the variation in axis ratio measurements between different data sets can be quite large, and moreover is often strongly correlated with galaxy properties, the choice of axis ratio measurement is critical.

Illustrating this, using SDSS axis ratios rather than those of S11 results in significantly increased attenuation measurements. This increase is quite large – up to 0.5 in slope in the u band – and is by far the strongest among the brighter galaxies along the star-forming main sequence. As with the modelmags, this is likely due to the presence of significant bulge components in these galaxies. These result in much rounder measured axis ratios than would otherwise be expected for populations of randomly-inclined disc galaxies, narrowing the axis ratio distributions within each bin and therefore steepening the slopes of the colour-axis ratio relationships in those bins. Notably, this effect is strongest for the brightest disc galaxies, and is great enough that when using these axis ratios the measured attenuation is also strongest for these brightest galaxies, rather than peaking at intermediate luminosities as we observe.

Similarly, using 2MASS axis ratios also results in significantly increased attenuation measurements. This increase is even greater than for the SDSS measurements, reaching more than 0.7 in slope in the u band. This effect tends to be slightly larger for the most luminous galaxies, likely reflecting the same influence of bulges as in the SDSS, but overall is much more widespread. This is likely due to the lower resolution of 2MASS data, which (as noted in §2.2.2) results in unreliable shape measurements for the smaller galaxies which comprise most of our sample. For these small galaxies, seeing effects will tend to result in rounder measured axis ratios regardless of the presence (or absence) of a bulge, further

increasing measured attenuations across the board.

These strong effects emphasize the importance of very careful measurements of axis ratios, sharply highlight the limitations of low resolution, purely isophotal, or single-model measurements. We believe that S11's axis ratio measurements are the best currently available by a significant margin, but further developments in this area would be welcome, especially in longer-wavelength measurements. These effects also illustrate the limitations of this method of parametrizing attenuation, and we may attempt to mitigate this issue in future work.

2.5 Comparisons to previous work

Fig. 2.10 illustrates that attenuation is more significant at shorter passbands than longer ones, shows a strong dependence on our observational proxy for star formation activity ([12]–[3.4]) in that more intensely star forming disc galaxies are more attenuated than their less star forming counterparts, and shows a complex dependence on luminosity, in that attenuation is smaller for both less luminous and more luminous galaxies than the Milky Way (at $M_{3.4\mu\mathrm{m}} \approx -21.5$). The goal of this section is to compare our results to two immediately comparable works – Tully et al. (1998) (hereafter T98) and Maller et al. (2009) (hereafter M09).

Our work, T98's, and M09's use similar methods, in that all works assume that at sufficiently long wavelength galaxy luminosity is effectively independent of inclination. After removing the overall trend in optical–NIR colour vs. NIR luminosity, any remaining trends in $M_\lambda - K$ colour with inclination are interpreted as dust-induced attenuation, and are presented as the slope of the relation between optical–IR colour and the logarithm of axial ratio. Yet, the three works have significant differences that impede straightforward comparison of attenuation relation slopes: the works are based on different data, parametrize attenuation differently, and use different axial ratio measurements. Given that the intention of each of these works is to provide an inclination correction that can return galaxy magnitudes to their face-on values, the final inclination corrections themselves are a reasonable point of

comparison.

As such, to compare our work with that of T98 and M09, we calculate three different inclination corrections for each galaxy in our sample based on the parametrization and results of each work. For our work, we calculate an inclination correction using our SDSS g-band attenuation relation slope at the galaxy's given S11 axial ratio, $M_{3.4\mu\mathrm{m}}$ absolute magnitude and [12]–[3.4] colour. For M09, the SDSS g-band attenuation relation slope is derived according to the results in their Table 2, parametrized in terms of absolute K magnitude (from 2MASS) and concentration (from SDSS), and the inclination correction is calculated using that slope and SDSS model fit axial ratios. For T98, the attenuation relation slope is parametrized in terms of B-band absolute magnitude, which we derive from our SDSS magnitudes using PÉGASE (Fioc & Rocca-Volmerange, 1997) stellar population synthesis models. The inclination correction in B band is then calculated using that slope and S11's axial ratios, and translated back into SDSS g band using the attenuation curve of Calzetti et al. (2000). This yields a predicted inclination correction in SDSS g band for each galaxy using each of the three works' methods.

In Fig. 2.12, we compare the predicted inclination correction for our work with those of T98 and M09, in this case as a function of K-band absolute magnitude. Since T98 and M09 attempted to select disc-only samples, we restrict this comparison to include only galaxies which lie along the star-forming main sequence as defined by our $M_{3.4\mu\mathrm{m}}$ and [12]–[3.4] selection. In each case, the presented inclination correction is the average correction for the 20% most inclined members of the population at that magnitude, and the error bars are the scatter among that group.

We can see that at lower luminosities, all three methods predict a similar pattern of increasing inclination corrections with luminosity. M09's predictions match ours very closely, while T98 predicts stronger attenuation by up to 0.2 mag (the reasons for this discrepancy will be discussed below). At higher luminosities, however, both T98 and M09 predict much stronger attenuation, as their predicted corrections do not significantly decrease as ours do.

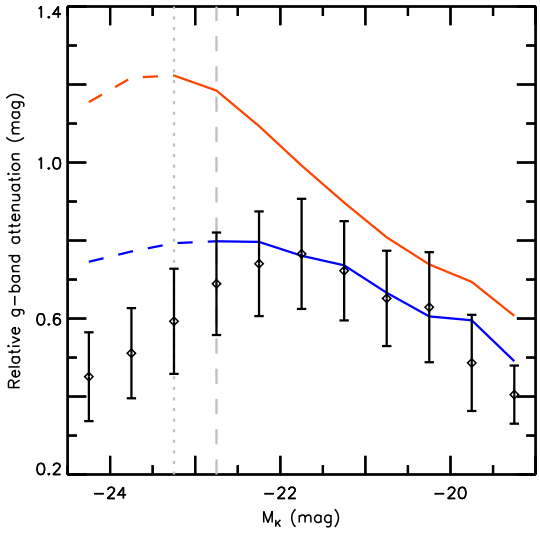

Figure 2.12: Predicted edge-on relative g-band attenuation of main sequence star-forming disc galaxies as a function of K-band luminosity. Black data points are our work, while red and blue lines are predictions based on the results of T98 and M09 respectively. The vertical dotted and dashed lines represents the approximate magnitude limits of the data used in those two works, and the switch to dashed lines beyond these limits shows that those attenuation estimates are extrapolations.

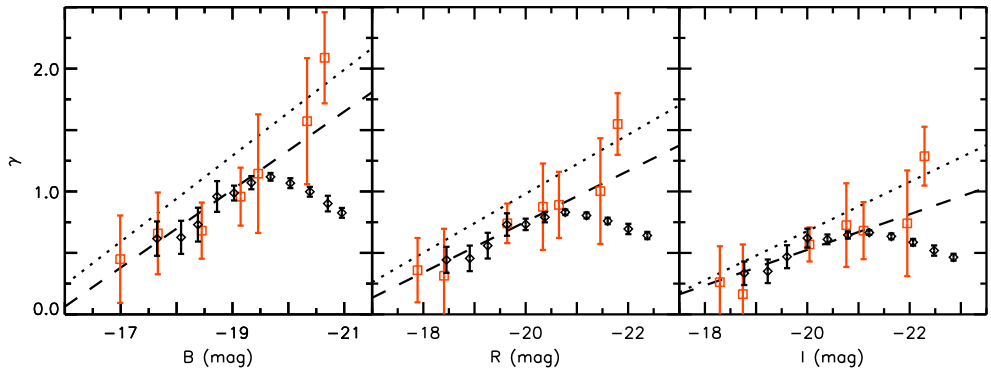

Figure 2.13: The strength of the attenuation parameter γ as a function of absolute B, R and I magnitudes. Diamonds are the values for star-forming galaxies from our sample, while red squares are data from T98. Dotted lines are T98's joint fits to their and Giovanelli et al. (1995)'s data, while dashed lines are fits to T98's data alone (neglecting the highest luminosity data point).

Both the overall discrepancy with T98 and the dramatic differences between our work and those of T98 and M09 at high luminosities appear concerning, and we investigate (and largely resolve) them below.

2.5.1 Comparison with Tully et al.

T98 measured inclination dependence in optical–NIR colours as a function of absolute magnitudes in BRI using a very similar methodology to ours. Their sample is much more limited, containing only 100 galaxies spread between two clusters, but both are relatively nearby and the quality of the data is generally good. Given the similarity of our methods, the offsets in inferred attenuation in Fig. 2.12 seem surprising.

In order to investigate this further, we choose to repeat the analysis of T98 using our joint *WISE*-2MASS-SDSS dataset. We convert the SDSS *ugriz* absolute magnitudes into *BRI* using the PÉGASE stellar population synthesis models and convert our attenuations into *BRI* using the attenuation curves of Calzetti et al. (2000), and bin the sample in K-band luminosity only rather than in both luminosity and [12]–[3.4] colour.

The results are shown in Fig. 2.13. The diamonds show our estimates of the slope of the

attenuation relation γ as a function of luminosity in different bins of absolute B (left panel), R (middle panel), or I (right panel) magnitude. Meanwhile, the squares are T98's estimates, and the dotted lines are the fits that T98 adopt for their final attenuation prescriptions (that is, T98's equations 3, 4, and 5). The dashed lines will be explained shortly.

As can be seen, our data are broadly consistent with T98's at low and intermediate luminosities, but depart from T98's results at the high end. Their highest luminosity data point, in particular, is very inconsistent with our data. Additionally, the final fits that T98 adopt are well above our (and their!) results. However, the agreement of their actual data points with ours at lower luminosities is very good. Accordingly, there are two issues to understand: the discrepancy between the presented fits (dotted lines) and the data (both ours and theirs), and the strong attenuation of their highest luminosity subsample.

T98's fits are a joint fit to both their data and data taken from Giovanelli et al. (1995), and it is the influence of both that data and T98's highest luminosity data point that combine to pull their final fits well above our results. It is apparent from a visual inspection of T98's data and fits in Fig. 2.13 that their overall fits are inconsistent with their lower luminosity data points. Indeed, fits simply to T98's data alone, discarding the highest luminosity data point (represented by the dashed lines in Fig. 2.13), match our results much more closely.

Fig. 2.14 shows why we believe that the highest luminosity data point is erroneous (this figure is an analogue of T98's figure 2). Each panel shows, for one bin in K luminosity, the $B-K$ colour residuals (after the removal of the overall trend in $B-K$ colour with K) as a function of axis ratio. The leftmost panel shows this relation for galaxies on the star-forming main sequence with $M_K < -21.65$, matching T98's highest luminosity bin. The 2-d histogram shows the distribution of galaxies from our sample, while the red circles are the galaxies from T98's sample. As can be seen, in this luminosity bin T98's sample has a very skewed distribution of axis ratios and contains *only one* galaxy more face-on than $b/a = 0.6$. Additionally, that one galaxy can be seen to lie (somewhat unfortunately) significantly below the average for its inclination. This causes T98's fit for γ in this bin (orange line) to be highly

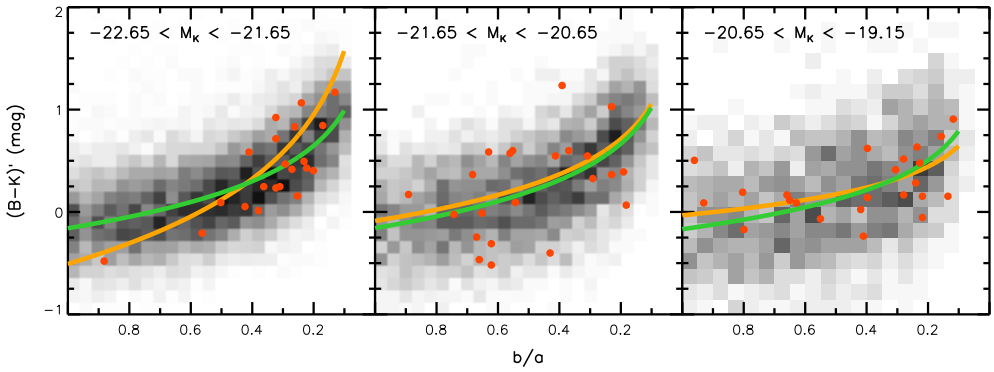

Figure 2.14: Galaxy $B-K$ colour residuals as a function of axis ratio for star-forming galaxies from our sample, divided into bins of K-band luminosity. Green lines are the best-fit relation between $\log(a/b)$ and colour for our sample. Orange lines and red circles are T98's fits and data, respectively.

inconsistent with the overall galaxy population, suggesting a far higher attenuation than is actually implied by our more comprehensive sample (green line).

Visually T98's relation may seem to be a better fit to the highly inclined end of the sample. However, we find no improvement in the quality of the fit by adopting a steeper slope at the high end, even if low inclination galaxies are excluded. This visual impression is caused by the fact that the distribution of $B-K$ colour for highly inclined galaxies is significantly non-gaussian. This non-gaussian distribution is in part explained by the [12]–[3.4] dependence in the attenuation explored in Fig. 2.10; the dependence of attenuation on morphological and structural parameters (e.g., bulge prominence) that we explore in chapter 4 also likely contributes to this.

The centre and right panels of Fig. 2.14 expand this comparison to include the luminosity bins $-21.65 < M_K < -20.65$ and $-20.65 < M_K < -19.15$, matching T98's next two bins. (T98's lowest luminosity bin, $-19.15 < M_K$, is very sparsely populated and shows almost no dependence of colour on axis ratio, so we do not include it.) In these cases there are no large skews in the axis ratio distributions, so our fits are much closer to T98's, and indeed the slopes match quite well.

To conclude, the discrepancy between our and T98's fit results is somewhat illusory – our data are consistent with their data (Fig. 2.14). The differences in our fit results are driven by two factors: T98 lacks a representative sample of face on luminous galaxies, driving their attenuation estimates to artificially high values, and that T98 (by hand) modifies their attenuation results to more closely mirror the results of Giovanelli et al. (1995), degrading the match between their 'fit' results and their (and our) data. We conclude that our results are both consistent with T98's data, and, owing to the larger and more representative sampling from SDSS/2MASS/*WISE*, are a more faithful representation of the actual trends in attenuation with galaxy properties than T98's analysis could probe.

2.5.2 Comparison with Maller et al.

In Fig. 2.12 it was shown that when both our methods and M09's are parametrized solely in terms of K-band magnitude, our results agree for galaxies less luminous than the upper limit of M09's sample, but disagree for brighter galaxies. In this section, we repeat M09's analysis to explore the origin of this seeming discrepancy.

M09 begin with a sample drawn from the NYU-VAGC, an optical catalog based on the SDSS which fits each galaxy with a Sérsic light profile to measure its Sérsic index n_s, half-light radius r_{50}, and axis ratio b/a. This sample is cross-matched with 2MASS for NIR magnitudes, and subjected to r-band absolute magnitude limits and a minimum r_{50} size limit. They then use a combination of cuts on Sérsic index and axis ratio ($n_S \leq 3.0$ or $b/a \leq 0.55$) to isolate disc galaxies. It is important to note that the NYU-VAGC sample is volume limited, and that this dramatically limits the number (and weight in the fits) of galaxies more luminous than $M_K < -22.75$.

We note that the use of optical half-light radii and Sérsic indices is potentially troublesome – both are likely to be affected by dust attenuation (Pastrav et al., 2013a), and may lead to biased fit results. We choose to simply mirror their fitting methodology for the present moment, deferring a full discussion of the effects of attenuation on galaxy structures for later;

a brief analysis on this topic is presented in chapter 5, which we will expand in future work.

M09 parametrize their results in terms of not only absolute K-band magnitude but also in terms of Sérsic index, and they fit the attenuation by a function of the form $\gamma = \alpha_0 + \alpha_K(M_K + 20) + \alpha_n n_s$ – in other words, a plane in the M_K-n_s parameter space. This parametrization is the only major mechanical difference between M09's analysis and ours, since we do not assume a functional form for the variation of attenuation across our parameter space.

A comparison between our methodology and M09's can be seen in Fig. 2.15. In the left panel, we redo our analysis in exactly the same way as in §2.4, but following M09's parametrization and input measurements rather than our own. (Namely, parametrizing the attenuation in terms of absolute K magnitude and r-band Sérsic index rather than $M_{3.4\mu\mathrm{m}}$ luminosity and [12]–[3.4] colour, using non-K-corrected[6] SDSS modelmags rather than K-corrected SDSS cmodelmags, and using SDSS r-band axis ratios rather than those of S11.) The centre panel shows the predicted strength of attenuation across the same parameter space derived from M09's fit, and the rightmost panel shows the difference between the two.

Overall, both our data and the results produced from it by our method are in substantial agreement with M09 for fainter and intermediate-luminosity galaxies with $M_K > -22.75$. The disagreement seen in Fig. 2.12 for brighter galaxies is a discrepancy with M09's extrapolation; we argue that their choice of a parameteric plane fit in the M_K-n_s plane is not well-motivated by the data, and leads to unfortunate behaviour towards the edges of parameter space, particularly when extrapolated beyond their magnitude limit. We do note that we consider the use of r-band Sérsic index as a controlling parameter for M09's analysis to be a concern and a potential bias, leading us to instead frame our sample selection in terms of attenuation-insensitive near- and mid-IR luminosities (Fig. 2.10).

[6]It is unclear whether or not M09 K-corrected their data. As they do not mention K-corrections at all in their work, we must assume they did not, but regardless this does not significantly affect the results.

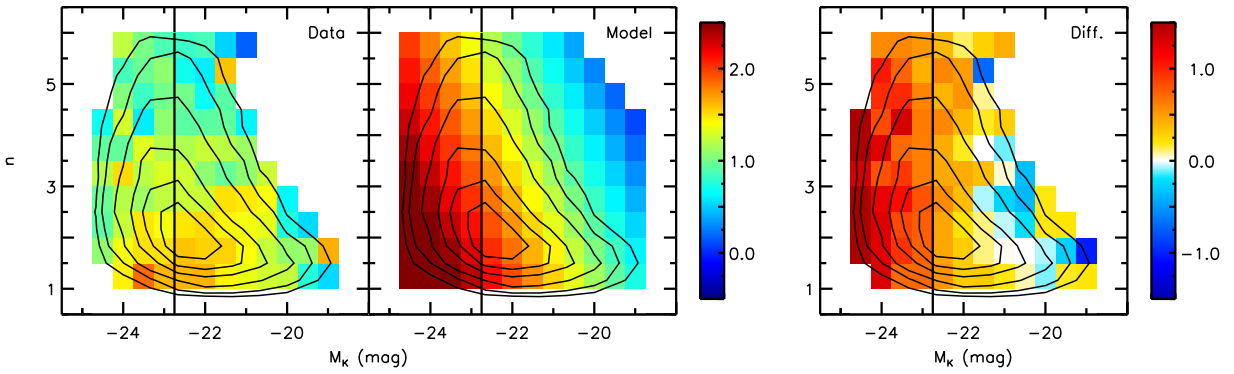

Figure 2.15: Dust attenuation amplitude parameter γ as a function of K-band luminosity and Sérsic index, in the g band. Contours show the distribution of galaxies within this parameter space. The dark vertical line shows the magnitude limit of M09's sample. Left panel: measured attenuation parameter using our method. Centre panel: predicted attenuation parameter using the results of M09. Note that, due to the magnitude limit of their sample, all values to the left of the dark vertical line represent an extrapolation. Right panel: Difference of our measured results (left panel) and M09's predicted results (centre panel).

2.6 Discussion

2.6.1 Qualitative comparison with previous works

In addition to the detailed comparisons presented in the previous section, it is instructive to compare our results in a briefer, qualitative sense with the conclusions of a few other works in this area. There have been a wide variety of approaches taken to the study of dust attenuation involving different methods and parametrizations, not all of which are as directly analogous to our own work as those of T98 or M09 but which are still worth mentioning.

Wild et al. (2011) study dust attenuation by comparing the SEDs of pairs of galaxies matched in the observed properties of metallicity, specific star formation, axis ratio, and redshift. Their analysis is significantly different than ours, with axis ratio as an explicit parameter rather than our method, and their results are presented almost exclusively in terms of the shapes of attenuation curves, rendering a direct comparison difficult. Nevertheless, it

is notable that they find the ratio of continuum to line opacity (representing the strength of the attenuation due to dust in the diffuse ISM) to vary strongly with specific star formation, in accord with our results. They do not directly include galaxy luminosity as a parameter, however they do parametrize on surface brightness, finding that higher surface brightness galaxies have stronger attenuation, but that the variation with surface brightness is not as strong as that with specific star formation.

Driver et al. (2007) derive dust/inclination corrections for disc galaxies in the Millennium Galaxy Catalog by matching the galaxy luminosity function at differing inclinations. Their iterative method relies on the fact that the turnover of the luminosity function should occur at the same magnitude regardless of inclination, and uses this to derive general inclination corrections independently for both the disc and bulge components. This method avoids the need to select identical subsamples as we do, but is limited to providing only a single general correction for the entire galaxy population rather than being able to quantify variation in attenuation among that population. They conclude that the average relative attenuation in the B band from face-on to edge-on is approximately 0.9 mag for discs and 1.8 mag for bulges. Comparatively, the nearest equivalent band in our work is SDSS g, where we observe a maximum total relative attenuation of approximately 1.0 mag. Their disc attenuations are in general agreement with our results, noting that these are relatively disc-dominated galaxies. However, since these are disc-dominated galaxies it is unclear how their bulge attenuations relate to our results, as the relative contribution of bulge attenuation to the total attenuation will depend on factors such as the distribution of B/T ratios and the geometry of bulges relative to discs.

Masters et al. (2010) studied dust attenuation in the SDSS in a very similar manner to our work, parametrizing attenuation in the same way and binning according to galaxy properties to measure the variation in attenuation. In their case, their longer wavelength comparison colour is SDSS z, rather than our 3.4μm, and the physical properties they use to parametrize the variation in attenuation are r-band luminosity and more 'bulgy' or 'discy'

morphology as measured by the r-band SDSS f_{DeV} parameter. Though their methodology is different from that of M09, they also find that less bulge-dominated galaxies have stronger attenuation, though the strength of this variation is somewhat weaker than the variation with luminosity. Given that we find the variation with luminosity to be weaker than that with specific star formation, this would argue that the variation with morphology should also be weaker than that with specific star formation; it will be interesting to see whether this is borne out by our future studies. It is also notable that, unlike older works, they also show a peak in attenuation at intermediate luminosities, in broad agreement with our work.

Cho & Park (2009) also study dust attenuation using very similar methodology to our work, again parametrizing attenuation similarly and binning according to galaxy properties. Relative to our work, they use 2MASS K band as their longer wavelength comparison, and parametrize the attenuation by dividing their galaxies according to their K-band luminosity and SDSS i-band concentration index. They conclude that attenuation is strongest for moderate concentrations and weaker for both the most and least concentrated galaxies, and as with other studies that attenuation is strongest for the most luminous galaxies. However, it is notable that the relationship between attenuation and luminosity noticeably flattens for the most luminous galaxies in their sample, which would be expected in light of our results that attenuation should decrease again for the very brightest galaxies. Another notable aspect is their experimentation with $u - r$ colour (with an attempted correction to the intrinsic, face-on values) as an additional parametrization for dust attenuation. Intrinsic optical colour is related to star formation activity, so based on our work one might expect bluer colours to correspond to greater attenuation. However, they find the opposite, that redder colours correspond to stronger attenuation. This is likely related to the fact that optical colour is also a dust-affected measurement, and so untangling these competing influences on colour is not necessarily straightforward.

2.6.2 Optical depth scaling relation predictions & the importance of star-dust geometry

Our methodology is purely observational, which, as noted previously, has the advantage of not relying on any assumed models. Nonetheless, it is instructive to attempt to reproduce the observed trends using physically motivated tools such as scaling relations. These are useful to gain a quick understanding of the physical principles underlying a set of observations, and it is illustrative to see in what ways these relatively straightforward calculations match our observations, and more interestingly, where they fail to capture the full range of factors that lead to our results.[7]

For this analysis, we use scaling relations to calculate model average dust optical depths for the galaxies in our sample, and then ask how these combine with star-dust geometry to give dust attenuation and how they might be expected to vary across our parameter space.

In the simplest model, the intrinsic optical depth of dust in a galaxy depends on the dust surface density as

$$\tau = \kappa \Sigma_d, \tag{2.1}$$

where κ is the dust opacity. The dust density is not a measured property of our sample, but it can be derived using scaling relations based on our catalog properties. One could assume that dust density scales with metal column density, which in turn scales with gas column and metallicity, and so

$$\tau = \kappa f Z \Sigma_g, \tag{2.2}$$

where Z is the metallicity, Σ_g is the gas surface density, and f is the fraction of metals in the form of dust. Finally, the gas surface density could be estimated from the star formation

[7] As mentioned in the preface, portions of this section have been superseded by the updated analysis presented in chapter 4. The basic model structure and assumptions remain the same, but we have updated some of the input measurements and the parameters of the radiative transfer model. More importantly, we also no longer attribute the downturn in attenuation at higher luminosities *solely* to geometrical bulge effects, but have come to recognize the strong influence of the relative scaling of the face-on and edge-on attenuations on this effect. For full details, see chapter 4.

rate using the Kennicutt-Schmidt relation (Kennicutt, 1998):

$$\tau = \kappa f Z \left(\frac{\mathrm{SFR}}{\pi r^2}\right)^{1/1.4}, \tag{2.3}$$

where $\mathrm{SFR}/\pi r^2$ is the star formation rate surface density.

To calculate the metallicity we use the stellar M/L vs. [3.4]–[4.5] colour relation from Cluver et al. (2014) along with the $M_{3.4\mu\mathrm{m}}$ luminosity to estimate stellar mass (following §2.3.2), combined with the mass-metallicity relation of Tremonti et al. (2004). The star formation rate is derived from the *WISE* 12μm-star formation rate relation of Wen et al. (2014), and this is combined with the SDSS r-band petrosian half-light radii to calculate star formation rate surface densities. The metal-dust fraction is estimated at 0.2 in Bell (2003) and at 0.5 in Draine & Li (2007); we use the latter value of $f = 0.5$. The dust opacity (assuming u band) is taken from Li & Draine (2001). Thus, using these scaling relations we can construct a model intrinsic (face-on) dust optical depth for each galaxy in our sample.

This is, by necessity, a relatively rough calculation. For example, $f = 0.5$ is uncertain and may vary from galaxy to galaxy (Draine & Li, 2007; Draine et al., 2007), and the $M_*(3.4\mu\mathrm{m}, 4.5\mu\mathrm{m})$, $Z(M_*)$, and SFR(12μm) scaling relations all have notable scatter. Additionally, the radius used is an optical one, and there is no guarantee that the optical radius and star-forming radius actually correspond. More importantly, this neglects all geometric effects such as dust clumping, relative stellar and dust scale lengths/heights, bulge effects, etc. As such, we do not expect the quantitative size of the predicted optical depths to necessarily match the true physical values. However, this still provides a useful qualitative estimate of the intrinsic dust optical depth, especially since for comparison with our results we are most concerned with the *variation* across our parameter space (which should be more accurately predicted by this model) rather than the absolute normalization.

The basic results of this calculation are presented in the top panel of Fig. 2.16, which shows the the average model dust optical depth across our parameter space presented in

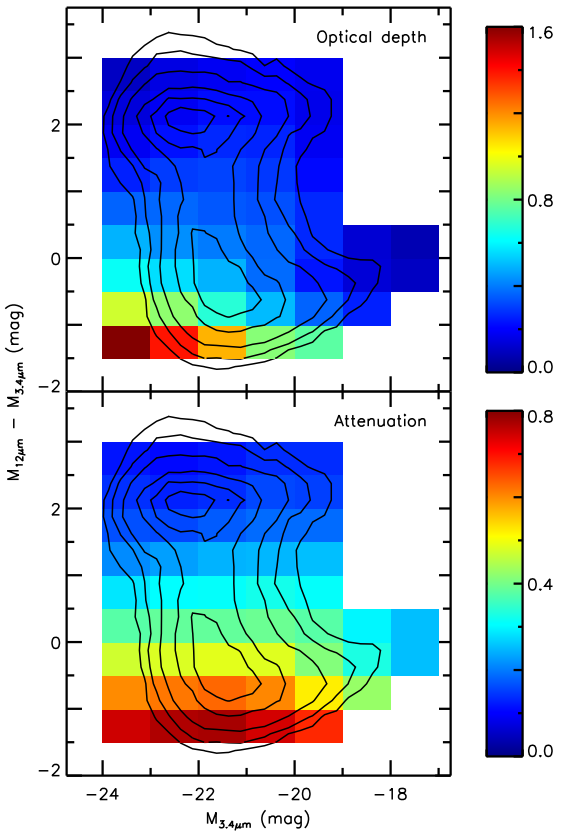

Figure 2.16: Top panel: predicted u band dust optical depth as a function of $M_{3.4\mu\mathrm{m}}$ luminosity and [12]–[3.4] colour, derived from scaling relations based on *WISE* luminosities and SDSS radii. The colour scale shows the intrinsic dust optical depth τ. Contours show the distribution of galaxies within this parameter space. Bottom panel: same as top panel, except the color scale shows the predicted relative face-on-to-edge-on attenuation, derived from the same scaling relations and Tuffs et al. (2004)'s disc attenuation models. The colour scale shows the attenuation in magnitudes.

the same manner as Fig. 2.10. We can see that the basic patterns apparent in the model calculation are similar to those found in the data. Like our data, the model optical depths show a strong dependence on specific star formation as parametrized by [12]–[3.4] colour, and likewise the models show a significant dependence on stellar mass as parametrized by $M_{3.4\mu\mathrm{m}}$ luminosity. Though this is an intentionally simplified model, this qualitative match is an encouraging sign that the parametrization we use does indeed correlate with variations in dust content, and helps inform intuition about the physical processes that lead to those variations. Moreover, the basic patterns we observe in this model are also seen in more complex ones. For example, Fontanot et al. (2009) predict, using a combination of semi-analytic models and radiative transfer simulations, that attenuation in disc galaxies should vary steeply with specific star formation rate as well as with stellar mass (see, e.g., their figure 4), matching our simplified model.

This model is useful, but it is important to remember that the basic model calculation gives only the (average) *intrinsic, face-on optical depth* – the total optical depth due to dust, through the entire thickness of the galaxy, as seen by an observer viewing the galaxy face-on. This is not the quantity we infer from our observations: we measure attenuation rather than optical depth, and not only that, we measure the *relative difference* in attenuation between the edge-on and face-on orientations rather than just the attenuation at one particular orientation. Thus, these measurements are not only sensitive to optical depth and star-dust geometry along a certain line of sight, but additionally depend on how the optical depth and geometry vary with viewing angle. Since galaxies contain multiple stellar and dust components with various characteristic shapes and scale lengths, the relationship between attenuation and optical depth can be complex as various components are more or less screened and become optically thick at different inclinations. Thus, the simple face-on optical depth does not necessarily correspond to the full relative attenuation between face-on and edge-on orientations. In order to compare more fully with our observations, we must convert our optical depth model into a relative attenuation model.

This is illustrated in the bottom panel of Fig. 2.16, which shows the results of using our scaling relation optical depths to construct a simple model for the relative face-on to edge-on attenuation. This construction makes use of the model dust attenuations of Tuffs et al. (2004) in modified form. Tuffs et al.'s models do not include any variation in galaxy morphology, and their model galaxy contains only a relatively small bulge deeply embedded in a dust disc, leading to very large relative attenuation of bulge light. Our parameter space contains a wide range of galaxy morphologies, and for our purposes we assume that, by the time a galaxy has a bright enough bulge for the attenuation of bulge light to make a significant contribution to the overall attenuation, the bulge is physically large enough to no longer be deeply embedded in the dust disc, in contrast with Tuffs et al.'s assumptions. Therefore, we approximate the overall relative attenuation with disc attenuations only, dividing using the galaxy B/T ratios from S11 and treating the bulge attenuation as being unchanged with inclination. While this is obviously an over-simplification, it is important to remember that this model is intended as a simple, qualitative approximation rather than a fully rigorous physical model. This also correctly treats the largely or entirely bulge-dominated quiescent galaxies as having attenuation largely unaffected by viewing angle. The attenuation for each galaxy is then calculated twice, once assuming a face-on orientation and once assuming an edge-on orientation, and the difference of the two attenuation models then represents the relative face-on to edge-on attenuation.[8]

As can be seen, this presents a quite different picture than the basic optical depth model. Most notably, the variation with luminosity is no longer sharply peaked at the highest luminosities, but rather is much more gradual and peaks at intermediate luminosities, matching the patterns we observe in our data. The normalization is significantly different, but this is not unexpected given the simplicity of this qualitative model, and overall the pattern of variations in predicted attenuation with [12]–[3.4] colour and $M_{3.4\mu\mathrm{m}}$ luminosity match our

[8]The corresponding attenuation parameter γ for disc galaxies would then be (1/0.85) times the relative attenuation (see footnote 5) – we report the relative attenuation here as it is the more physically meaningful property.

results quite closely throughout the parameter space. More broadly, while this particular relative attenuation model is only intended as a rough qualitative approximation, it illustrates the very strong effects that star-dust geometry and its variation with viewing angle have on attenuation – the qualitative variation in *observed* relative attenuation with galaxy properties is by no means necessarily the same as the variation in *intrinsic* dust optical depth with those same properties.

2.7 Conclusions

Dust attenuation affects nearly every observable property of gas-rich star forming galaxies in the ultraviolet and optical. Because of the strength of the effects of attenuation and ubiquity of dust, statistical study of the attenuation as a function of galaxy parameters has proven challenging – samples need to be selected and characterized in dust-attenuation insensitive bands, such as the near- or mid-IR, or HI.

With the advent of large, reasonably deep all-sky near-IR datasets (*WISE* and 2MASS), samples of galaxies detected in the near-IR – with spectroscopic redshifts in the optical and complementary optical luminosities – have become available for study. We have used such samples to systematically study the relative dust attenuation in disc galaxies and its variation with NIR luminosity and MIR-NIR colour. Our overall sample, inclination measurements, and photometric measurements are carefully selected to be as free from biases with inclination as possible. We choose to select and classify galaxies using near- and mid-IR measurements where possible (with the only exception being the relatively robust optical axis ratio from S11) in order to avoid any possible dust-induced confusion (and attendant biases). By selecting our samples in these ways and by using solely observational metrics for our analyses rather than derived physical quantities, we avoid the need for uncertain and model-dependent corrections to our analyses.

With this data set and classifications, we divide our sample into bins of galaxies which are intrinsically similar in $M_{3.4\mu\mathrm{m}}$ luminosity and [12]–[3.4] colour and measure the relative

attenuation between face-on and edge-on galaxies in each bin, thus quantifying the variation in relative attenuation across this parameter space. Our main results are as follows.

The strength of the relative attenuation is very strongly dependent on [12]–[3.4] colour (a proxy for specific SFR, or SFR per unit stellar mass). Galaxies with [12]–[3.4] colours greater than 0.5 show almost no relative attenuation, while below this value attenuation increases very rapidly with decreasing colour (increasing specific SFR) as you move across the star forming main sequence. At greatest, this can represent variation in face-on vs. edge-on attenuation of up to 1.1 mag (in the u band) over a span of 2 mag in colour (or roughly an order of magnitude in specific SFR). We conclude that relative dust attenuation is a strong function of specific star formation rate.

The strength of the relative attenuation is also strongly dependent on $M_{3.4\mu\mathrm{m}}$ luminosity (a proxy for stellar mass). However, the variation in relative attenuation with $M_{3.4\mu\mathrm{m}}$ luminosity over the length of the star-forming main sequence (roughly an order of magnitude in stellar mass), while still significant, is generally slightly smaller than the variation with [12]–[3.4] colour. Additionally, the variation in attenuation is not monotonic with luminosity, but rather increases with luminosity to a maximum near $M_{3.4\mu\mathrm{m}} \approx -21.5$ (corresponding to $M_* \approx 3 \times 10^{10} M_\odot$) and then decreases again for more luminous galaxies. We conclude that dust attenuation is also a strong function of stellar mass, though not quite as strong as specific star formation.

Relative to previous results, our result that the strength of the relative attenuation decreases for the most luminous galaxies was somewhat unexpected. Comparing our results in detail with those of T98 and M09, we learn that while our final fit results differ, all the actual datasets match well over the ranges where they overlap. The primary differences between the results come from our probing to brighter luminosities, where we could clearly discern and characterize the downturn in attenuation at bright luminosities where many previous works could or did not. In particular, T98's fits were affected by a somewhat unfortunate unrepresentative small sample at high luminosities, while M09's choice to fit the run of attenuation

with luminosity and Sérsic index with a plane leads to unrealistically high attenuation at high luminosities where their data was sparse.

Simple dust density scaling relations reproduce the strong correlations between dust content, specific star formation rate, and stellar mass, in broad accord with our observational inferences. Making more detailed comparisons with the variation in attenuation across our parameter space, however, requires the use of more complex models that attempt to model the relative face-on to edge-on attenuation. In particular, models which account for differences in star-dust geometry reproduce the non-monotonic variation of attenuation with $M_{3.4\mu\mathrm{m}}$ luminosity, which is not seen in the simple dust density model. We therefore suggest that this behavior is not caused solely by variations in dust density but rather is due to a combination of density variations and geometric effects, but a full investigation of this will depend on the availability of inclination-independent measurements of galaxy structure, which we turn to in the next chapter.

CHAPTER III

Inclination-independent structural measurements

Abstract

As a follow-up to our previous work, we wish to measure the dependence of relative attenuation on galaxy structure. However, most traditional measurements of structure use optical observations and techniques that leave them vulnerable to biases due to inclination and dust, rendering them unsuitable for use with the inclination test. Therefore, we develop techniques for measuring inclination-independent galaxy brightness profiles and structural measurements. We use dust-penetrated infrared survey imagery from the UKIRT Infrared Deep Sky Survey (UKIDSS) to avoid biases due to dust attenuation, and construct 'linear' galaxy brightness profiles by collapsing the light down onto the major axis – this technique is inclination-independent by construction. We investigate the properties of our measurements by using synthetic images of dust-free galaxies of known parameters, finding that our technique produces reliable structural measurements with reasonable errors throughout our parameter space, and showing that these measurements indeed do not vary with inclination. Applying this measurement technique to our sample of UKIDSS galaxies, we verify that it does produce largely inclination-independent results in observations, and examine the distribution of galaxy morphologies in the parameter space defined by these new measurements. We also compare our measurements with traditional structural metrics, finding that they do correlate with each other, that there is indeed an intrinsic spread in the structures of

galaxies at a given stellar mass and star formation rate, and that our measurements can usefully quantify these differences.

3.1 Introduction

In chapter 2 of this thesis, we developed inclination-independent measurements of galaxy stellar mass and specific star formation rate in order to isolate samples of intrinsically similar galaxies in a manner that is free of biases due to dust and inclination. However, these two properties, while informative, do not constitute a full description of a galaxy. They provide a useful census of the physical composition of the galaxy, but they do not give any information about how those physical components are distributed. That, rather, is the domain of galaxy structural measurements, and their inclusion is required to gain a full understanding of the galaxies in our sample. However, creating structural measurements that are inclination independent is a key challenge that must be overcome.

Galaxy structural measurements, apart from the simple descriptive value, give information about a wide range of galaxy properties. Galaxy size and brightness profile shape can inform us about angular momentum content and evolution (e.g. Mao et al. 1998; van den Bosch et al. 2001), reflects orbital dynamics and hence the demographics of rotation or dispersion support (van der Wel et al., 2009b), correlates with star formation history (e.g. Kauffmann et al. 2003b; Franx et al. 2008), and through its evolution with redshift encodes the growth of disks and spheroids (van der Wel et al., 2014b), merger rates (Jogee et al., 2009), and the history of quiescence (e.g. Bell et al. 2012; Lang et al. 2014b). Galaxy morphology also can have a profound effect on overall dust attenuation, even for identical dust and stellar contents, by changing the degree to which stars are screened by dust at various viewing angles – for example, making the bulge of a disk galaxy physically larger causes it to protrude further from the dust disk, altering the amount of dust between much of the bulge and the viewer at many orientations. As such, it is critical to be able to classify galaxies according to their structural properties as well as to their bulk composition.

However, as with the measurements of stellar properties, in order to be useful our measurements of galaxy structure must be inclination-independent. The basic task of a structural measurement is to provide a robust parameterization of the light distribution of a galaxy. However, that is only the second half of a two-stage process – before we make our measurements, the universe converts the intrinsic three-dimensional light distribution into the projected two-dimensional distribution we observe. This first step is often overlooked, yet it is extremely important because the mapping from three-dimensional light distribution onto two-dimensional projected light distribution is not necessarily one-to-one. Rather, changes in viewing angle will result in the exact same galaxy being mapped onto many different potential two-dimensional images, both through purely geometrical projection effects and through varying dust attenuation. The critical point is, *any variation in the mapping between three-dimensional light/mass distribution and two-dimensional projected light distribution* ***will*** *affect the resulting structural measurements,* unless the measurements in question are designed to account for these effects. As such, when initially constructing a structural parameter it should be an explicit design goal that it be robust to such inclination effects.

In general, this has frequently not been done. As a result, many traditional structural measurements are found to suffer from biases with inclination – we explore this more fully in chapter 5 of this thesis. As such, these measurements are not suitable for our purposes - we require *inclination independent* measurements to avoid biases in our study of the variation of attenuation and dust content with galaxy properties.

Therefore, we must create new measurements of galaxy structures that *are* designed to be inclination independent. We do this by making use of dust attenuation-independent NIR imagery, and from these images measuring linear major-axis brightness profiles that are by construction blind to the projection effects of varying inclination. These measurements will allow us to explore the structures of galaxies with confidence that our results are not due to hidden inclination biases.

The construction and properties of these measurements are the subject of this chapter.

We begin in §3.2 by describing the data we base our structural measurements on, and describe in detail the procedures for measuring the linear brightness profiles and constructing structural measurements from them. In §3.3 we study the reliability and error properties of our measurements using synthetic images, and confirm using these simulations that our method does indeed produce inclination-independent measurements. In §3.4 we then examine the distribution of our metrics with inclination for our galaxy sample in order to test their inclination independence for observational data. In §3.5 we explore the distribution of structural properties in our sample as a function of the previously measured stellar properties, in §3.6 we briefly compare our structural measurements to more traditional measurements, and in §3.7 we present our conclusions.

3.2 Constructing inclination-independent structural measurements

In order to create inclination-independent structural measurements, there are two major obstacles that must be avoided. First, one must deal with the effects of dust attenuation, which, in optical wavelengths, strongly alters the observed projected light distributions of galaxies in a manner that varies with inclination. Second, one must deal with geometric projection effects, which alter the projected light distribution in an inclination dependent manner even in the absence of dust. Both of these must be accounted for in order to create inclination independent measurements – dust attenuation with long-wavelength observations, and projection with careful design of the measurement algorithms.

3.2.1 Data

To create inclination-independent measurements of galaxy structures we need to avoid the effects of dust attenuation. It is difficult at best to dust-correct optical observations to a degree sufficient to measure reliable structural measurements; in addition, it is arguably circular to attempt to apply dust corrections to derive inclination-independent measurements that will ultimately be used to (among other things) study variation in dust attenuation.

As such, we avoid the dust attenuation issue to the greatest possible extent by measuring our structural properties in the NIR K band rather than at optical wavelengths. Dust attenuation in the NIR is typically an order of magnitude lower than the attenuation at optical wavelengths (e.g. Li & Draine 2001), and while radiative transfer effects can be complex, overall attenuation should be less than 0.3 mag even for galaxies with very high optical opacities viewed at nearly edge-on orientations (Tuffs et al., 2004). Thus, in the K band galaxies are optically thin for almost all viewing angles, preventing any significant inclination-dependent attenuation effects.

Our K band imagery comes from the UKIRT Infrared Deep Sky Survey (UKIDSS) Large Area Survey (Lawrence et al., 2007). This survey is chosen for its large survey area, the overlap between its survey area and that of the SDSS (a requirement to be able to use these measurements to extend the analyses we conducted in chapter 2), and its good resolution and sensitivity (typical seeing of ∼0.6 arcsec, 0.4 arcsec pixel scale, and K band point source limit of 18.2 mag; Lawrence et al. 2007) allowing for robust structural measurements.

As in chapter 2, we continue to make use of data from the Sloan Digital Sky Survey (SDSS) DR10 (Eisenstein et al., 2011) and the Wide-field Infrared Survey Explorer (WISE) All-Sky Data Release (Wright et al., 2010). In §3.6 we also make use of optical galaxy Sérsic indices and half-light radii measured by Simard et al. (2011) for comparison with our results. We use SDSS optical spectra-based redshifts and the derived distances to set size scales and calculate absolute magnitudes, and we use the WISE-based color and luminosity metrics we developed in chapter 2 to discuss the distribution of structural parameters throughout the stellar mass-specific star formation rate parameter space. As such, the sample presented in this chapter is a subset of the one studied in chapter 2; of the 78,721 galaxies in the SDSS-WISE cross-matched sample from chapter 2, a total of 24,427 of them fall within the UKIDSS survey area and therefore may be measured using our techniques.

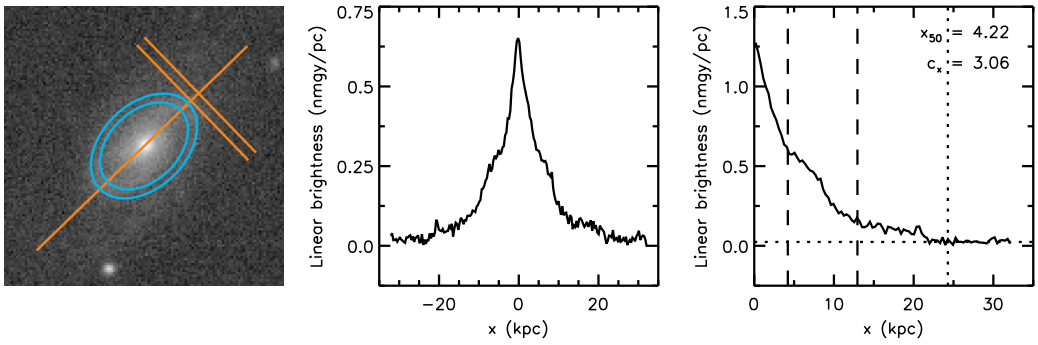

Figure 3.1: Left panel: Example K-band galaxy stamp, with example elliptical annulus and major axis cut. Center panel: Raw measured linear brightness profile. Right panel: Final folded linear brightness profile and structural measurements. Dotted lines indicate the measured sky level and profile 'edge' location, and dashed lines indicate measured x_{50} and x_{90} locations.

3.2.2 The linear brightness profile method and linear structural metrics

Conventional disk galaxy photometry is generally done by measuring the surface brightness in concentric rings, either circular (e.g. SDSS petrosian photometry) or ellipses of constant axis ratio. This is illustrated in Fig. 3.1 (blue rings in the leftmost panel). However, this leaves these parameters vulnerable to varying geometrical projection effects with inclination. The portions of a galaxy projected within a circular aperture obviously change drastically with inclination, but even elliptical apertures are not immune due to the effects of vertical structure. An elliptical aperture only maps to a ring of constant radius in the limit of an infinitely thin galaxy – for a realistic galaxy with a bulge and a disk of non-zero thickness viewed at any significantly inclined angle an elliptical aperture mixes light from a variety of radii. Therefore, even in the absence of dust effects many traditional measurements will suffer from inclination dependence.

Our photometric method sidesteps these issues in a very simple manner. We take cuts along each galaxy's major axis, extending them to cover the full width of the galaxy regardless of its inclination. All light within each cut is then summed and collapsed down onto the major axis to produce a *linear*, rather than radial, brightness profile. This process is also illustrated

in Fig. 3.1 (orange lines in leftmost panel). This method has the very important advantage over traditional photometry that, in the absence of dust, it is completely independent of galaxy inclination.

From the viewpoint of an external observer, by definition varying the inclination of a galaxy does not alter the projected distance along the major axis of any point within its disk, but rather only changes the perpendicular distance of that point from the major axis. It is this varying projection that causes the issues with traditional measurements. Since in our method all light within each cut is collapsed down onto the major axis equally, regardless of its distance from that axis, this technique is therefore *by construction* completely blind to inclination.

An example raw linear brightness profile resulting from this technique is shown in Fig. 3.1 (center panel). Turning this into a final profile and structural metrics requires dealing with a variety of complicating factors. One must account for the fact that galaxies do not have sharp edges, along with the effects of centering, sky background levels, noise, and potential contamination from other sources; here we describe our procedures for correcting for these factors and producing the structural metrics.

First, we check for centering errors. As a result of uncertainty in catalog coordinates or centroiding, it is possible for the peak of the profile to be offset from the zero point of the major axis. To correct this, we fit the central peak of the profile with a gaussian, and check whether the center point of this fit coincides with the zero of the axis. (The overall shape of the profile is generally not a gaussian, but the main peak is close enough that a gaussian fit provides a good, noise-resistant estimate of the location of the center.) If the difference is non-zero, we then shift the profile laterally to compensate. In the common case that the shift is not an integer number of pixels, the shifted profile is linearly interpolated from the raw profile. This may seem questionable, but a one-dimensional linear interpolation preserves flux and in our tests we find that the ability to correct for sub-pixel centering errors significantly reduces biases.

Second, we check for contamination by exploiting the expected symmetry of the linear brightness profiles. In the absence of contamination, a linear brightness profile should be highly symmetric around the center of the galaxy. This applies even in the presence of non-axisymmetric but regular features such as bars or spiral structure, since the process of collapsing light down onto the major axis has a smoothing effect and many features which are not fully axisymmetric still exhibit rough reflection or two-fold rotation symmetry. However, contamination from other sources will not follow this pattern, instead resulting in profiles which show significant differences between the two halves, and we exploit this property to detect contamination. Comparing the two halves of the profile, we measure the local difference in brightness (in nmgy/arcsec) at equal distances from the center as well as the difference in total integrated brightness (in nmgy). If the maximum local brightness difference between the two halves is greater than 15% of the central galaxy brightness and the difference in total integrated brightness between the two halves is greater than 10%, we flag the galaxy as contaminated. (These values for these thresholds are chosen to balance sensitivity versus the possibility of false positives; future tweaking in this area is likely.) This combination of tests ensures that the asymmetry is both significant as well as localized, indicating true contamination rather than being caused by, e.g., a consistent small offset due to a sub-pixel centering error. If the profile does not show contamination, we fold the halves of the profile together to generate a combined one-sided average profile for the galaxy. On the other hand, if contamination is detected, the one-sided profile is instead taken solely from the uncontaminated side. Using only one half of the profile results in a noisier measurement and likely reduced reliability, but is superior to the wildly erroneous measurements which generally result from contamination.

Third, we estimate the sky value. As is apparent in Fig. 3.1, even after initial processing the profiles often show residual non-zero sky levels. To estimate the sky level in our profiles we create a smoothed copy of the brightness profile (to minimize noise), and then find the minimum value of this profile. This minimum value by definition corresponds to the column

of the profile containing the least light, so the minimum value cannot be higher than the sky value and therefore puts a lower limit on the sky value. Similarly, the profile by definition cannot be lower than the sky value, so this minimum plus some measure of noise amplitude puts an upper limit on sky value. Therefore, we use the mean absolute difference between the normal and smoothed profile to estimate the noise, and clip the profile to within 4 times this value of the smoothed minimum to isolate the regions close to the sky value. We then fit for the sky value within that range that minimizes the residuals. This procedure will fail if the profile is so contaminated that there are no columns that do not contain light from either the primary object or contaminating objects, or if the sky value is not constant across the profile, but both of these cases are very uncommon and will result in an essentially unusable profile anyway.

Finally, we must define a maximum size for the profile. Galaxies do not have sharp edges, and so by definition no finite limit can encompass 100% of the extended light of a galaxy, but for the purposes of measuring structural properties it is necessary to assign them a size and an edge beyond which light will not be included. To define an edge for our galaxies we use the slope of their linear profiles – this is analogous to the relative surface brightness limit used to define a Petrosian radius. We define the edge of the galaxy to be the smallest distance where both the slope of the smoothed profile drops below 5% of the average slope near the profile center and the difference between the smoothed profile level and the sky level is less than 5% of the total profile height. (Again, the values for these thresholds have been chosen to attempt to balance detection of the outskirts of galaxies versus errors due to noise, and we will likely continue to tweak these in the future.) It is important to note that the sizes and structural parameters are measured from the actual profile, *not* the smoothed version, which is only used for determining the sky level and cutoff location.

Thus, after all corrections we have a single-sided light profile, folded or unfolded depending on whether contamination was detected, sky-subtracted and truncated to a realistic outer limit. This profile is then used to measure the 50% and 90% distances (henceforth

denoted as x_{50} and x_{90}) by analogy with r_{50} or r_{90} in traditional circular or elliptical aperture photometry - these are the linear distances outward from the center which contain 50% or 90% of the total integrated brightness. The linear concentration (henceforth denoted c_x) is calculated as the ratio x_{90}/x_{50}, again in analogy to traditional photometry (e.g. Blanton et al. 2001). An example of this is shown in the rightmost panel of Fig. 3.1. The linear size x_{50} and linear concentration c_x are then our inclination-independent structural parameters.

3.3 Simulation tests of the linear structural metrics

In order to test our method and explore the properties of our structural metrics, we create and analyze synthetic images of simulated galaxies. This allows us to quantify the bias and scatter in our method using simulated data of known properties. Importantly, this also allows us to confirm that our method achieves its primary goal of producing inclination-independent results. The construction and properties of these simulated images and the resulting uncertainty estimates and inclination independence tests are discussed in this section.

3.3.1 Construction of the simulations

We construct simulated galaxies of two basic types: disk galaxies composed of an axisymmetric disk and bulge, and triaxial elliptical galaxies. For disk galaxies the luminosity density of the disk at any point is given by the well-known double-exponential distribution:

$$\rho(r, z) = \rho_{0,d} e^{-(r/R_{0,d})-(|z|/h)}, \tag{3.1}$$

where $R_{0,d}$ and h are the scale length and scale height of the disk, respectively, and $\rho_{0,d}$ sets the normalization. Meanwhile, for the luminosity density of bulges and elliptical galaxies we

use the triaxial density model of Terzic & Sprague (2007):

$$\rho(m) = \rho_{0,b} \left(\frac{m}{R_{0,b}} \right)^{-p} e^{-b_n (m/R_{0,b})^{1/n}}, \tag{3.2}$$

where n is the Sérsic index, p and b_n are functions of n, $R_{0,b}$ is the scale length of the system, $\rho_{0,b}$ again is a normalizing constant, and

$$m = \sqrt{\frac{x^2}{a^2} + \frac{y^2}{b^2} + \frac{z^2}{c^2}} \tag{3.3}$$

is an ellipsoidal 'radial' coordinate where $a : b : c$ defines the axial ratios of the system. This is their standard triaxial density model, with no power-law core.

Synthetic image stamps are constructed from these models by overlaying a pixel grid coordinate system rotated to an arbitrary viewing angle and, for each pixel (x, y) in the image plane, numerically integrating the total model luminosity along the z axis to derive the brightness in that pixel. In the case of disk galaxies, the bulge and disk components are simulated separately and their normalizations individually adjusted to produce a desired bulge-to-total (B/T) flux ratio in the combined image. For elliptical galaxies, to account for rapidly changing brightness near their centers these regions are oversampled by a factor of 5 in all three dimensions.

Simulated disk galaxies are constructed with an exponential disk component with a variable horizontal scale length $R_{0,d}$ and a scale height $h = 0.1R_{0,d}$, plus a bulge component with scale length $R_{0,b} = 0.15R_{0,d}$, an oblate spheroid shape given by $a : b : c = 1 : 1 : 0.5$, and a Sérsic index of $n = 4$. Simulated elliptical galaxies are constructed solely of a bulge component with a variable Sérsic index n, and are oblate spheroids whose flattening varies from $c = 0.75$ to $c = 0.25$ based on magnitude. It should be noted that these structural choices should not be taken as attempting to perfectly match in detail all real galaxies, but rather are intended to broadly represent 'generic' galaxies over a wide range of galaxy properties drawn from our sample.

When creating the synthetic image stamps, the size of the pixels is chosen to match that of the UKIDSS imaging data at a desired galaxy size, and the overall normalization of the stamp is set to produce a desired total galaxy magnitude. These synthetic image stamps are then inserted into real UKIDSS images for measurement via our standard pipeline.

3.3.2 Simulation analysis of structural metric error and inclination properties

In order to study the behavior of our linear structural measurements for galaxies of varying brightness and structure, using our simulations we create a suite of synthetic galaxy observations whose apparent magnitudes, scale lengths, and central concentrations are chosen to sample as completely as practical the distributions of these properties observed in our sample.

We begin by creating a set of synthetic galaxies covering a wide range of physical scale lengths and B/T ratios (for disks) or Sérsic indices (for spheroids), and measuring their x_{50} and c_x values in the limit of high brightness, precisely known total luminosity, and zero noise or background. This gives us a mapping between the physical 3-d structure of our simulated galaxies and the 'true' structural parameters that result, which allows us to compare the measured structural parameters for more realistic synthetic observations to the ideal case.

We then create a larger set of synthetic galaxies, covering both the ranges of physical parameters expected to reproduce the ranges of structural parameters observed in our data (based upon the mapping above), as well as covering a range of apparent magnitudes (and, hence, surface brightnesses and S/N ratios) similar to that of our sample as well as a variety of inclinations. In total, we create simulated galaxies covering the ranges 1" $\leq x_{50} \leq$ 6", $2 \leq c_x \leq 5$, and $11.5 \leq m_K \leq 13.5$. We then repeatedly project these simulated galaxies onto real images and record the measured structural parameters, in order to understand both the bias and the variance in our structural parameter measurements as a function of galaxy properties.

It is important to note that, while our simulations are built using physical parameters

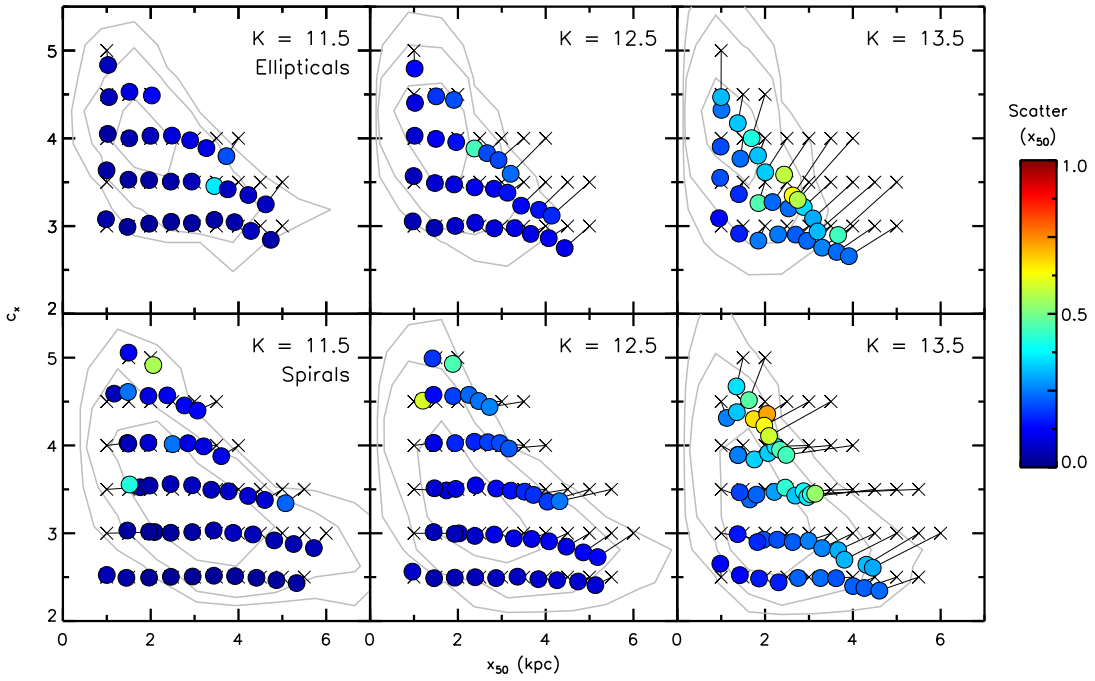

Figure 3.2: Bias and relative scatter in measured x_{50} as a function of simulated galaxy angular size, concentration, and apparent magnitude. Displacement between x symbols (true values) and circles (measurement averages) shows bias, and circle color shows relative scatter in x_{50}. Top row shows results for elliptical galaxies and bottom row shows disks. Background contours show observed galaxy distributions for similar samples.

such as galaxy scale lengths in kiloparsecs, total brightnesses in absolute magnitudes, etc, our use of these simulations to study the properties of our structural metrics is exclusively framed in terms of the *observed* quantities of linear concentration, *angular* linear size, and apparent magnitude, as these are the quantities that reflect the actual galaxy 2-d light distributions in our images. This is why we choose physical parameter ranges solely to reproduce the distribution of observed structural parameters, rather than attempting to precisely determine 'realistic' physical parameters and letting the measured structural parameters fall where they may – we are not attempting to understand the variation in our measurements with intrinsic 3-d galaxy light distribution, but rather the variation with the projected 2-d light distribution that we actually measure.

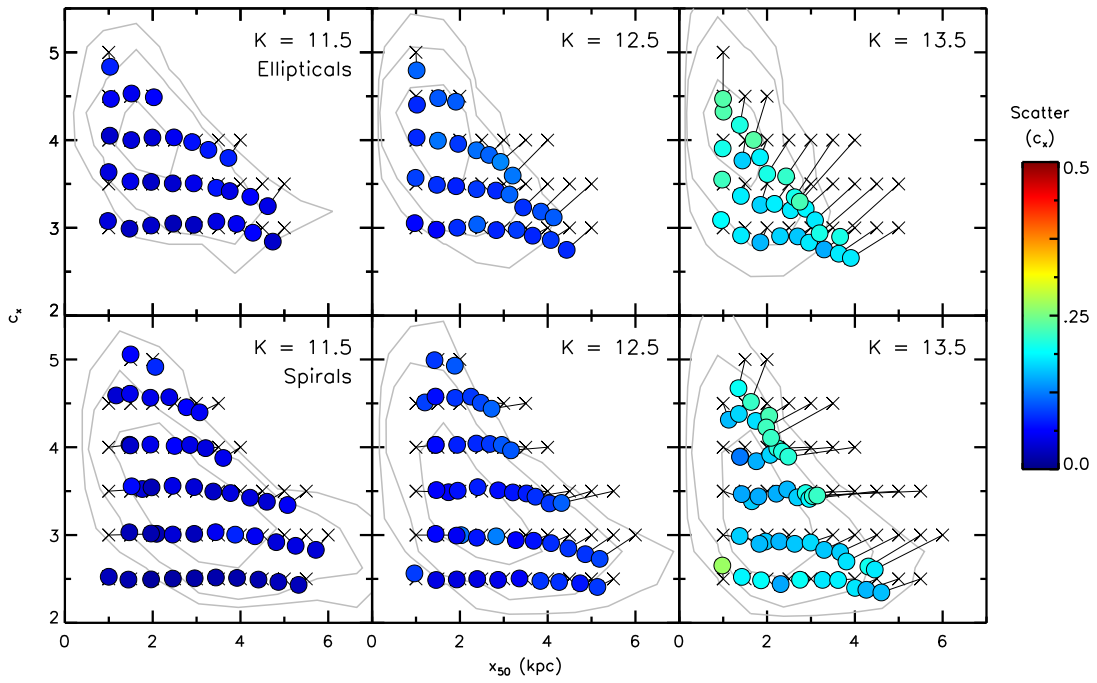

Figure 3.3: Bias and relative scatter in measured c_x as a function of simulated galaxy angular size, concentration, and apparent magnitude. Displacement between x symbols (true values) and circles (measurement averages) shows bias, and circle color shows relative scatter in c_x. Top row shows results for elliptical galaxies and bottom row shows disks. Background contours show observed galaxy distributions for similar samples.

The error estimate results of this exploration are presented in Figs. 3.2 and 3.3. Each plot shows the bias and scatter in c_x or x_{50}; the different panels cover disk or elliptical galaxies and various values of apparent magnitude m_k. In each panel, the black x symbols show the 'true' value of c_x and x_{50} for a given simulated galaxy; these are then connected to the circles which show the average recovered values of c_x and x_{50} for that galaxy. The displacement between these thus shows the bias in the measurements of c_x and x_{50} at that location in the intrinsic galaxy property parameter space. The circles themselves are color-coded to show the relative scatter in the recovered values of x_{50} (Fig. 3.2) or c_x (Fig. 3.3), thus showing the variation in these measurements. The background contours show the distribution of structural parameters measured for the *observed* galaxies (see §3.5) that correspond with the sample in that panel.

One can see that for brighter galaxies, the bias and scatter in these measurements is relatively small. The recovered average values of c_x and x_{50} track the 'true' values well across most of the parameter space, and the measured scatter is generally 10% or less for c_x and 20% or less for x_{50}. Unsurprisingly, though, both measurements become less reliable as the apparent magnitude of the simulated galaxies becomes fainter. The measured c_x and x_{50} values are still close to their 'true' values over portions of the parameter space, but become increasingly biased for galaxies with larger angular sizes and higher concentrations. Similarly, while the scatter is only modestly higher for the smaller and less concentrated galaxies, the ones showing strong biases also have quite significant relative scatter. It is important to note, however, that the measurements remain quite usable over a significant portion of the parameter space, especially for disk galaxies.

It is apparent from the results for the dimmest galaxies that it is not intrinsic c_x or x_{50} alone that determines where the measurements become unreliable, but rather a combination of the two. This indicates that the true limiting factor is surface brightness, particularly of the outermost regions. As a galaxy becomes larger at a given magnitude, the same amount of flux is spread out over more pixels, and thus the outermost regions of the galaxy become

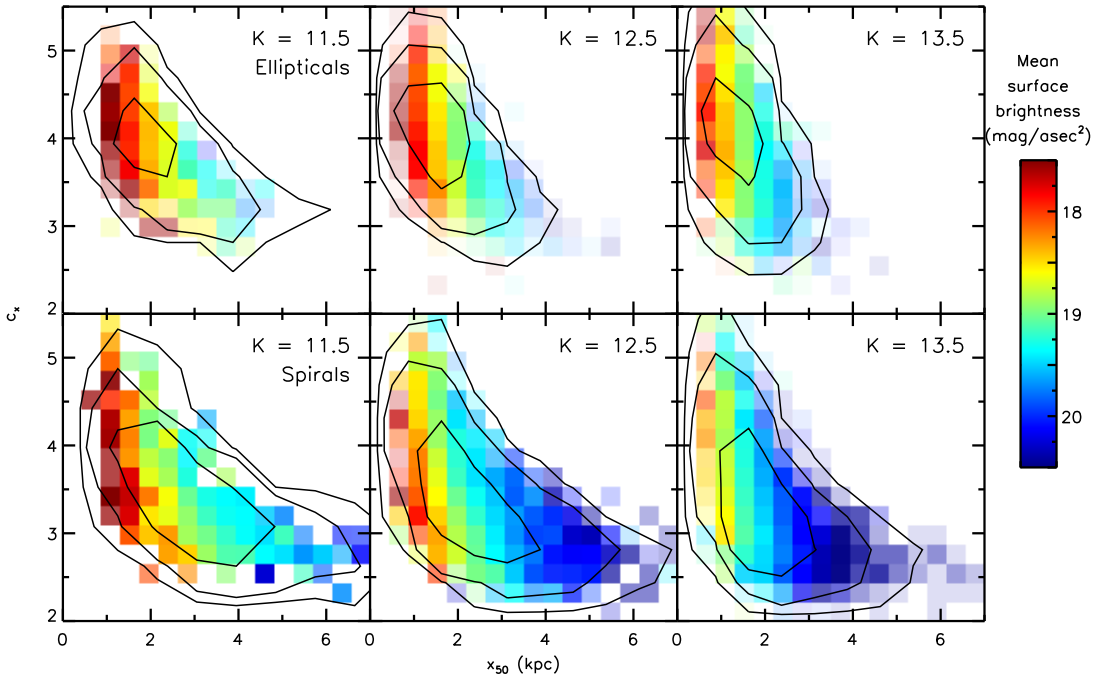

Figure 3.4: Colors show observed galaxy mean surface brightness as a function of galaxy angular size, concentration, and apparent magnitude. Top row shows results for elliptical galaxies and bottom row shows disks. Background contours show the observed galaxy distributions for these samples.

too low surface brightness to be detected above the noise background. This causes the measured size values to drop, as the outskirts of the galaxy simply cannot be detected; it is apparent that the values of x_{50} effectively saturate as size continues to increase. Similarly, as concentration increases more of the flux is shifted to the central regions, likewise lowering the surface brightness of the outskirts – this causes the above-mentioned loss of detectability to set in at a lower overall size threshold, as the shape of the light profile changes. This loss of detectability also affects the measurements of c_x; one can see that there is a trend towards erroneously low values of c_x for the affected galaxies, particularly in the case of the ellipticals. This arises because, while the measured x_{90} and x_{50} are both lowered by this effect, x_{90} is more strongly affected as it is measured farther out along the light profile. This is especially apparent for the ellipticals, whose outer profiles are shallower.

It can be seen that there are certain regions of the measured parameter space that simply

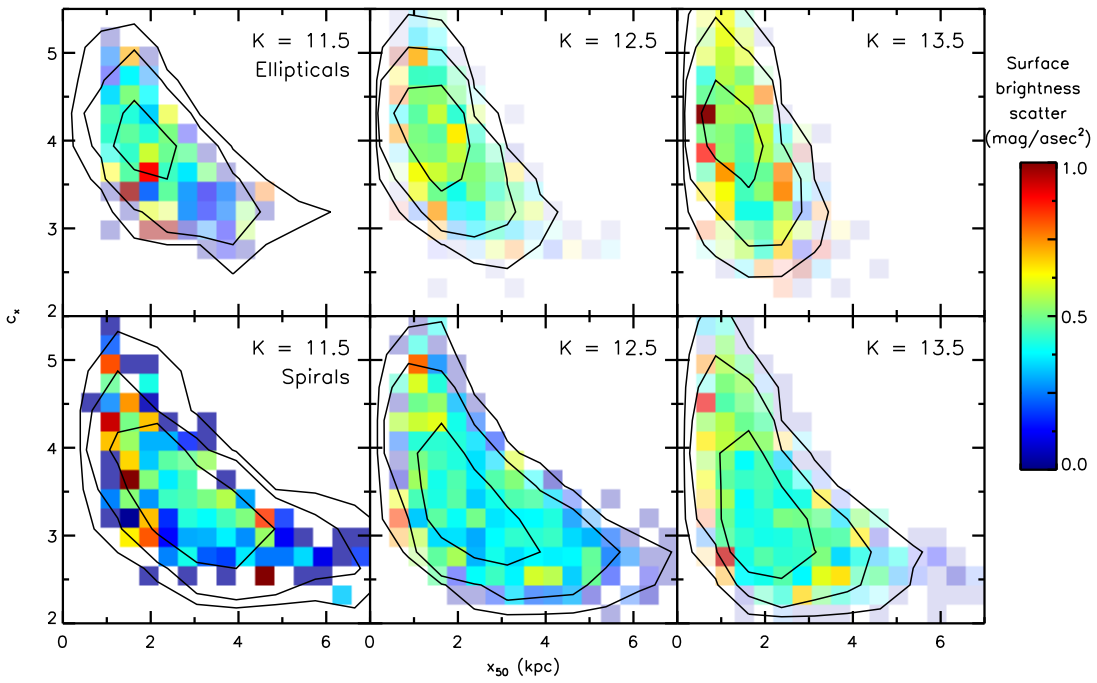

Figure 3.5: Colors show the scatter in observed galaxy surface brightness as a function of galaxy angular size, concentration, and apparent magnitude. Top row shows results for elliptical galaxies and bottom row shows disks. Background contours show the observed galaxy distributions for these samples.

will not be populated; namely, regions with relatively large values of c_x and/or x_{50} at dimmer magnitudes. Unsurprisingly, we can see in Figs. 3.2 and 3.3 that the observed distribution of parameters follows suit, with those regions of parameter space being nearly empty at dimmer magnitudes. The observed distribution extends up to the edge of those regions, though, so there could also be galaxies in those regions that we are not able to see. This would be worrisome if true, as it would imply the existence of a population of galaxies whose intrinsic parameters we are not able to accurately measure. However, we do not believe this to be the case; rather, it appears to us that these regions of parameter space are actually intrinsically sparsely populated.

We believe this for two reasons. First, if there truly were a large population of galaxies whose intrinsic structural parameters would lie in those regions, as we can see in Figs. 3.2 and 3.3 the distribution of the *observed* parameters for those galaxies should lie in a line along the edge of the accurately measurable region. However, as we can see from the contours in Figs. 3.2 and 3.3, there is no pile-up of galaxies along the edge, rather, the distribution peaks near the center and drops off smoothly towards the edges. Thus, if there is any such population of galaxies, their numbers cannot be a large fraction of the total.

Second, the distributions of surface brightnesses for our sample also suggest that there is no significant population of displaced galaxies. We construct simple surface brightnesses for our sample from K band magnitudes and inclination-corrected SDSS petrosian radii; these are unlikely to be rigorously correct but suffice for diagnostic purposes. Fig. 3.4 shows the distribution of mean surface brightnesses; we can see that the distribution of surface brightness varies smoothly right up to the edge of the observed distribution, rather than undergoing any abrupt changes. Moreover, if there truly was a large population of displaced galaxies, the *spread* in surface brightnesses should increase at the edges of the distribution, as galaxies with a variety of intrinsic surface brightnesses pile up at the edge of the accurately measurable region. However, we can see in Fig. 3.5 that this is not the case; indeed there are no particular trends in the surface brightness scatter with any parameter. Thus, if there

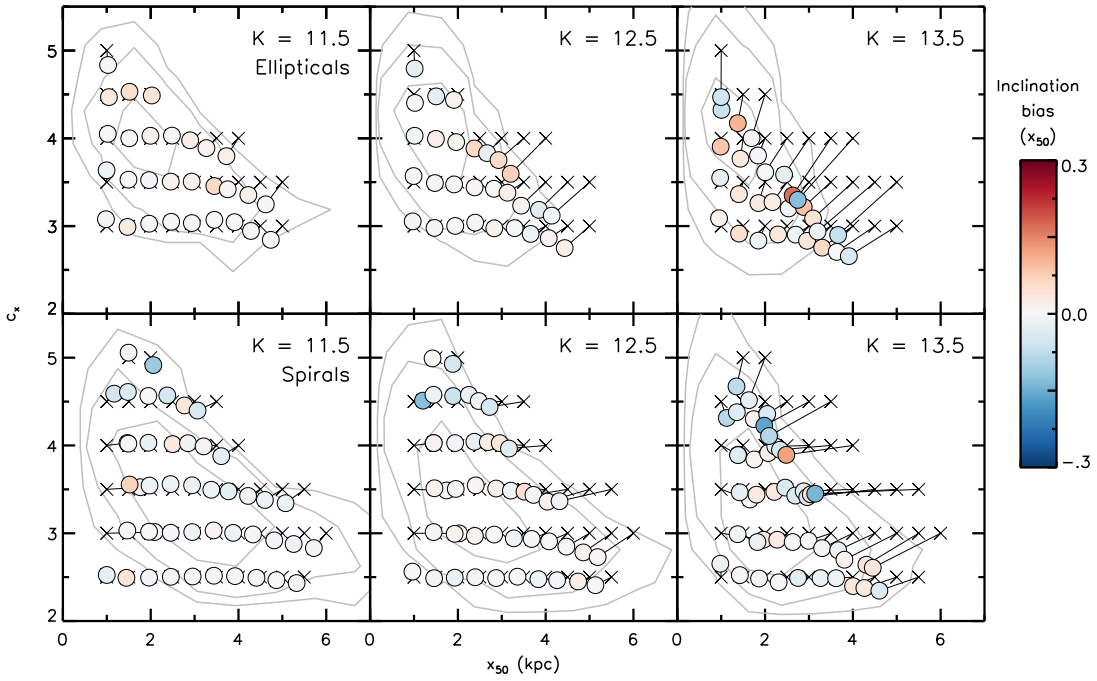

Figure 3.6: Bias and relative variance with inclination in measured x_{50} as a function of simulated galaxy angular size, concentration, and apparent magnitude. Displacement between x symbols (true values) and circles (measurement averages) shows bias, and circle color shows relative inclination bias in x_{50}. Top row shows results for elliptical galaxies and bottom row shows disks. Background contours show observed galaxy distributions for samples of galaxies with similar magnitudes and morphologies.

are any such galaxies, not only must their numbers be small relative to the total population, but they also must be fewer than the subset of the population whose surface brightnesses intrinsically lie along the edges of the accurately measurable region. As such, it appears that it is plausible that much of the problematic regions of parameter space are, in fact, unphysical.

The results of our simulated tests for inclination independence are shown in Figs. 3.6 and 3.7. The format of these figures is similar to that of Figs. 3.2 and 3.3, with the panels dividing by magnitude and type, the location of the points indicating the bias in x_{50} and c_x, and the contours again showing the observed galaxy distribution. However, in this case the color-coding of the points shows the relative variation in either x_{50} (Fig. 3.6) or c_x (Fig. 3.7)

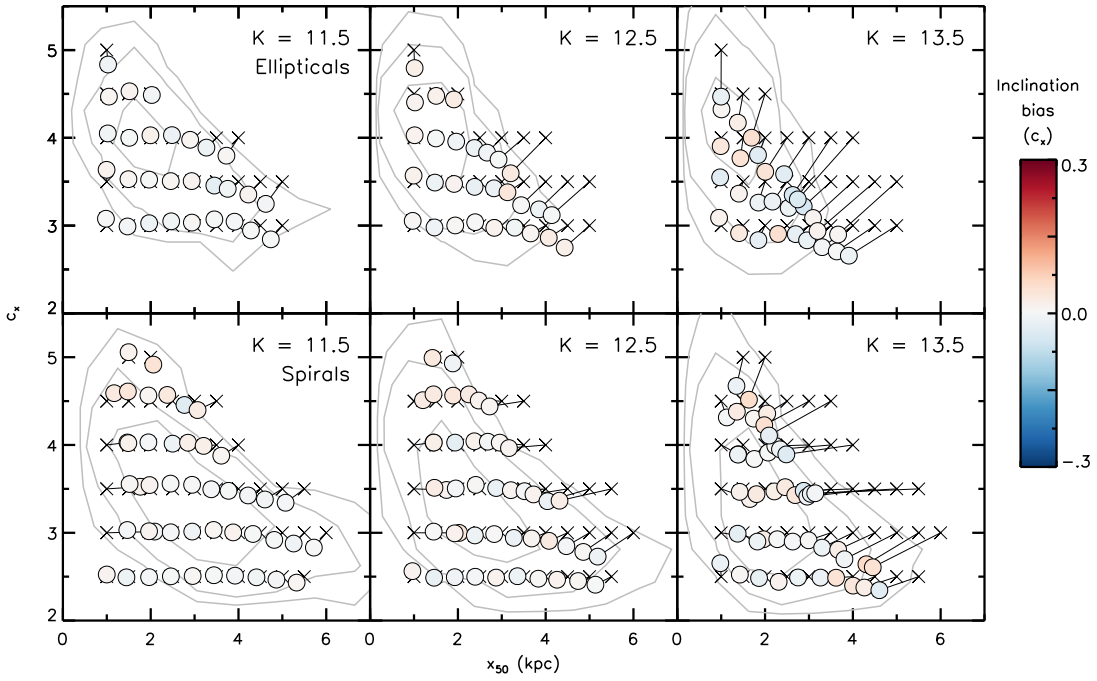

Figure 3.7: Bias and relative variance with inclination in measured c_x as a function of simulated galaxy angular size, concentration, and apparent magnitude. Displacement between x symbols (true values) and circles (measurement averages) shows bias, and circle color shows relative inclination bias in c_x. Top row shows results for elliptical galaxies and bottom row shows disks. Background contours show observed galaxy distributions for samples of galaxies with similar magnitudes and morphologies.

between the face-on view and the edge-on view at that location in parameter space; positive values indicate an increase as the galaxy tilts from face-on to edge-on, while negative values indicate a decrease with increasing inclination.

It is easily seen that our measurements show effectively zero inclination dependence over almost the entirety of the parameter space, even for fainter apparent magnitudes - less than 5% in almost all cases, and often less than 2-3%. Moreover, for the minor inclination dependence that is present, there is no overall preference for positive or negative dependence, suggesting that said dependence is driven by noise rather than any systematic effect. This is reinforced by noting that this minor dependence occurs most strongly in the low surface brightness regions of parameter space noted above to have unreliable measurements.

This is a very important test of our method, as it is in these simulations that one can be certain that the results are not being affected by the various difficult to quantify hazards that affect observational data. With these results, we can be confident that the method itself *works* – that, when presented with a wide variety of realistic galaxies, it does indeed quantify their two-dimensional projected light distributions in a manner that is independent of the angle at which they are projected.

3.4 Inclination independence in observations

We have seen that our method works for producing inclination-independent structural measurements for simulated images, but it is also necessary to determine to what degree we achieve similar results for actual observations. Given the results for our simulated galaxies we expect good performance in the real universe as well, but observational data are subject to real-world limitations such as sample selection uncertainties, binning issues and finite sample sizes, residual dust attenuation, etc. As such we do not necessarily expect perfect results, but it is important to check how close we come.

Therefore we use our method to measure structural parameters for our full galaxy sample and examine the distribution of our structural parameters with inclination, dividing our

sample in mass and specific star formation rate as was done in chapter 2. Figs. 3.8 and 3.9 show these distributions. The contours show the distribution of our sample in $M_{3.4\mu\mathrm{m}}$ and [12]–[3.4], representing stellar mass and specific star formation rate, and the inset panels show the distribution of c_x (Fig. 3.8) or x_{50} (Fig. 3.9) with inclination at each location in the parameter space.

The division of the sample according to mass and star formation is useful due to the variation that is present in the structural parameters across this parameter space; one can see that both size and concentration vary as a function of $M_{3.4\mu\mathrm{m}}$ and [12]–[3.4], and therefore any trends with inclination would not be easily visible were the entire sample to be considered at once. Indeed, even once this is done there remains some spread in structural parameters within some bins. The distribution of structure with mass and star formation rate and the variation within bins will be explored in more detail in §3.5 and §3.6; for now we focus on the variation with inclination.

As can be seen, while there is notable scatter in both c_x and x_{50} within most bins of parameter space, there are no major systematic trends with inclination apparent to the eye. (This stands in contrast to traditional structural measurements, as we examine in §3.6 and chapter 5.) For both star-forming disks of all masses and for the dimmer, less massive quiescent ellipticals with sufficiently disky structures to have broad enough (a/b) distributions for any trends to be meaningful, the distribution of structural parameters appears broadly the same for both the low and high ends of the inclination distribution within each bin.

More careful examination using linear fits to the $\log(c_x)$ and $\log(x_{50})$ versus $\log(a/b)$ distributions confirm this visual impression for the most part, but does show some small, but still notable, variation.

The concentration c_x appears to be quite close to truly inclination-independent, with the maximum difference between the most edge-on and face-on galaxies in each bin being less than 0.03 dex across all bins. This is in all cases much smaller than the scatter within each bin.

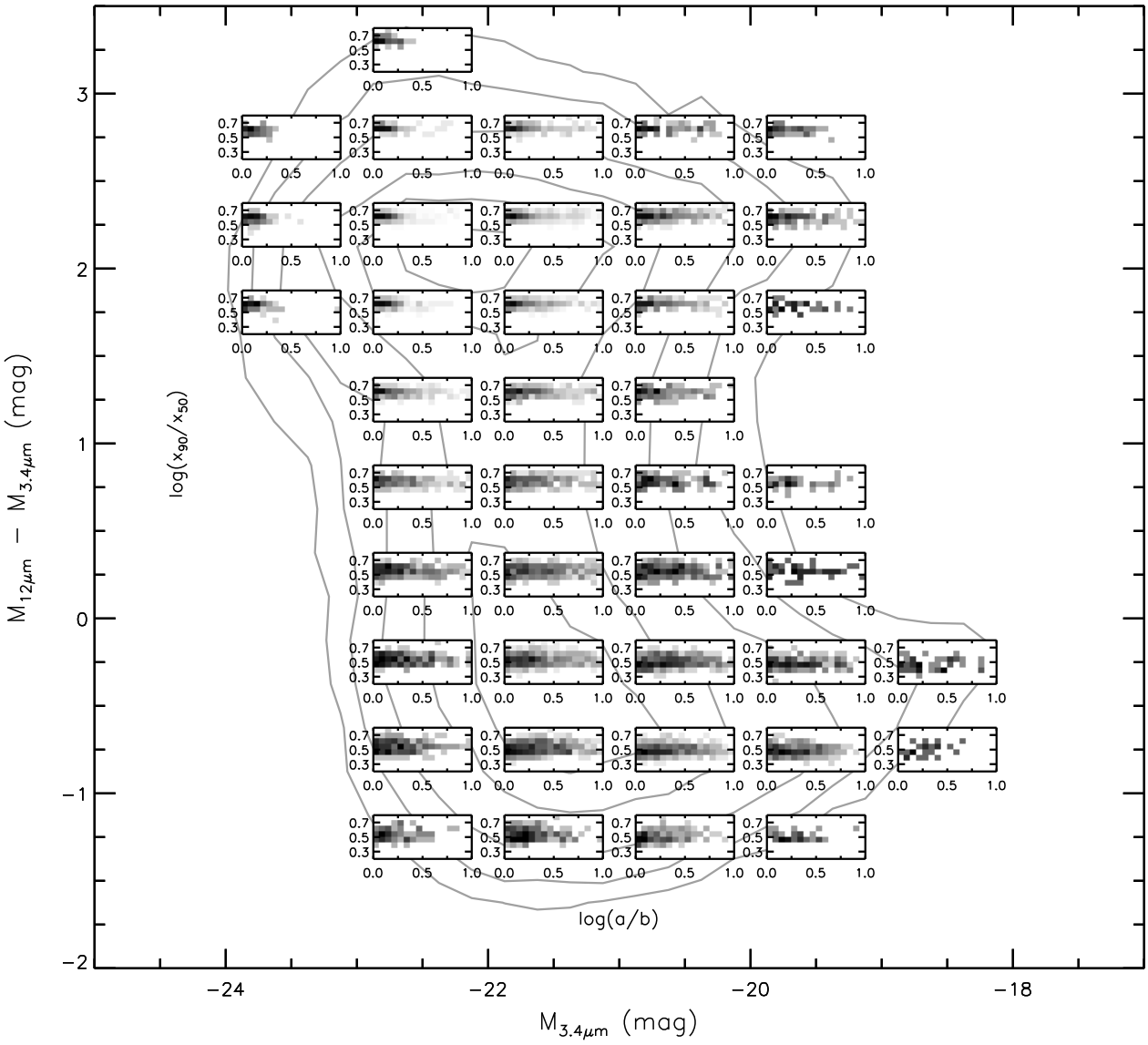

Figure 3.8: Background contours show the distribution of galaxies in $M_{12\mu\mathrm{m}} - M_{3.4\mu\mathrm{m}}$ vs $M_{3.4\mu\mathrm{m}}$ space. The inset panels show the distribution of $\log(c_x)$ as a function of $\log(a/b)$ for galaxies at that location in $M_{12\mu\mathrm{m}} - M_{3.4\mu\mathrm{m}}$ vs $M_{3.4\mu\mathrm{m}}$ space.

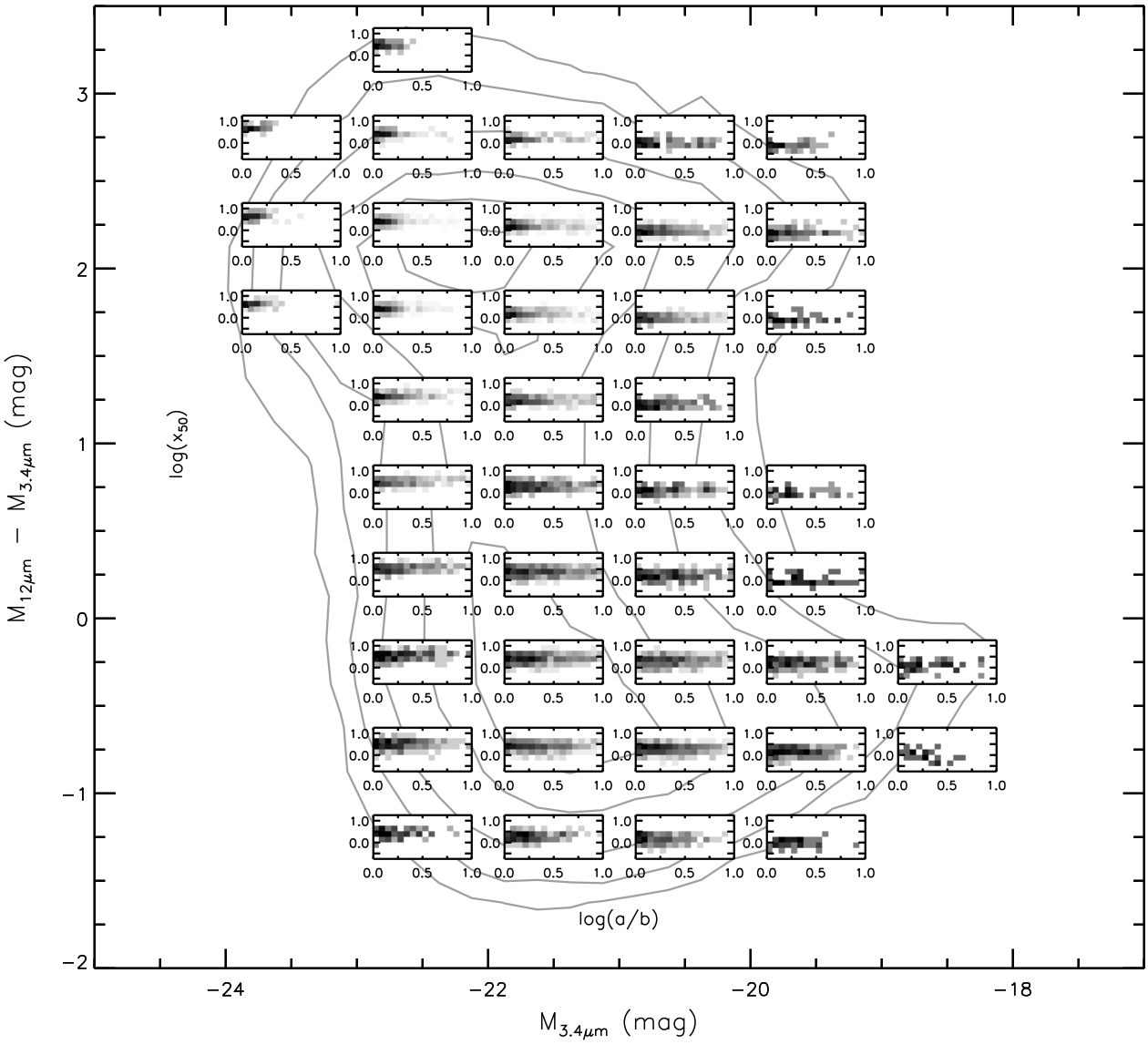

Figure 3.9: Background contours show the distribution of galaxies in $M_{12\mu\mathrm{m}} - M_{3.4\mu\mathrm{m}}$ vs $M_{3.4\mu\mathrm{m}}$ space. The inset panels show the distribution of $\log(x_{50})$ as a function of $\log(a/b)$ for galaxies at that location in $M_{12\mu\mathrm{m}} - M_{3.4\mu\mathrm{m}}$ vs $M_{3.4\mu\mathrm{m}}$ space.

The size measurements x_{50} are somewhat less universally reliable – while the difference between edge-on and face-on is below 0.05 dex across much of the parameter space, there are a number of bins with variation in the 0.05-0.1 dex range. This occurs primarily for the highest luminosity bins and some bins in the transitional region between starforming disks and quiescent ellipticals, and is significant enough to be marginally visible in some of the leftmost bins in Fig. 3.8. Thus, although the method works in general, we do see a slight tendency towards larger measured sizes for more highly inclined galaxies in some bins. We believe this to be due largely to spread in structural properties within each bin, specifically mixtures of smaller, more concentrated and intrinsically rounder (and hence narrower a/b distribution) and larger, less concentrated and intrinsically flatter (and hence wider a/b distribution) populations. This would cause the high a/b populations to appear systematically larger even with accurate measurements, simply because we do not have infinite sample sizes and therefore cannot bin our sample infinitesimally narrowly. Such mixing is quite plausible for transitional bins or bins of the most massive (and hence, containing the most prominent bulges) disk galaxies, and we observe that the inclination dependence decreases by up to ~50-60% if the galaxies within a bin are also selected for a narrow range in c_x, supporting this hypothesis. Part of the dependence may also be due to residual dust attenuation, which is small in K band but not completely zero, would act to increase measured half-light radii due to most strongly affecting the central regions of galaxies, and would be strongest for the most massive galaxies (see chapter 4). It is important to note, however, that even for the most strongly affected bins the variation is still smaller than the scatter, and is *much* smaller than the variation suffered by traditional structural metrics (as seen in §3.6 and chapter 5).

Overall, therefore, we see that our structural measurements remain inclination independent for the most part even when dealing with observational data and all of its associated uncertainties. We regard our c_x measurements as being reliably inclination independent in all cases, and we regard our x_{50} measurements as reliably inclination independent in most cases and still vastly better than traditional measurements in the worst cases.

3.5 The distribution of galaxy linear structural parameters

Returning from our discussion of error and inclination independence, it is instructive to explore the overall distribution of galaxies in our parameter space. This expands on the discussion in chapter 2, adding the dimensions of size and concentration to those of mass and star formation rate. Fig. 3.10 shows this distribution. The contours show the distribution of our sample in $M_{3.4\mu\mathrm{m}}$ and [12]–[3.4], and the inset panels show the distribution of c_x and x_{50} for galaxies at each location in parameter space.

Confirming the visual impressions of Figs. 3.8 and 3.9 earlier and of Fig. 2.6, there is a clear variation of size with luminosity – for all galaxy types, more luminous galaxies are systematically larger. This is the expected behavior (e.g. Shen et al. 2003; van der Wel et al. 2014a), so it is good to see that our structural measurements recover this property. Similarly, there is a notable variation in concentration with specific star formation rate, with the less actively star-forming galaxies in the upper half of the figure tending towards higher concentrations. Again, this is expected, as star formation rate is known to correlate strongly with morphology (e.g. Wuyts et al. 2011).

The range of concentrations present within each bin also varies across the parameter space. Bright quiescent galaxies have very little variation in concentration; again referring to Fig. 2.6 these are large (likely triaxial) ellipticals, which appear to have relatively uniform light profile shapes. As one moves towards lower luminosities and/or higher star formation rates the spread of concentrations within each bin increases; this may reflect the transition from single-component triaxial elliptical morphologies to two-component bulge+disk morphologies.

For star-forming galaxies, the maximum concentration within each bin increases slightly with increasing luminosity, though this effect is not large. This likely arises from the increased prominence of bulges in more massive disk galaxies.

For bins of galaxies which contain a significant range in concentration (mostly the star-forming disks), concentration is notably correlated with size. As the measured size is an

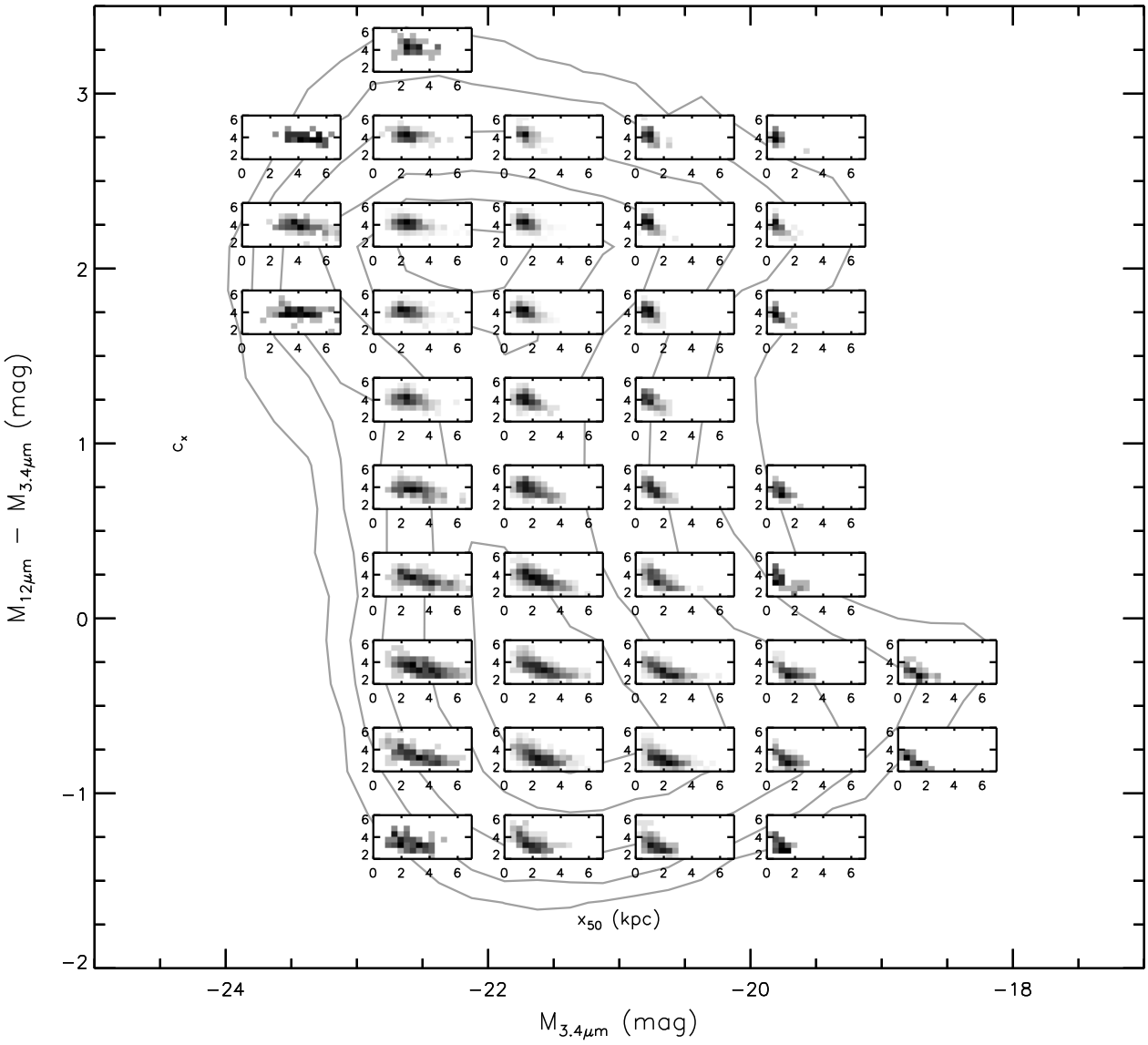

Figure 3.10: Background contours show the distribution of galaxies in $M_{12\mu\mathrm{m}} - M_{3.4\mu\mathrm{m}}$ vs $M_{3.4\mu\mathrm{m}}$ space. The inset panels show the distribution of c_x and x_{50} for galaxies at that location in $M_{12\mu\mathrm{m}} - M_{3.4\mu\mathrm{m}}$ vs $M_{3.4\mu\mathrm{m}}$ space.

analogue of a half-light radius, changing the overall light profile shape, whether by trading off light between two components with different profile shapes and scale lengths (e.g. bulges and disks) or simply by altering the profile of a single component (e.g. ellipticals with varying Sérsic indices) will necessarily alter size as well as concentration. This is unfortunate, as it means that these are not completely independent measurements – altering structure will to some extent bleed into altering size and vice-versa, which somewhat complicates the interpretation of the data when both are varying. However, this is an inevitable drawback of this sort of non-parametric size measurement – a parametric measurement such as a two-component bulge-disk model would not show this effect, but only at the cost of potentially introducing model-dependent systematics. And as we will see in §3.6 below, this does not prevent us from isolating usefully independent variation in both parameters in samples of similar galaxies.

3.6 Comparison with traditional structural measurements

One of the major purposes for which we create our structural measurements is to use them to analyze the inclination dependence of the measurements derived from more traditional methods; we carry out a comparison for this purpose in chapter 5 of this thesis. However, such a comparison is also useful as a diagnostic of our method; while our measurements are not expected to exactly match the traditional ones, they should broadly correlate with them. Here we show the results of a brief comparison of our measurements of size and concentration with traditional measurements of those quantities.

For this purpose we assemble a sample of galaxies selected to have $-22.5 \leq M_{3.4\mu\mathrm{m}} \leq -20.5$ and $-1.0 \leq [12]-[3.4] \leq 0$. This is a population of 'average' starforming disk galaxies roughly in the middle of the starforming main sequence. Fig. 3.11 shows the distributions of linear structural parameters (c_x, x_{50}) and traditional structural parameters (r-band Sérsic index – a measure of central concentration – and half light radius R_{chl} from Simard et al. 2011) for this sample, with contours showing the distributions for the entire sample and

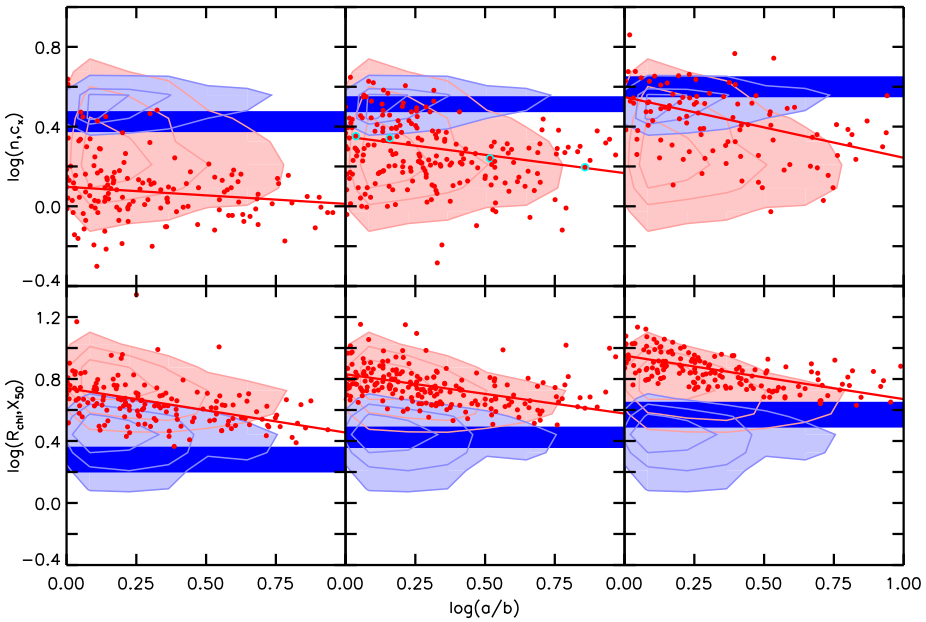

Figure 3.11: Contours show distribution of structural parameters c_x (blue, top) and n (red, top) and size measurements x_{50} (blue, bottom) and R_{chl} (red, bottom) for the sample of disk galaxies described in this section. Blue highlights show selection of subsamples of linear structural parameters c_x or x_{50}, and red points and line show traditional structural parameter values n or R_{chl} and linear fit for those selected subsamples. Top: left to right, subsamples of low, moderate, and high c_x, with x_{50} held at moderate values. Bottom: left to right, subsamples of low, moderate, and high x_{50}, with c_x held at moderate values.

highlighted regions/points showing the distributions in multiple sub-bins divided by linear concentration and linear size.

One can see that, as feared, traditional structural measurements suffer from significant inclination dependence; we quantify this in our later analysis in chapter 5. This inclination dependence is notably far larger than any suffered by our measurements; the variation here is quite obvious to the eye, in contrast to the lack of variation visible in Figs. 3.8 and 3.9. However, inclination dependence aside, the traditional and linear structural measurements do broadly correlate with each other – subsamples of higher or lower c_x or x_{50} indeed roughly correspond to subsamples of higher or lower Sérsic index and half light radius. This is a useful diagnostic of our method; while the linear structural measurements do not quantify size or

concentration in exactly the same way as traditional structural measurements and thus should not be expected to return identical results (even ignoring that our linear structural measurements are inclination-independent while the traditional measurements are not), they do measure the same concepts and thus should correlate with each other as seen here.

We can also see that (as noted in §3.4 and §3.5) even within a sample of similar star-forming disk galaxies there is considerable spread in structural properties. Some of this will be due to simple measurement error, but as evidenced by the correlated variations in linear and traditional measurements noted above much of it is intrinsic. This illustrates the usefulness of having reliable measurements of galaxy size and concentration – while selections on mass and star formation activity can define samples of broadly similar galaxies, measurements of galaxy structure do indeed encode additional information about astrophysically relevant physical variations in galaxy properties that are not captured by integrated luminosity-based selections alone. Unlike traditional measurements, our inclination-independent linear structural metrics allow these intrinsic differences to be clearly observed without confusion from additional inclination-induced variations.

3.7 Conclusions

Recognizing the need for measurements of galaxy structure that are reliably free of biases due to inclination and dust effects, we have developed a way to measure inclination-independent brightness profiles of galaxies. To do so we use dust-penetrated NIR imagery, and create linear, rather than radial, brightness profiles by collapsing each galaxy's light distribution down onto the major axis – this technique is by construction immune to geometric inclination effects. Using these profiles, we can create inclination-independent measurements of galaxy size and central concentration.

Using simulated galaxy images to investigate the properties of our measurements, we find that the primary limitation on reliability is surface brightness. For reasonably bright galaxies our measurements are relatively unbiased and show scatter of 10-20% or less across the full

parameter space of reasonable sizes and concentrations. For dimmer galaxies both bias and scatter grow, but the most severely affected regions of parameter space (combinations of high concentration and large size that result in the lowest surface brightnesses) seem to be sparsely populated in the real universe. Our simulations also show that our method does indeed produce inclination-independent measures of galaxy structures, with essentially zero variation in measured structural properties between edge-on and face-on simulated galaxy images.

Applying these techniques to our full observational sample, we find that, although observational limitations slightly affect the results, our measurements of structure do remain largely inclination-independent when applied to real data. Concentration measurements are almost completely inclination independent in all cases. Size measurements are inclination-independent for most areas of the stellar mass-star formation rate parameter space and only slightly inclination-dependent for the most massive galaxies; we tentatively attribute this small variation with axis ratio to a spread in bulge prominence (giving a subsample of galaxies that can never have large values of a/b) and/or minor residual dust attenuation in K band. In all cases the variation with inclination is smaller than the scatter in the structural parameters, and is much smaller than the variation suffered by traditional structural metrics.

We explore the distribution of galaxy structures measured using our techniques as a function of stellar mass and specific star formation rate. Unsurprisingly, we find that quiescent galaxies tend to have higher central concentrations than star-forming galaxies, and that the *range* of concentrations in quiescent galaxies is lower than in star-forming galaxies. Galaxy size is found to vary with luminosity, again in accord with expectations.

In comparison to traditional structural metrics, while the traditional measurements are found to be biased with inclination (unlike ours), our measurements do correlate with the traditional ones, indicating that they do indeed measure the same concepts in comparable ways. We also note the significant spread in structural measurements for a sample of a given mass and star formation rate, confirming that there is astrophysically relevant information

to be gained from adding our structural measurements on top of our previous selection tools.

The addition of these inclination-independent structural measurements completes our toolkit of dust and inclination-independent galaxy property metrics. With this full set of inclination-independent measurements in hand, we are now well positioned to apply them to measure the dependence of relative attenuation on galaxy structures as well as on stellar mass and star formation rates, which is the subject of the next chapter.

CHAPTER IV

Relative attenuation as a simultaneous function of stellar mass, specific star formation rate, size, and concentration

Abstract

Using our new inclination-independent galaxy structural metrics in concert with our previous inclination-independent galaxy property measurements, we measure the dependence of optical–NIR relative attenuation and face-on color on the intrinsic galaxy properties of stellar mass, specific star formation rate, size, and concentration. In agreement with chapter 2, we find that the relative attenuation (defined as the difference in optical–NIR color between face-on and edge-on views) increases sharply with specific star formation rate, and varies non-monotonically with mass, peaking at intermediate masses and declining for the most and least massive galaxies. For galaxies of a given stellar mass and specific star formation rate, relative attenuation varies with galaxy structure in a complicated fashion, in some cases peaking for the largest and least concentrated galaxies, and in others peaking at small to intermediate sizes and concentrations. Face-on color is a strong function of both stellar mass and specific star formation rates, becoming redder with both increasing mass and with decreasing star formation rate. For galaxies of a given stellar mass and specific star formation rate, face-on color is a very strong function of size, with smaller galaxies showing

redder colors. Scaling relation-based models where optical depth scales only with gas density and metallicity are found to predict the observed patterns in relative attenuation and face-on color surprisingly closely. Using the insights offered by these models we are able to construct a unified conceptual framework to explain the patterns we see in our measurements, allowing us to understand how the face-on color can serve as a diagnostic of face-on attenuation, and how the relative attenuation does not vary monotonically with the optical depth due to varying bulge/disk geometry and radiative transfer effects that lead to the saturation of relative attenuation at high optical depths.

4.1 Introduction

In chapter 3 of this thesis we constructed and investigated the properties of new inclination-independent galaxy structural measurements. These measurements are useful in their own right, but our initial purpose in developing them is to expand our inventory of inclination-independent galaxy property measurements. With these added to our toolbox, we now have the ability to select samples of galaxies which are simultaneously intrinsically similar in stellar mass, star formation rate, size, and concentration. In this chapter we make use of this capability to expand our analysis from chapter 2 to measure the variation in dust attenuation with galaxy structure as well as with stellar mass and specific star formation rate.

This is important because our analysis in chapter 2, informative as it may have been, is incomplete. We have investigated how dust attenuation varies with stellar mass and specific star formation rate, but not in terms of galaxy structure. And yet, there is ample reason to expect that dust attenuation should also depend on galaxy structure.

Galaxy structure correlates with star formation activity and star formation history (Wuyts et al., 2011), which we have already seen is related to dust attenuation. Additionally, radiative transfer effects mean that structure can have a very strong influence on attenuation. At a basic level, for a given total dust *amount*, the dust *density* will depend on galaxy size. Yet, as noted in chapter 1, it is dust density that determines optical depth; thus, dust atten-

uation should depend on size. Similarly, variations in morphology can affect attenuation by altering the extent to which stellar populations are screened by or embedded within dust at different viewing angles; e.g. changes in disk galaxy bulge prominence that cause the bulge to physically protrude from the dust disk. Notably, these effects will act to cause varying attenuation even for identical stellar populations and dust quantities. As such, even with our inclination-independent measurements of mass and star formation rate, if we do not include structural measurements we will still be missing half of the story in terms of understanding what controls dust attenuation.

Understanding the variation of dust attenuation with galaxy structure is important if one wishes to understand the effects of dust on all of the galaxy properties that structure *correlates* with – e.g. quiescence (Lang et al., 2014b), formation history (van der Wel et al., 2014a), angular momentum content (van den Bosch et al., 2001), or star formation rates (Wuyts et al., 2011). One must also be able to parameterize the variation of dust effects with structure if one wishes to understand the effects of dust on traditional (i.e. dust-affected) measurements of structure themselves.

Additionally, even absent concerns such as these, measuring the variation of dust attenuation with galaxy structure as well as with stellar mass and star formation rate is a valuable undertaking in its own right. Previous studies of the variation of attenuation with structure did not use inclination-independent structural measurements (e.g., Maller et al. 2009 used optical Sérsic indices, and Cho & Park 2009 used optical concentrations); thus, it is unclear the degree to which one can trust those results, particularly in light of the biases with inclination and dust that we uncover for those structural measurements in chapter 5. As such, this is a relatively under-explored question.

As well, while there have been a number of works that have studied the variation of dust attenuation with one or two galaxy properties at a time (e.g. Tully et al. 1998; Maller et al. 2009; Cho & Park 2009; Masters et al. 2010), there have not been any studies that have simultaneously measured the variance of dust attenuation on *all four* galaxy parame-

ters of mass, star formation rate, size, and concentration, even ignoring the question of the inclination-independence of the parameter measurements. Therefore, this offers us the opportunity to quantify the relative importance of each of these four parameters in controlling dust attenuation (which one affects dust attenuation the most?) as well as the ability to explore the variance with one parameter as a function of another parameter (e.g. 'does dust attenuation vary with size more for star-forming galaxies than it does for quiescent ones?') – *and* to do so with confidence that the parameters we use are truly intrinsic and unbiased, for the first time.

In this chapter we also expand our study of galaxy dust effects to include consideration of the face-on colors of galaxies in addition to their relative attenuation. This property is measured by the inclination test method as part of measuring the relative attenuation, but we did not consider it separately in our initial analysis in chapter 2. However, the face-on color turns out to offer additional insight into the dust content and properties of galaxies, independently of the relative attenuation, and thus is worth exploring.

We carry out the bulk of our investigation in §4.2; we review our method and parameters in §4.2.1, and present our results of the variation of relative attenuation with mass, star formation rate, size, and concentration in §4.2.2. The remainder of the chapter is devoted to interpreting these results. In §4.3 we update the scaling relation-based relative attenuation model we used in chapter 2 and show that it predicts the patterns we see in the relative attenuation with surprising accuracy. We then discuss the implications of this in §4.4, using the insights offered by our model to construct a conceptual framework that can explain the patterns we observe in our relative attenuation measurements, and conclude in §4.5.

4.2 Relative attenuation as a function of intrinsic galaxy properties

With the addition of our inclination-independent structural measurements, we can now measure the relative attenuation (defined as the difference in optical–NIR color between face-on and edge-on views) of galaxies as a function of not only stellar mass and star formation rate, but also galaxy size and concentration. In order to do so, we repeat the analysis detailed in chapter 2, additionally dividing our sample by the two additional structural parameters.

4.2.1 Method

We shall briefly review this procedure here; for full details see chapter 2. In order to measure the relative attenuation within a bin of galaxy properties (however selected), we measure the variation in $M_{optical} - M_{3.4\mu\mathrm{m}}$ color with inclination (parameterized by axis ratio). Since these galaxies are selected to be identical, they should have the same intrinsic luminosity. The optical magnitude will be affected by dust attenuation while $M_{3.4\mu\mathrm{m}}$ will not, and the attenuation will be much stronger when viewed edge-on as the galaxy's light must pass through a greater depth of dust in this orientation. Therefore, the $M_{optical} - M_{3.4\mu\mathrm{m}}$ color will vary with inclination, and the expectation is that the stronger the dust attenuation, the greater this variation will be. (However, as we show below, this naive expectation does not always hold.) We parameterize the relative attenuation in each bin as $A_\lambda = \gamma_\lambda \log(a/b)$, where A_λ is the attenuation relative to face-on in the passband λ, a/b is the ratio of the semi-major to semi-minor axis (inverse of the axial ratio), and γ_λ is the resulting attenuation amplitude parameter in that band. To measure the attenuation amplitudes, we fit a linear relationship to the $M_{optical} - M_{3.4\mu\mathrm{m}}$ vs. $\log(a/b)$ distribution of galaxies in each bin – the slope of this relationship is the relative attenuation amplitude parameter γ_λ in this bin.

Previously we had parameterized our sample by dividing it into bins of identical $M_{3.4\mu\mathrm{m}}$ luminosity and [12]–[3.4] color. In this section we continue this practice, but additionally

subdivide each bin into sub-bins of identical c_x and x_{50} in order to explore the variation with these additional parameters.

For this study we divide our sample into fourteen bins in magnitude and color. This is a somewhat coarser binning than employed in chapter 2, but this is necessary to have a sufficient number of galaxies in each sub-bin of structural properties, and the fine variation with color and magnitude has already been explored in chapter 2. We select fully quiescent galaxies with $[12]-[3.4] \geq 1.5$, and divide them into three bins of luminosity as $M_{3.4\mu\mathrm{m}} \leq -22.5$, $-22.5 \leq M_{3.4\mu\mathrm{m}} \leq -21.0$, and $M_{3.4\mu\mathrm{m}} \geq -21.0$. We select mostly quiescent intermediate galaxies with $0.5 \leq [12]-[3.4] \leq 1.5$, and divide them into three bins of luminosity as $M_{3.4\mu\mathrm{m}} \leq -22.0$, $-22.0 \leq M_{3.4\mu\mathrm{m}} \leq -21.0$, and $M_{3.4\mu\mathrm{m}} \geq -21.0$. Finally, we select moderately star-forming galaxies with $-0.5 \leq [12]-[3.4] \leq 0.5$ and strongly star-forming galaxies with $[12]-[3.4] \leq -0.5$, and divide each of these into four bins of luminosity as $M_{3.4\mu\mathrm{m}} \leq -22.0$, $-22.0 \leq M_{3.4\mu\mathrm{m}} \leq -21.0$, $-21.0 \leq M_{3.4\mu\mathrm{m}} \leq -20.0$, and $M_{3.4\mu\mathrm{m}} \geq -20.0$.

In each bin of color and luminosity, we sub-divide by structural properties in the range $0.5 \leq x_{50}(kpc) \leq 6.5$ and $2.0 \leq c_x \leq 5.0$, with bins 1.0 kpc wide in x_{50} and 1.0 units wide in c_x. As noted in chapter 2, this parameter space is not necessarily fully populated in all bins of color and luminosity, but this encompasses roughly the range of parameters present in the overall sample.

To this point we have only discussed the slope of the linear fit, as the relative attenuation amplitude. However, there are *two* components to a linear fit – not only the slope, but the intercept as well. The slope describes the relative attenuation between face-on and edge-on, but the intercept also describes a physically relevant property – namely, the face-on optical–NIR color of the galaxies within a bin. This color depends on both the stellar populations of the galaxies in question and their total dust content and dust distribution, and thus also encodes useful information about the physical properties of these galaxies. Thus, the intercept provides a complementary source of information to the slope for the study of dust attenuation.

In this case, the intercept proves particularly powerful as an analysis tool because of our ability to select samples which are similar in stellar mass and specific star formation rate. These two properties control the metallicity and stellar population, and thus fix the *intrinsic* color within each bin. Therefore, any variations in *observed* color with structure within a bin are likely due entirely to dust attenuation – thus, the face-on colors that the intercept provides give information on the face-on dust attenuation, which the inclination test method cannot normally probe.

4.2.2 Results

The results of this study are presented in Fig. 4.1. As before, this figure shows the background distribution of galaxies in our $M_{3.4\mu\mathrm{m}}$ - [12] − [3.4] parameter space; the inset panels then show the relative attenuation amplitude as a function of x_{50} and c_x for galaxies at that location in the parameter space. (In this chapter we examine the u band attenuation, as this band has the highest dust opacity and thus the resulting trends are the largest and easiest to see.) We describe the trends in relative attenuation and face-on color in this section, and analyze the significance of these results in context with our models in the discussion section below.

As previously noted, fully quiescent galaxies (panels a–c) show essentially no relative attenuation, even for the lower luminosity galaxies with intrinsically flattened disk-like shapes. One can perhaps suggest that the higher concentration members of the lowest luminosity group (panel c) have very slightly more relative attenuation, but the difference is negligible. The mostly quiescent intermediate galaxies (panels d–f) also show little relative attenuation for the most part, though not zero. We also see the first hints of coherent trends in relative attenuation with structural properties here, with the two more luminous bins (panels d and e) showing a modest trend for the largest and least concentrated galaxies to have greater relative attenuation.

The various bins of star-forming galaxies (panels g–n), on the other hand, show not only

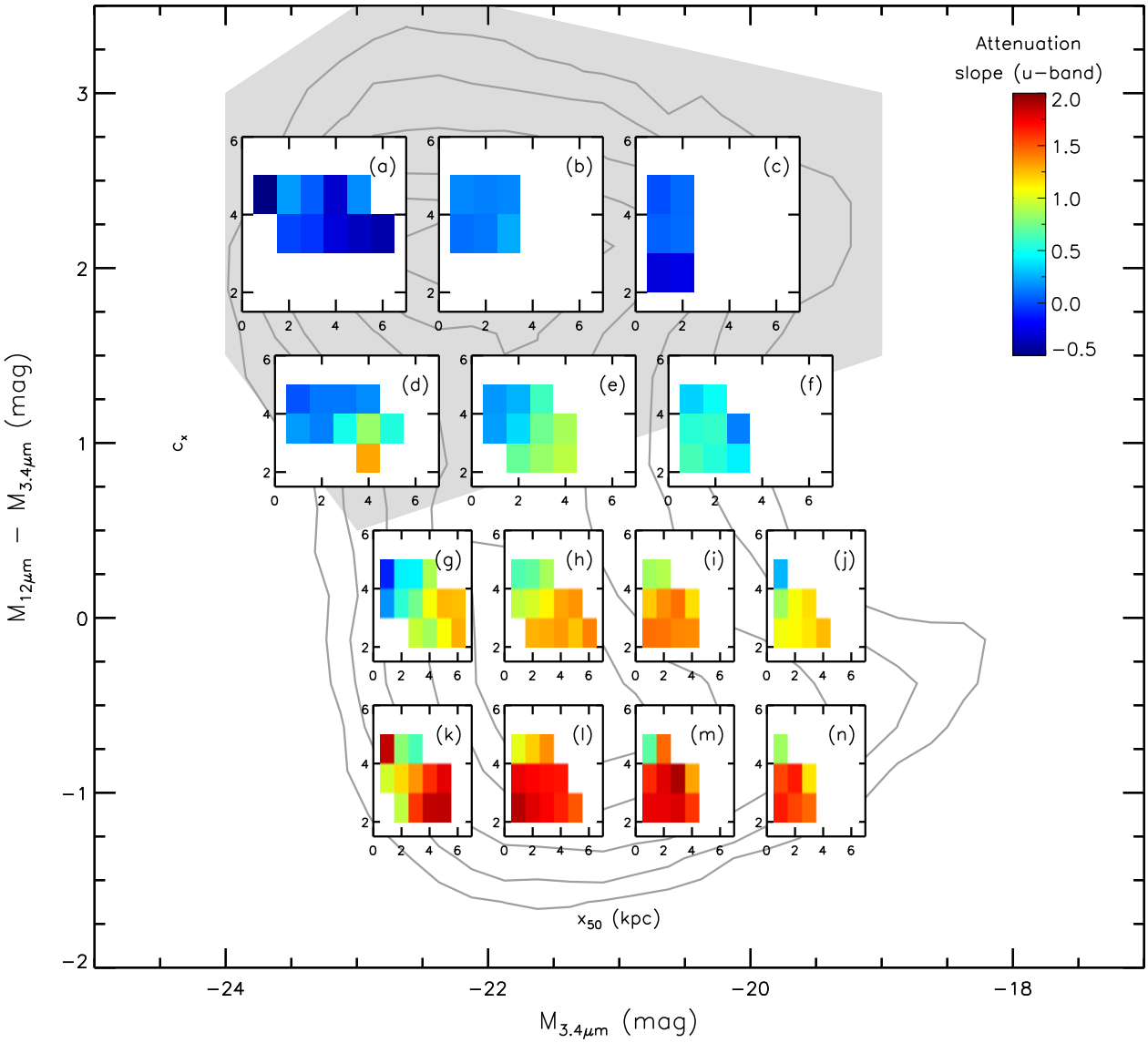

Figure 4.1: Relative attenuation slope as a function of specific star formation rate, mass, size, and concentration. Background contours show distribution of galaxies in [12]–[3.4] and $M_{3.4\mu m}$. Each inset panel shows the relative attenuation slope (denoted by color) as a function of c_x and x_{50} for a subsample of galaxies at that location in the [12]–[3.4] - $M_{3.4\mu m}$ parameter space.

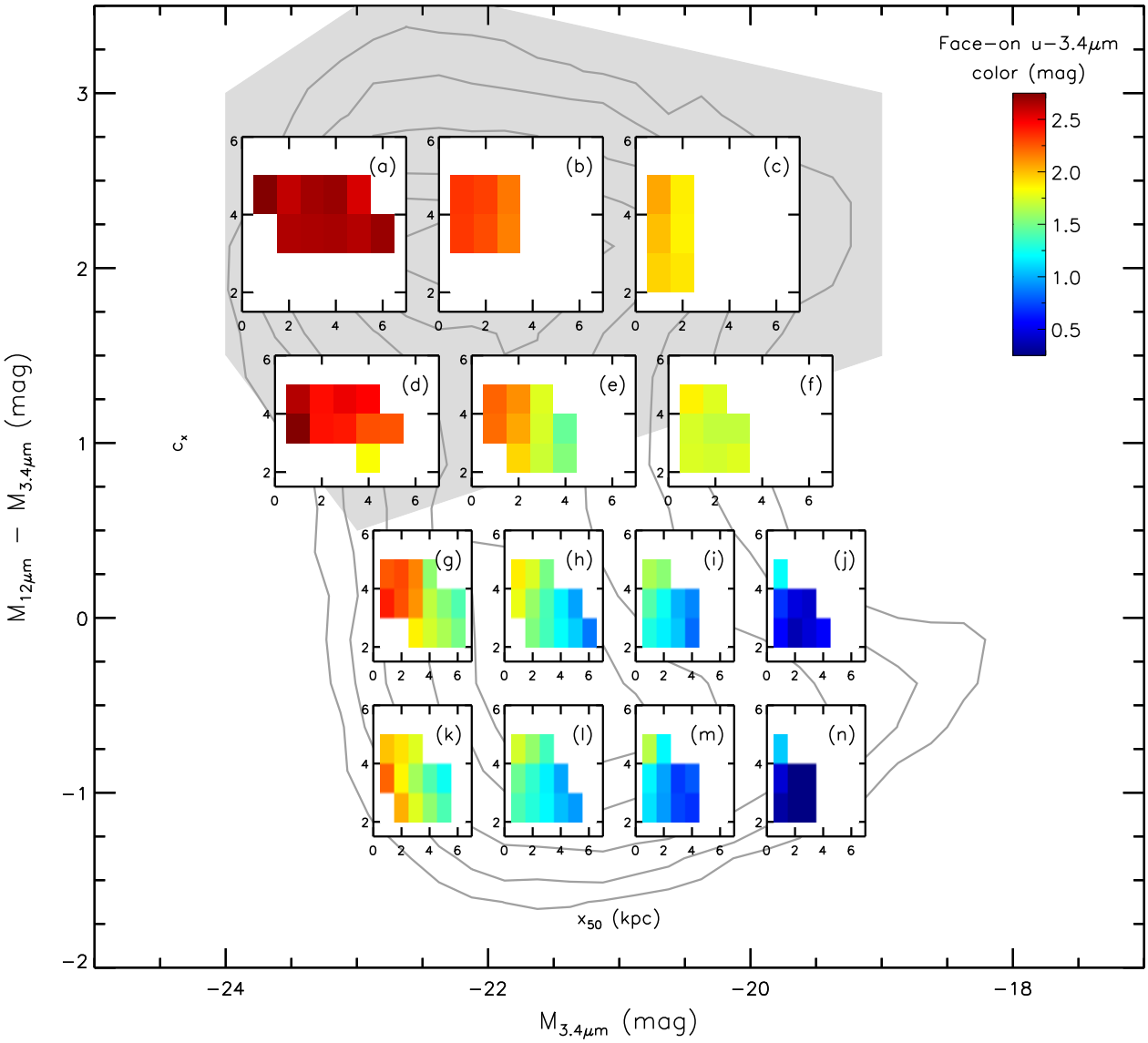

Figure 4.2: Face-on color as a function of specific star formation rate, mass, size, and concentration. Background contours show distribution of galaxies in [12]–[3.4] and $M_{3.4\mu\mathrm{m}}$. Each inset panel shows the face-on color (denoted by color) as a function of c_x and x_{50} for a subsample of galaxies at that location in the [12]–[3.4] - $M_{3.4\mu\mathrm{m}}$ parameter space.

significantly greater overall relative attenuation, but also strong trends in relative attenuation with structure. As already seen in the analysis in chapter 2, the strongly starforming galaxies (panels k–n) show higher overall relative attenuation than the moderately starforming ones (panels g–j), and the intermediate luminosity bins (panels h–i and l–m) show higher overall relative attenuation than the most or least luminous bins (panels g, j, k, and n). In terms of structure, for the two most luminous bins of moderately starforming galaxies (panels g–h) and the most luminous bin of strongly starforming galaxies (panel k) we can see a similar trend as the mostly quiescent galaxies of increasing relative attenuation for the largest, least concentrated galaxies. For the less luminous bins of both categories (panels i–j and l–n) the trend with size weakens; rather than a strong linear trend, the strongest relative attenuation is found in galaxies with small to intermediate sizes and low concentrations, with relative attenuation decreasing towards large sizes (and, in some cases, towards very small sizes) and towards more concentrated galaxies.

In Fig. 4.2 we show the fit face-on color as a function of MIR–NIR color, NIR luminosity, size, and concentration in the same manner as the slope is shown in Fig. 4.1; as before, the background shows the distribution of galaxies in color-luminosity space and the inset panels show the face-on color as a function of x_{50} and c_x at that location in parameter space.

At a given [12]–[3.4] color, overall face-on color is a function of luminosity, with the more luminous galaxies (left bins) in general having redder face-on colors. Face-on color also varies with [12]–[3.4] color, with less actively starforming galaxies (upper bins) likewise having redder face-on colors. These trends are likely due to simple variation in stellar populations and metallicity with star formation rate and mass, as we explain further in our discussion below.

Within a given bin of [12]–[3.4] color and $M_{3.4\mu\mathrm{m}}$ luminosity, stellar population parameters are expected to be constant, leading to the expectation of a constant face-on color in the absence of the effects of dust in face-on orientation. Yet, for all but the most luminous quiescent galaxies (panel a) *the face-on color is a strong function of structure.* For the most

part the face-on color varies most strongly with size, with the smaller galaxies showing redder colors. In some bins there is also a slight tendency towards redder colors with increasing concentration, though this trend is small compared to the dominant trend in color with size. In contrast to the variations in face-on color between bins, as we explain more fully below, in this case we attribute this trend to differences in the face-on attenuation driven by variation in dust density.

4.3 Scaling relation model analysis

As discussed in chapter 2 of this thesis, while we intentionally use purely observational and non-parametric methods in order to avoid relying on any assumed models, it is nevertheless interesting to attempt to *reproduce* our results using physically motivated models. These models are not intended to be rigorously predictive, but rather as tools to gain insight into the physical processes that give rise to our observations.

As with the previous section, our model methodology and analysis follows that of chapter 2 closely; for a full description see chapter 2. Briefly, we use simple scaling relations to produce predicted dust optical depths for each galaxy from its observed catalog properties. Optical depth depends on dust surface density, which depends on gas surface density combined with metallicity, and gas density can be related to star formation rate surface density through the Kennicutt-Schmidt relation (Kennicutt, 1998). The optical depth can therefore be parameterized as

$$\tau = \kappa f Z \left(\frac{\mathrm{SFR}}{\pi r^2} \right)^{1/1.4}, \tag{4.1}$$

where τ is the face-on optical depth, κ is the dust opacity, f is the fraction of metals in the form of dust, Z is the metallicity, and $\mathrm{SFR}/\pi r^2$ is the star formation rate surface density.

None of these quantities are measured directly in our catalogs, but they may be derived from them using scaling relations. Metallicity is derived from a modified form of the $M_{3.4\mu\mathrm{m}}$ luminosity-stellar mass relation of Meidt et al. (2014) to measure stellar mass, combined

with the mass-metallicity relation of Tremonti et al. (2004). The star formation rate is estimated using the $M_{12\mu\mathrm{m}}$ luminosity-star formation rate relation of Wen et al. (2014), which is combined with inclination-corrected SDSS r-band petrosian half-light radii to calculate star formation rate surface density. The metal-dust fraction f is estimated as 0.5, and the dust opacity (assuming u band) is taken from Li & Draine (2001). The above calculation returns the average optical depth inside the half-light radius for our galaxies; we convert this to a central optical depth for input to the radiative transfer models we use below by assuming an exponential profile for the stellar and dust disks, which results in a conversion factor of $\tau_{\mathrm{central}} \approx 2.8\,\tau$.

Using these scaling relations, we can estimate a face-on dust optical depth for each galaxy in our sample, which is shown in Fig. 4.3. One can see that, as expected from the scaling relations in our model, the optical depth is higher for the more actively star-forming bins and for the most massive bins, and within each bin the optical depth is higher for the smaller galaxies where the dust is more concentrated. However, while the optical depth is physically meaningful and informative, the observations we wish to compare with are the face-on galaxy color and face-on to edge-on relative attenuation. These measurements depend on the optical depth but are not identical to it, and as we have seen this relationship can be complex.

As such, we combine our optical depth estimates with the dust attenuation radiative transfer models of Tuffs et al. (2004) to predict face-on and edge-on dust attenuations for each of our galaxies. Their model consists of a galaxy containing thick and thin double exponential stellar disks, each with an associated dust component (diffuse only for the thick disk, diffuse plus clumpy for the thin disk), plus a dust-free flattened de Vaucouleurs bulge. Their radiative transfer model then predicts the attenuation (due to both absorption and scattering) suffered by each of the three stellar components individually, for a variety of viewing angles and dust densities (parameterized by the central face-on dust optical depth). For our model we use our predicted dust optical depths for each galaxy to set the dust density in the radiative transfer models, and then use their derived face-on and edge-on disk

and bulge attenuations to construct a predicted relative attenuation for that galaxy.

However, the geometry of the Tuffs et al. model is not appropriate for all galaxies – specifically, ellipticals and disks with large bulges – as it consists of a star+dust disk with a relatively small, deeply embedded bulge. As such we modify the attenuation predictions, reducing the edge-on bulge attenuation for more bulge-dominated galaxies by replacing it with a linear combination of the face-on and edge-on bulge attenuations based on bulge-to-disk ratio. For galaxies with $B/T \geq 0.6$ the edge-on bulge attenuation is completely replaced by the face-on attenuation, which more or less correctly treats the diffuse dust present in the highly or fully bulge-dominant quiescent elliptical populations. For galaxies with $0 \leq B/T < 0.6$ the predicted edge-on bulge attenuation is gradually phased in (e.g. at 50% for a galaxy with $B/T = 0.3$), which approximately mimics the expected reduction in relative attenuation as physically larger bulges begin to significantly protrude above and below the dust disk. This is necessarily a somewhat ad-hoc correction, necessitated by the limited geometry of the radiative transfer model. However, it is required to plausibly capture the physical behavior we expect, and as we will see below it produces predicted relative attenuations that match the patterns we observe in the data.

Relative to our previous models in chapter 2, the model used in this chapter incorporates updated estimates of stellar mass, applies inclination corrections to the radii used, uses an improved translation from predicted optical depth to the parameters of Tuffs et al. (2004)'s models, and has a somewhat less aggressive scheme for reducing the edge-on bulge attenuation in disk galaxies.

Using this, we can predict the average face-on color and the relative face-on to edge-on attenuation as a function of $M_{3.4\mu\mathrm{m}}$, [12]–[3.4], x_{50}, and c_x. Figs. 4.4 and 4.5 show the results of this model, presented in the same manner and using the same binning scheme as in the previous section. One note is that the models predict face-on attenuation rather than face-on color. However, as each sub-bin consists of galaxies with the same stellar mass and specific star formation rate, to first order all of the galaxies in that bin should have the same *intrinsic*

face-on color; thus, the observed variations in face-on color across the bin must be due to the varying face-on attenuation. Therefore we fit a constant offset to each bin, effectively marginalizing over the nuisance parameter of the intrinsic face-on color (which arises from stellar populations) in order to focus on the predicted variation in color with structure (due to the dust effects we study); the plotted color is this constant face-on color offset plus the predicted face-on attenuation, for comparison to our observations.

One can see that overall there is surprisingly good agreement between these models and our observations. The predicted relative attenuation slopes for fully quiescent galaxies (panels a–c) are all notably too large, but inaccuracies in this area are not surprising as the attenuation model is intended for disk galaxies rather than bulge-dominated ones. The mostly quiescent galaxies (panels d–f) show a similar slight overprediction of measured relative attenuation, but the patterns of variation within each bin do match those present in the data. Meanwhile, for the moderately starforming (panels g–j) and strongly starforming (panels k–n) galaxies, both the overall size of the predicted relative attenuation and the patterns within each bin match quite well. Notably, the models are able to reproduce the pattern of variation seen in some bins of the relative attenuation first increasing and then decreasing again as one moves from the largest and least concentrated galaxies to the smallest and most concentrated. Interestingly, this is only the case with the bulge attenuation correction described above – models that lack this correction do not reproduce the observed patterns of attenuation.

Similarly, there is very good agreement between the predicted face-on colors and the observed ones. While the normalization of the intrinsic face-on color offset in each bin is fit to the data, the patterns within each bin match the data almost perfectly, notably reproducing the observed strong dependence of face-on color on size across most of the parameter space.

It is worthy of note that this agreement arises with very little fine-tuning of the models required. The scaling relations are among the simplest possible ways to predict dust optical depth from the observed galaxy properties, and the radiative transfer models are relatively

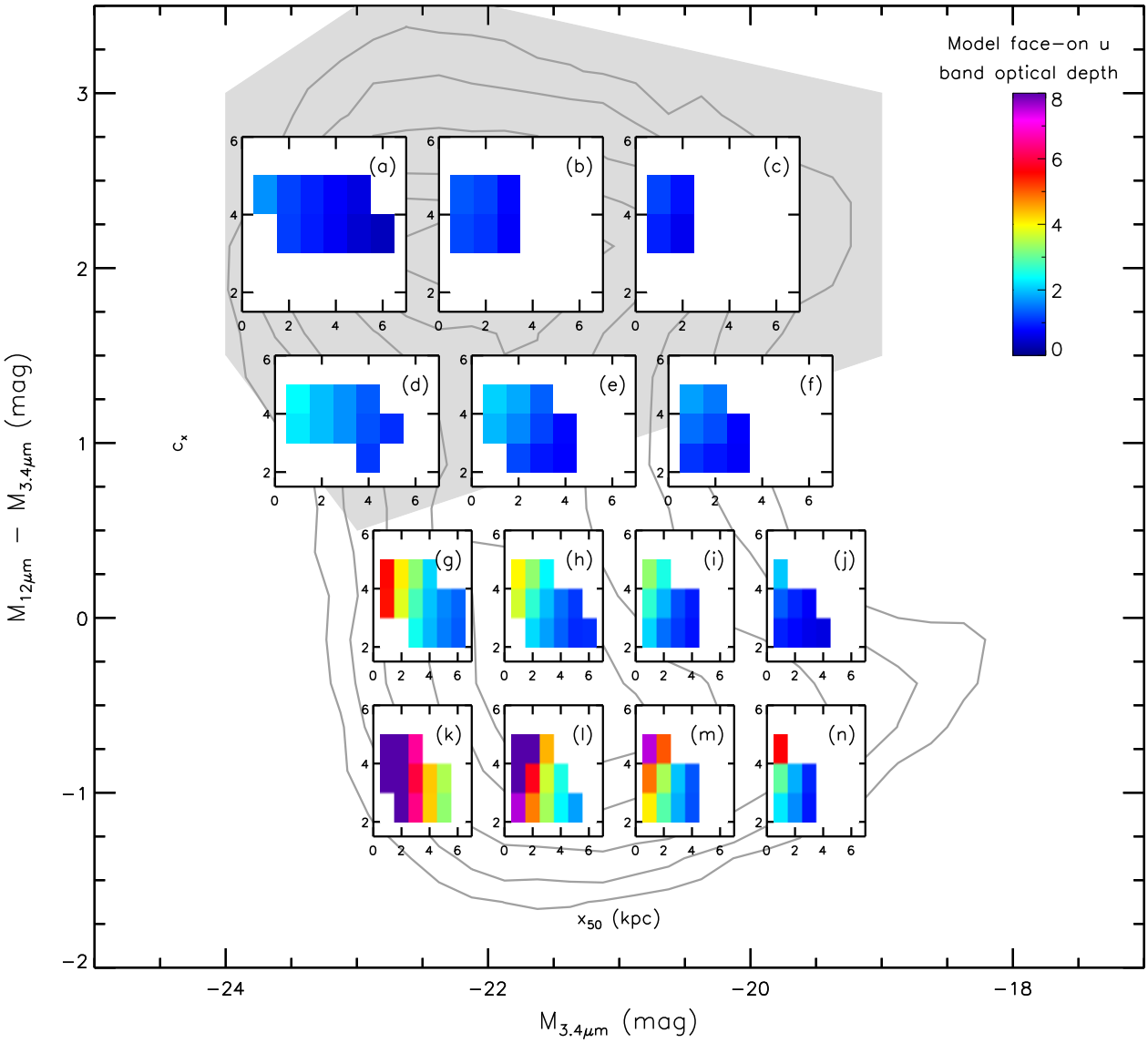

Figure 4.3: Model face-on optical depth as a function of specific star formation rate, mass, size, and concentration. Background contours show distribution of galaxies in [12]–[3.4] and $M_{3.4\mu\mathrm{m}}$. Each inset panel shows the model face-on optical depth (denoted by color) as a function of c_x and x_{50} for a subsample of galaxies at that location in the [12]–[3.4] - $M_{3.4\mu\mathrm{m}}$ parameter space.

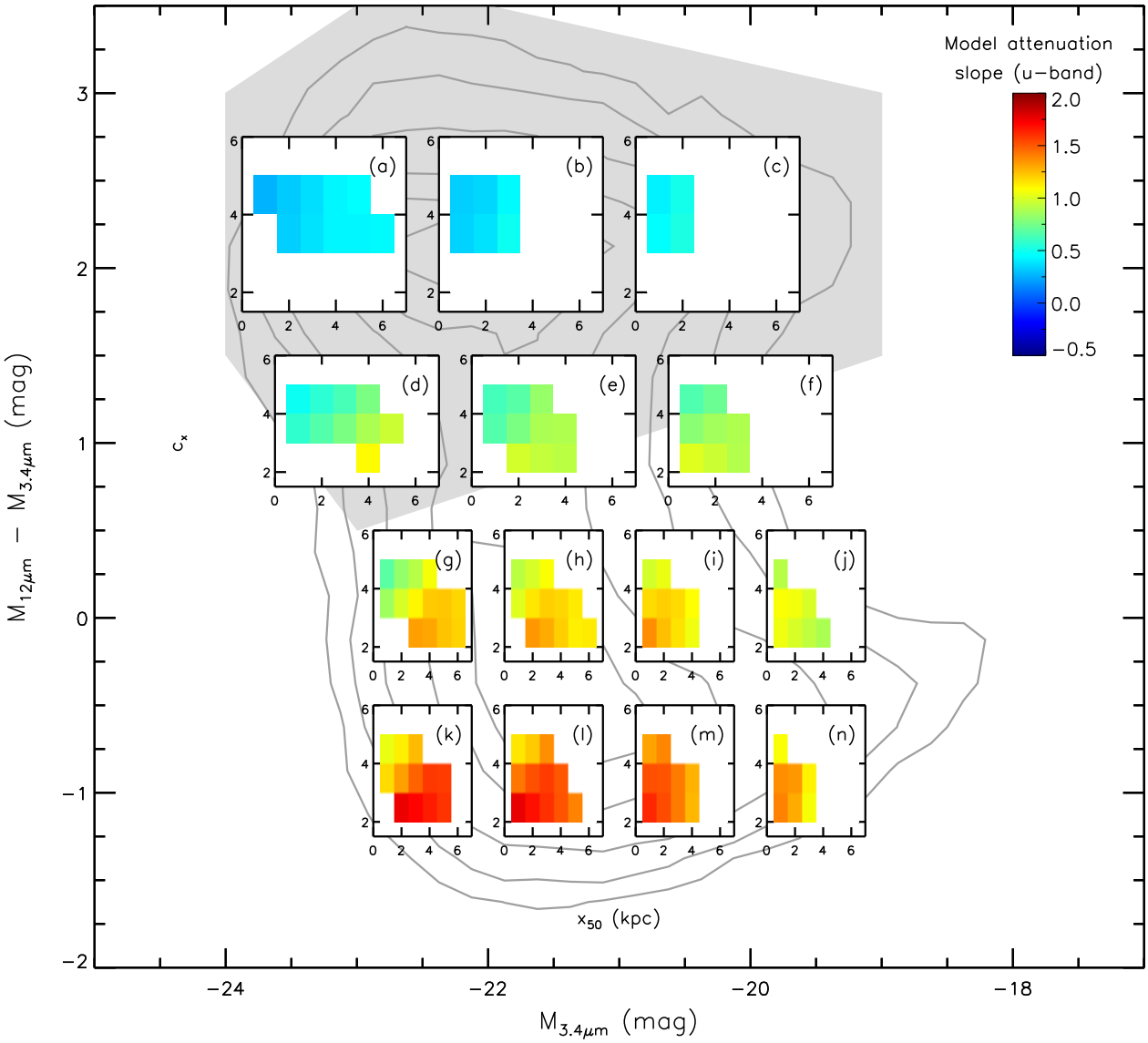

Figure 4.4: Model relative attenuation slope as a function of specific star formation rate, mass, size, and concentration. Background contours show distribution of galaxies in [12]–[3.4] and $M_{3.4\mu m}$. Each inset panel shows the model relative attenuation slope (denoted by color) as a function of c_x and x_{50} for a subsample of galaxies at that location in the [12]–[3.4] - $M_{3.4\mu m}$ parameter space.

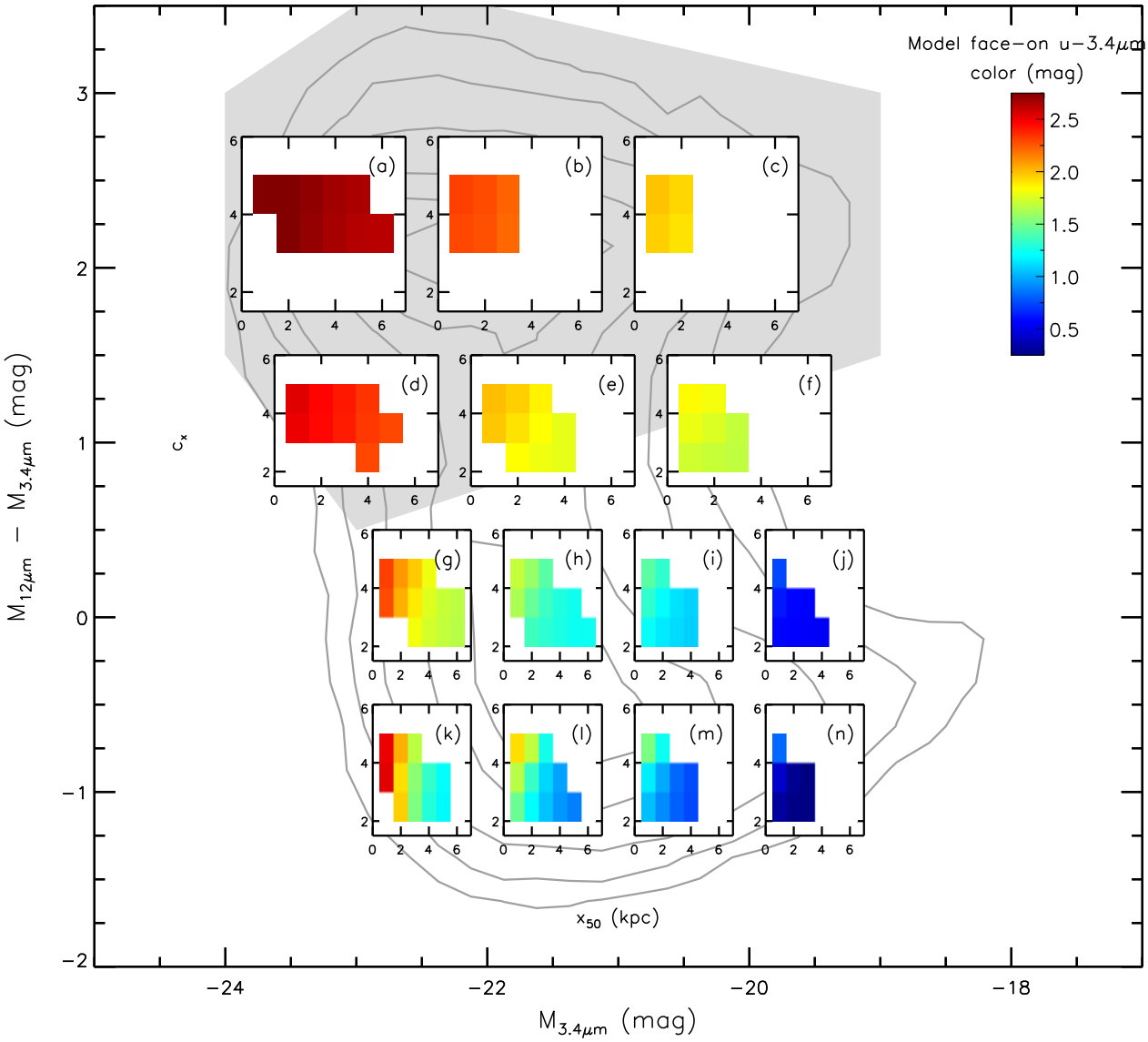

Figure 4.5: Model face-on color as a function of specific star formation rate, mass, size, and concentration. Background contours show distribution of galaxies in [12]–[3.4] and $M_{3.4\mu\mathrm{m}}$. Each inset panel shows the model face-on color (denoted by color) as a function of c_x and x_{50} for a subsample of galaxies at that location in the [12]–[3.4] - $M_{3.4\mu\mathrm{m}}$ parameter space.

simple as well. There are only two real free parameters in this model – first, the combination of the metal-dust fraction in the calculation of dust optical depth and the translation from average optical depth to the central optical depth required for input into the radiative transfer model, which combine into a single simple multiplicative factor, and second, the scheme for correcting the bulge attenuation based on B/T ratio – and neither of these require the assignment of implausible values in order to reproduce the data quite well. In short, it seems quite likely that the models are correctly capturing the basic physics behind the patterns we see in the data.

4.4 Discussion

The good agreement between the models and data gives us confidence that we can use our models to gain some insight into the physical causes of the patterns seen in the data. By examining the physical dependencies of the model, we can build a conceptual framework to explain the observations we make. For our model, in addition to the physical scaling relations themselves this framework rests on four key concepts:

1. Dust optical depth depends on dust *surface density*, not solely on the absolute quantity of dust present.

2. Dust attenuation depends on dust optical depth in a non-linear fashion, particularly when combined with the effects of galaxy geometry and viewing angle.

3. The varying relative geometry of dusty (disk) and dust-free (bulge) portions of a galaxy affects how much of a galaxy's light is subject to both attenuation in general and *varying* attenuation with viewing angle in particular.

4. The observations we make of *relative* attenuation depend not on the absolute amount of attenuation (at *any* particular orientation), but on the *difference* between the face-on and edge-on attenuation.

These scaling relations and principles, taken together, allow us to explain both the overall patterns in relative attenuation and face-on color as a function of MIR–NIR color and NIR luminosity as well as the variations as a function of concentration and size. In particular, if one compares Fig. 4.3 with Figs 4.1 and 4.4, it becomes apparent that the relative attenuation does not correspond directly to the optical depth, both between bins and within individual bins – in some cases increasing optical depth corresponds with increasing relative attenuation, but in other cases increasing optical depth corresponds with *decreasing* relative attenuation. This complex behavior demands explanation.

For some regions of parameter space, relative attenuation increases with increasing optical depth. For example, relative attenuation is observed to increase with decreasing MIR–NIR color. Dust density depends on gas density, which correlates with star formation rate density, and so galaxies with more negative MIR–NIR color (a measure of specific star formation rate) will have higher dust optical depths (as can be seen in Fig. 4.3) and, all other properties equal, would be expected to have higher relative attenuation. Similarly, for less luminous star-forming galaxies, relative attenuation is observed to increase with increasing luminosity. For a given specific star formation rate and gas density, the dust density will depend on the metallicity, which increases for more massive galaxies. Therefore, more luminous (and therefore massive) galaxies will have higher dust optical depths (as can also be seen in Fig. 4.3) and, all else equal, higher relative attenuation.

On the other hand, for some regions of parameter space the relative attenuation decreases with increasing optical depth. For more luminous star-forming galaxies the relative attenuation is observed to decrease with increasing luminosity after it reaches its maximum at intermediate luminosities, even though the overall dust density is still increasing due to increasing mass and metallicity as we can see in Fig. 4.3. Furthermore, for star-forming galaxies, within a given bin of MIR–NIR color and NIR luminosity the relative attenuation is observed to vary with structure in a complex fashion, frequently (though not always) declining for the smallest and most concentrated galaxies even though these galaxies can be

seen in Fig 4.3 to have the highest dust densities. This seemingly counter-intuitive behavior of the relative attenuation decreasing for the galaxies with the highest dust densities can be explained in terms of a combination of the points above.

As dust optical depth increases, our views of edge-on galaxies change in a different manner than our views of face-on galaxies (point 2). Due to the long path lengths through the disk, an edge-on galaxy rapidly becomes optically thick for even a moderate density of dust. Therefore, the observed edge-on attenuation increases rapidly with increasing dust density at first, but once the galaxy has become strongly optically thick adding even more dust does not further increase the attenuation nearly so dramatically – it's *already* optically thick, so the attenuation increases only slowly. Meanwhile, a face-on galaxy remains mostly optically thin for moderate densities of dust, so the observed face-on attenuation does not increase quickly with increasing dust density – it only becomes optically thick and highly attenuated for quite high densities of dust, and the increase in attenuation with increasing dust density is always gradual. Therefore, while attenuation increases with dust density for both edge-on and face-on galaxies, the rate and behavior of that variation is quite different between the two. This is significant because the *relative* attenuation we measure is the *difference* between these two measures (point 3). For very low dust densities, both the edge-on attenuation and the face-on attenuation are low, and so the difference between them is small. For intermediate dust densities, the edge-on attenuation is high and the face-on attenuation is still low, so the difference between them is large. However, in the transition from intermediate to *high* dust densities, the edge-on attenuation no longer increases dramatically – rather, it increases at a similar rate as the face-on attenuation. Therefore, for the dustiest galaxies the *difference* between the two (and so the measured *relative* attenuation) saturates and ceases to increase, *even though the absolute attenuation is still increasing.* This effect is illustrated in Fig. 4.6, which shows predicted face-on and edge-on attenuations as a function of face-on optical depth for an example galaxy in our model. One can see that the difference between these attenuations no longer increases once the optical depth becomes high.

In addition to this effect, the geometry of the bulge and disk and the relative distribution of light between these components also plays an important role. The bulge is located at the center of the stellar disk, where the associated dust is densest, and so in the face-on orientation the bulge light suffers from greater attenuation than the disk light. As such, galaxies with higher bulge to total ratios suffer from greater overall face-on attenuation for a given overall dust density. However, as the size and prominence of the bulge increases, it increasingly protrudes above and below the star and dust disk. Thus, for these galaxies more of the bulge's light does not change in attenuation with inclination, as it originates from stars lying either completely behind or completely in front of the dust disk. Therefore, galaxies with higher bulge to total ratios do not have their attenuation increase as dramatically with increasing attenuation for a given overall dust density. As the relative attenuation is the difference between the face-on and edge-on views, this effect acts to lower the relative attenuation. Fig. 4.6 also illustrates this effect; the solid lines show the model predictions for a galaxy with a B/T ratio of 0.15, while the dashed lines show the model predictions for a B/T ratio of 0.4. One can see that the galaxy with the larger bulge suffers from a greater face-on attenuation but a lower edge-on attenuation, and therefore a lower relative attenuation. We note that the bulge attenuation correction that leads to this effect is a 'by hand' addition to the radiative transfer model, but it is not an artificial or implausible correction in the sense that it is physically motivated and leads to a very good agreement of our models with the data, and so therefore we believe this interpretation to be reasonable.

The combination of these two effects can explain the variation of the relative attenuation with luminosity and with structure for star-forming galaxies. As luminosity increases, overall dust content also increases due to increasing metallicity. The relative attenuation increases with increasing luminosity at first, but after intermediate luminosities it saturates and ceases increasing due to the radiative transfer effects described above. One can see in Fig. 4.6 that the saturation occurs beyond a face-on optical depth of roughly 3–4; this corresponds to green–yellow and redder colors in Fig. 4.3, which dominate the brighter bins. Simultaneously,

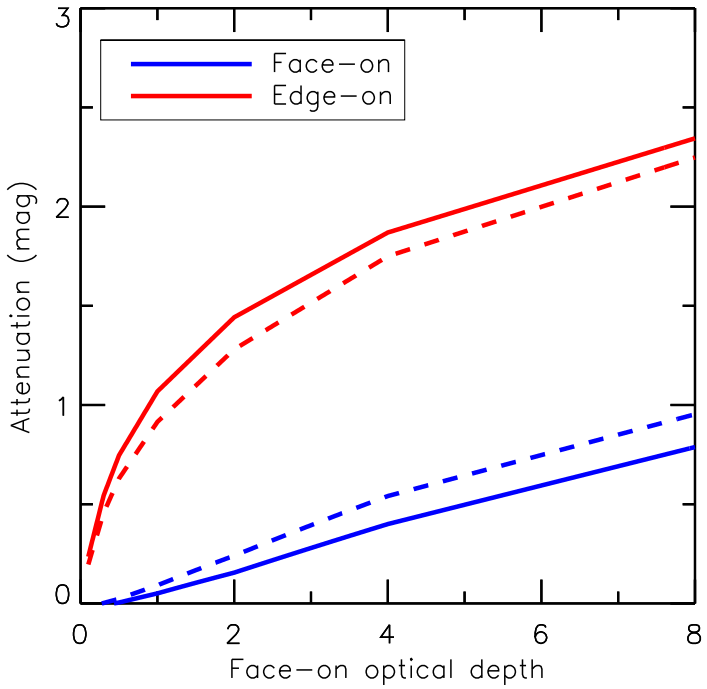

Figure 4.6: Predicted model attenuation as a function of galaxy face-on optical depth for an example galaxy in our models. Blue lines show the face-on attenuation, while red lines show the edge-on attenuation. Solid lines are for a model galaxy with B/T = 0.15, while dashed lines are for a model galaxy with B/T = 0.4.

the average bulge prominence of star-forming disk galaxies also increases with increasing luminosity. Fig. 4.7 illustrates this, showing the average B/T ratios of our sample divided in the same binning scheme as used throughout this chapter. One can see that the brighter bins along the star-forming main sequence (bins h, i, and especially g and k) have significantly higher B/T ratios than the less luminous bins. Therefore, with the relative attenuation saturated and no longer increasing with increasing face-on optical depth, the geometry effects described above cause the relative attenuation to decrease again in the highest luminosity bins.

Similarly, within each individual bin of MIR–NIR color and NIR luminosity there is also a variety of dust densities and structures present. While the star formation rate is fixed within each bin, the dust *density* will vary significantly with varying size across the bin, simply due to the dust content being spread out over a larger or smaller area. Thus, the larger galaxies will have lower dust densities and the smaller galaxies will have higher dust densities, and each bin will repeat in miniature portions of the same pattern of increasing and then decreasing relative attenuation with increasing dust density. For bins with an overall lower dust content, such as the lower luminosity bins, as can be seen in Fig 4.3 the relative attenuation will either not saturate or will only somewhat saturate. These bins thus show a pattern of relative attenuation either increasing for the smaller galaxies with higher dust densities, or remaining relatively constant with size while decreasing for the most concentrated galaxies due to the bulge effects. For bins with overall higher dust content, such as the highest luminosity bins, the relative attenuation saturates easily as the size decreases and dust density increases, and thus these bins have the relative attenuation decreasing significantly for the smallest and most concentrated galaxies as the geometric bulge effects take over.

In contrast to the complex variations in relative attenuation, the variation in face-on color is rather simpler to explain. Overall face-on color is observed to vary with both MIR–NIR color and NIR luminosity, becoming redder for the more luminous and less star-forming bins.

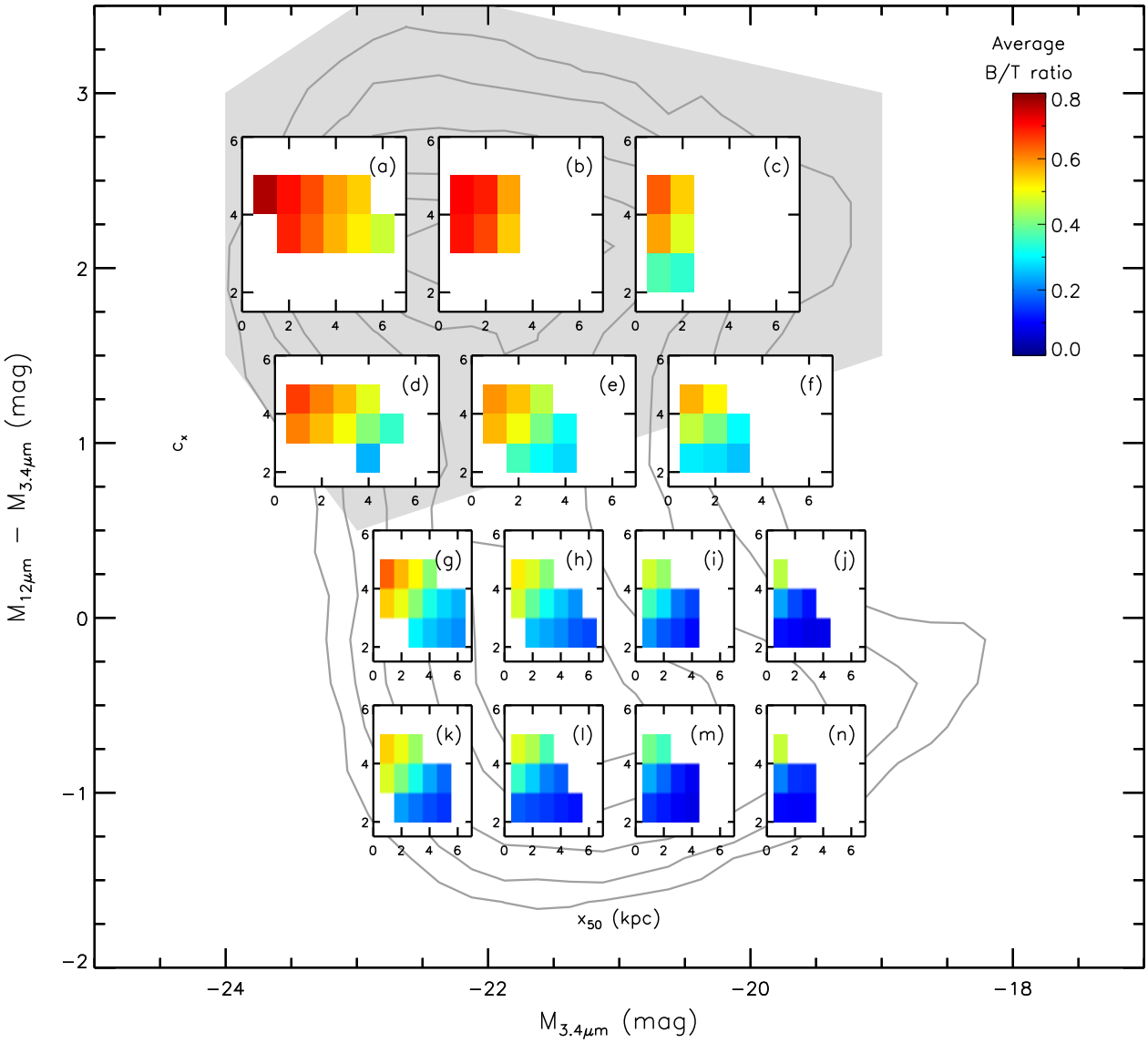

Figure 4.7: Bulge to total ratio as a function of specific star formation rate, mass, size, and concentration. Background contours show distribution of galaxies in [12]–[3.4] and $M_{3.4\mu\mathrm{m}}$. Each inset panel shows the bulge to total ratio (denoted by color) as a function of c_x and x_{50} for a subsample of galaxies at that location in the [12]–[3.4] - $M_{3.4\mu\mathrm{m}}$ parameter space.

This is not included in our model, as it is mostly due to stellar population variations that our model does not cover. Metallicity increases with increasing luminosity, which results in redder stellar population colors, while the less starforming galaxies have older, and hence also redder, stellar populations.

For essentially all galaxies except the most luminous and least starforming quiescent galaxies, within a given bin of MIR–NIR color and NIR luminosity the face-on color is observed to depend quite strongly on size, with smaller galaxies quite consistently showing redder colors. The stellar populations (and thus, intrinsic face-on colors) within each bin should be identical, so these variations must be driven by varying attenuation. This is a relatively straightforward consequence of the dependence of attenuation on dust density – as above, the total amount of star formation within each bin is relatively fixed, and so the dust density will vary significantly with size. This can be seen quite clearly in Fig 4.3. The overall patterns are simpler than those of the relative attenuation, as the face-on color is only dependent on the face-on attenuation rather than on the difference between the face-on and edge-on attenuation. Thus, we simply observe increasing face-on attenuation, and therefore redder face-on color, as dust density increases due to decreasing galaxy size.

4.5 Conclusions

Using our ability to make inclination-independent measurements of the structural properties of galaxies, we expand our study of the dependence of relative attenuation on galaxy properties to cover the full four-dimensional parameter space of galaxy specific star formation rate, stellar mass, size, and central concentration. We also expand this study to consider both relative attenuation and the observed face-on optical–NIR color.

In addition to the previously observed patterns of relative attenuation increasing with increasing specific star formation rate, and being the strongest for intermediate luminosity galaxies for the star-forming galaxies that have significant relative attenuation, we observe that for galaxies of a given star formation rate and mass the relative attenuation depends

significantly on size and concentration in a complex manner. For more luminous galaxies with significant relative attenuation, the relative attenuation is stronger for larger and lower concentration galaxies, while for the less luminous galaxies the relative attenuation is strongest at intermediate sizes. Meanwhile, we observe that face-on color varies significantly with mass and specific star formation rate, becoming redder with increasing mass and with decreasing star formation rate. We also observe that for galaxies of a given star formation rate and mass, face-on color is a strong function of galaxy structure. For almost all galaxies, there is a strong trend towards redder colors with decreasing size, with an additional slight bias towards redder colors with increasing concentration.

We implement scaling-relation based models similar to those of chapter 2 to predict the dust optical depths and relative attenuations of the galaxies in our sample. These models parameterize the dust density in terms of galaxy metallicity (derived from stellar masses) and gas density (derived from 12μm-based star formation rate densities using the Kennicutt-Schmidt relation), and convert dust optical depths into relative attenuations using a radiative transfer model that models both bulge and disk attenuations. We find that our models are capable of reproducing the observed trends in face-on color and relative attenuation remarkably well throughout our full parameter space with almost no fine-tuning. The good agreement between our models and data suggests that the dust content of galaxies can indeed be understood as a simple product of metallicity and gas content, as well as reinforcing the general geometric model of a dust/stellar disk combined with a bulge that protrudes from the disk to a degree which depends on bulge-to-total ratio. Our models also suggest that the face-on color of galaxies is strongly affected by dust attenuation, as well as showing that the relative attenuation does not directly vary with dust optical depth, but rather is a complex non-monotonic function of both optical depth and star-dust geometry.

CHAPTER V

Inclination dependence of traditional galaxy structures and other optical measurements

Preface

This chapter was originally published in the *Monthly Notices of the Royal Astronomical Society Letters*, Vol 468L, 31 (Devour & Bell, 2017), under the title *Revealing strong bias in common measures of galaxy properties using new inclination-independent structures*, coauthored with Eric Bell. Portions of this chapter overlap substantially with portions of chapter 3, but in the interests of retaining consistency with the published version I have not modified these portions. The only alteration from the published version is the restoration of Fig. 5.5 and accompanying text, which were originally cut for space reasons.

Abstract

Accurate measurement of galaxy structures is a prerequisite for quantitative investigation of galaxy properties or evolution. Yet, the impact of galaxy inclination and dust on commonly-used metrics of galaxy structure is poorly quantified. We use infrared datasets to select inclination-independent samples of disc and flattened elliptical galaxies. These samples show strong variation in Sérsic index, concentration, and half-light radii with inclination. We develop novel inclination-independent galaxy structures by collapsing the light distribution

in the near-infrared onto the major axis, yielding inclination-independent 'linear' measures of size and concentration. With these new metrics we select a sample of Milky Way analogue galaxies with similar stellar masses, star formation rates, sizes and concentrations. Optical luminosities, light distributions, and spectral properties are all found to vary strongly with inclination: when inclining to edge-on, r-band luminosities dim by >1 magnitude, sizes decrease by a factor of two, 'dust-corrected' estimates of star formation rate drop threefold, metallicities decrease by 0.1 dex, and edge-on galaxies are half as likely to be classified as star forming. These systematic effects should be accounted for in analyses of galaxy properties.

5.1 Introduction

An accurate understanding of galaxy structure – the physical, three-dimensional distribution of light and/or mass – is a cornerstone of the study of galaxies. Apart from their purely descriptive value, the structures of galaxies give insight into a range of physical ingredients and processes. Galaxy sizes and brightness profiles encode angular momentum content and its evolution (e.g. Mao et al. 1998; van den Bosch et al. 2001). Galactic structure correlates with the orbital structure of stars in galaxies and thus captures the demographics of rotation-supported and dispersion-supported galaxies (van der Wel et al., 2009b). Galaxy structure correlates strongly with star formation history (e.g. Kauffmann et al. 2003b; Franx et al. 2008). Redshift evolution of the mix of galaxy structures quantifies disc and spheroid growth (van der Wel et al., 2014b), changes in the merger rate (Jogee et al., 2009), and the emergence of quiescent galaxies (e.g. Bell et al. 2012; Lang et al. 2014b). As such, the astronomical community has devised many types of structure measurements – e.g., Sérsic index (Sérsic, 1963), concentration (Strauss et al., 2002), f_{DeV} (Abazajian et al., 2004), and bulge-to-disc or bulge-to-total ratios (de Jong, 1996a).

Ideally a structural measurement should provide an unbiased description of a galaxy's light distribution. Yet, the projection of the light distribution onto the plane of the sky is a central challenge. Inclination differences lead to the same galaxy being mapped onto differ-

ent two-dimensional projections owing both to geometry and varying dust attenuation with inclination. Unless structural measurements are designed to be viewing angle-independent, this will lead to inclination dependence in these measurements. Radiative transfer models suggest that structural measures should be wavelength and inclination-dependent (e.g. Möllenhoff et al. 2006; Pastrav et al. 2013b), in accord with measurements of more concentrated light profiles at longer wavelengths for dusty galaxies (e.g. Vulcani et al. 2014). Unfortunately, the *inclination*-driven biases of many commonly-used structural metrics are currently poorly understood.

The goal of this chapter is to quantify the inclination dependence of commonly-used structural measurements and illustrate the impact of these systematic effects on our understanding of galaxy properties. We use inclination-independent metrics to select samples of similar galaxies, revealing that common structural measurements systematically vary with inclination for a variety of galaxy types (§5.2). In §5.3 we introduce a novel *inclination-independent* technique for measuring galaxy structures. In §5.4 we use these new measures to select an inclination-unbiased sample of Milky Way analogs and quantify the inclination dependence of their SDSS optical catalog quantities. All magnitudes are in the AB system, all logarithms are base-10, and where necessary we assume $\Omega_M = 0.3$, $\Omega_\Lambda = 0.7$, and $H_0 = 70$ km s^{-1} Mpc^{-1}.

5.2 Widely-used structural metrics are biased by inclination

Our analysis technique is conceptually simple. Using a sample of intrinsically similar galaxies observed from a variety of viewing angles, one can measure how galactic properties vary with inclination. Since the galaxies are intrinsically similar, differences between edge-on and face-on measures represent systematic errors due to dust and geometry. This method is used widely to measure the attenuation of galaxy luminosity with inclination (e.g. Tully et al. 1998; Devour & Bell 2016); our use of it to explore the inclination dependence of galaxy structures and other properties is relatively novel.

This method requires that the metrics used to select the 'intrinsically similar' galaxies do not depend on inclination. If an inclination-dependent metric (e.g., attenuation-dependent optical luminosity) is used to select similar galaxies, then the low and high inclination members of that sample are substantially different galaxies. Therefore, the critical challenge is to devise selection metrics which are inclination-independent. We briefly review such a selection and its properties here; for full discussion see Devour & Bell (2016).

Our initial galaxy sample consists of the crossmatch of all galaxies with both elliptical aperture photometry from the Wide-field Infrared Survey Explorer (WISE; Wright et al. 2010) and spectroscopic redshifts from the Sloan Digital Sky Survey (SDSS) DR10 (Eisenstein et al. 2011, Ahn et al. 2014). We then select galaxies based on their WISE elliptical aperture W1 (3.4μm; henceforth $M_{3.4\mu\mathrm{m}}$) absolute magnitudes and WISE W3–W1 (12μm − 3.4μm) colours (henceforth [12]–[3.4]), as illustrated in Fig. 5.1. Dust attenuation at these wavelengths is small, < 0.1 mag attenuation between edge-on and face-on (Devour & Bell, 2016). Dust emission at 3.4μm is also small, and variations in stellar M/L are expected to be no more than 0.3 dex (Meidt et al., 2014), so $M_{3.4\mu\mathrm{m}}$ luminosity is a reasonable proxy for stellar mass. Meanwhile, 12μm emission arises from warm dust and PAH molecules (Calzetti, 2013), and for star forming galaxies tracks overall star formation rate to within $\sim$0.1 dex (Wen et al., 2014), making [12]–[3.4] colour a good proxy for star formation rate (SFR) per unit stellar mass (specific SFR).

We adopt the r-band disc inclinations from the two-component Sérsic models of Simard et al. (2011) to derive axis ratios a/b. For intrinsically flattened galaxies (like the ones examined here) the axis ratio is a direct proxy for inclination, particularly as these model fit axial ratios account for the presence of a bulge in disc galaxies (which would otherwise increase the measured axis ratio). Ideally one would use a near-infrared axis ratio measurement to avoid any possible dust effects; in practice the axis ratios of Simard et al. (2011) are the best currently available. (For full discussion of the suitability of this metric, see Devour & Bell 2016.)

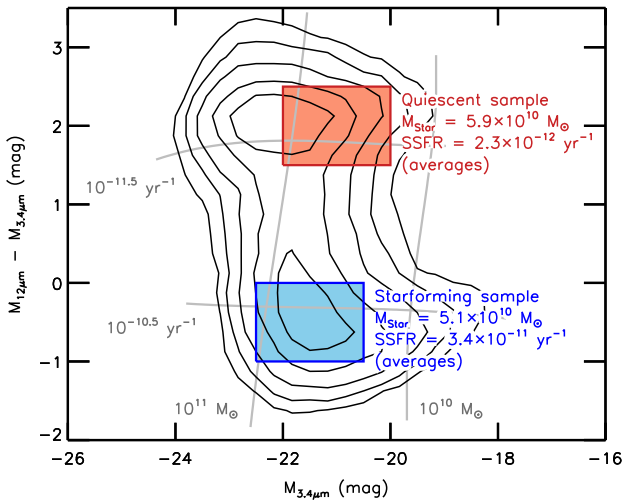

Figure 5.1: Contours show the distribution of galaxies in $M_{3.4\mu\mathrm{m}}$ - [12]–[3.4]. Gray lines and labels show approximate values of stellar mass and specific SFR. Colour insets show the locations of our quiescent and star-forming samples and their average properties.

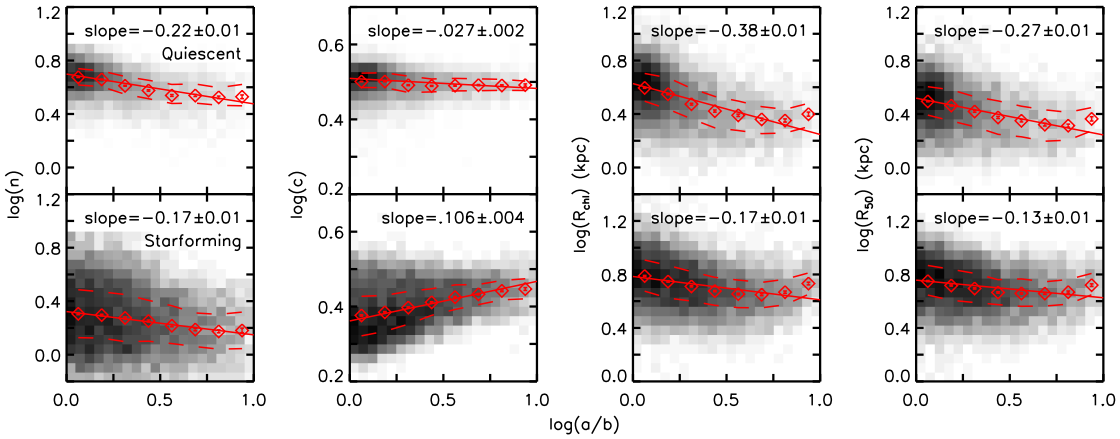

Figure 5.2: Trends in structural parameters and sizes with $\log_{10}(a/b)$ for quiescent (top) and star-forming (bottom) disc galaxies. From left to right: Sérsic index n, circular concentration c, Sérsic fit circular half-light radius R_{chl}, and circular Petrosian half-light radius R_{50}. Diamonds and dashed lines show the sample median and interquartile range, and the solid line shows a linear fit to the running median.

By selecting galaxies as above (Fig. 5.1), we quantify how galaxy structure measurements vary with inclination for samples of intrinsically similar disc and flattened elliptical galaxies. We select star forming galaxies to have $-22.5 \leq M_{3.4\mu\mathrm{m}} \leq -20.5$ and $-1.0 \leq [12]-[3.4] \leq 0$, corresponding to star forming main sequence galaxies with $3 \times 10^{10}\ M_{\odot} < M_{*} < 6 \times 10^{10}\ M_{\odot}$. Our quiescent sample has $-22.0 \leq M_{3.4\mu\mathrm{m}} \leq -20.0$ and $1.5 \leq [12]-[3.4] \leq 2.5$, corresponding to discy quiescent galaxies with $4 \times 10^{10}\ M_{\odot} < M_{*} < 8 \times 10^{10}\ M_{\odot}$. The parent sample contains 78,721 galaxies; these subsamples contain 7044 and 6239 galaxies, respectively, 75 per cent of which have $0.0279 \leq z \leq 0.0635$.

In Fig. 5.2, we show the variation with inclination (quantified by $\log_{10}(a/b)$) of r-band Sérsic indices n and circular half-light radii R_{chl} from the two-component Sérsic fits of Simard et al. (2011), and r-band concentrations c and Petrosian circular half-light radii R_{50} from SDSS. In each panel, we show the slope of a linear fit to the running median of that structural parameter with $\log_{10}(a/b)$; uncertainties in the slopes are calculated using bootstrap resampling.

Both Sérsic index and concentration strongly depend on inclination for star-forming disc galaxies, likely reflecting some combination of differential dust attenuation and geometric effects. Interestingly, Sérsic index also shows a strong dependence on inclination for the flattened quiescent (dust-free) galaxies. Concentration shows almost no trend with axis ratio for quiescent galaxies. Both Sérsic-derived half light radius R_{chl} and Petrosian half-light radius R_{50} vary significantly with inclination, decreasing significantly and then increasing slightly in size as galaxies tilt towards edge-on.

This is a major concern; commonly-used metrics of galaxy structure depend on inclination at a level comparable to the dispersion of structural metrics within a population.

5.3 Inclination-independent galaxy structural measurements

There are two primary obstacles to inclination-independent measurements of galaxy structure.

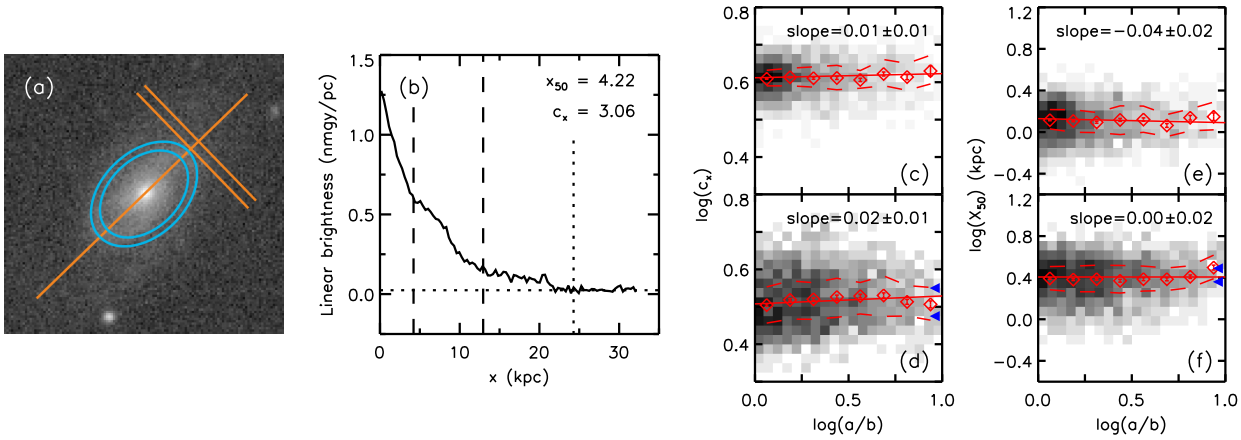

Figure 5.3: Panel a: K-band galaxy stamp, with example elliptical annulus and major axis cut. Panel b: Folded linear brightness profile and structural measurements. Dotted lines indicate the measured sky level and profile 'edge' location, and dashed lines indicate measured x_{50} and x_{90}. Panels c-f: Trends in linear concentration c_x (left) and linear half-light distance x_{50} (right) with $\log_{10}(a/b)$ for quiescent (top, panels c and e) and star-forming (bottom, panels d and f) disc galaxies. Diamonds and dashed lines show the median and interquartile range, and the solid line shows a linear fit to the running median. Blue carets in panels d and f bracket the c_x and x_{50} selections in §4.

The first is dust attenuation. Currently it is impossible to dust-correct the optical light distribution to the accuracy demanded by current analyses. Accordingly, we choose to analyze the galaxy structures in K band (2.2μm) from the UKIRT Infrared Deep Sky Survey (UKIDSS) Large Area Survey (Lawrence et al., 2007). Dust attenuation at K band is $1/5 - 1/3$ of the optical attenuation (depending on poorly-understood radiative transfer effects; Tuffs et al. 2004), and is generally < 0.3 mag even for nearly edge-on galaxies with high optical opacities; galaxies are therefore close to transparent across almost all viewing angles in K band, avoiding significant dust-induced inclination dependence.

The second obstacle is the differing projection suffered by face-on and edge-on galaxies. Many structural parameters are calculated using elliptical or circular apertures or annuli, as illustrated in Fig. 5.3 (blue rings in panel a). Circular annuli and apertures are obviously strongly affected by inclination, as the portions of a galaxy which are projected within a

circular aperture change dramatically with inclination. Elliptical annuli/apertures mitigate this obvious issue, but still suffer from inclination-dependent projection effects. An elliptical annulus only maps to a region of constant galactocentric radius in the limit of an infinitely thin disc. Towards larger inclination, an elliptical annulus becomes substantially more influenced by the vertical structure of a disc and mixes light from a variety of galactocentric radii (e.g. for a disc with an intrinsic $b/a = 0.1$ viewed from 60° inclination, an elliptical annulus mixes light from a range of radii corresponding to ∼35 per cent of its radial scale length). Furthermore, any variations in the vertical light profiles of galaxies will lead to further variation of structural measurements derived using elliptical annuli or apertures.

The issues with traditional metrics arise from the varying projection of light along the minor axis with inclination. Our technique sidesteps this issue. We take cuts parallel to the minor axis, collapsing all light down onto the major axis to form a *linear*, rather than radial, brightness profile, as illustrated in Fig. 5.3 (orange lines in panel a). This method has the decisive advantage that in the absence of dust attenuation it is inclination-independent *by construction*.

Each galaxy's linear brightness profile is folded across the centre, correcting for contamination and sky background. We then measure the 50 and 90 per cent distances (henceforth x_{50} and x_{90}) by analogy with r_{50} or r_{90} in circular or elliptical aperture photometry – these are the linear distances from the centre which contain 50 or 90 per cent of the total brightness. The linear concentration (henceforth $c_{\rm x}$) is then the ratio x_{90}/x_{50}, again in analogy to the traditional measurement. We illustrate this process in panel b of Fig. 5.3. The linear sizes x_{50} and concentrations $c_{\rm x}$ are then inclination-independent structural parameters. A full discussion of the process, uncertainties, and the galaxy parameter distribution is presented in chapter 3.

These parameters show little systematic dependence on inclination for either disc-dominated star forming or quiescent galaxies (Fig. 5.3, rightmost panels). A linear fit to the running median of $\log(c_{\rm x})$ or $\log(x_{50})$ (kpc) with $\log(a/b)$ gives variations between face-on and edge-

on of < 0.04 dex (c.f., variations of 0.1–0.4 dex for most widely-used galaxy structures in Fig. 5.2). The distributions of $c_{\rm x}$ and x_{50} appear noisier owing to smaller sample sizes, as only $\sim$30 per cent of our sample has UKIDSS imaging, but the *scatter* in $c_{\rm x}$ or x_{50} is comparable to the scatter in Sérsic index and concentration, or $R_{\rm chl}$ and R_{50}, respectively, for the same populations. Typical uncertainties in $c_{\rm x}$ and x_{50} are < 0.1–0.2 dex respectively, thus, much of the scatter in $c_{\rm x}$ and x_{50} in a given bin of WISE absolute magnitude and colour is intrinsic.

5.4 How does our view of Milky Way analogues vary with inclination?

With these inclination-independent structural metrics, we can sharpen our selection of intermediate-mass star-forming main sequence disc galaxies to also have a relatively narrow range in linear concentrations and sizes: we select galaxies to have $-22.25 \leq M_{3.4\mu{\rm m}} \leq -20.75$, $-1.0 \leq [12]-[3.4] \leq 0$, $0.475 \leq \log(c_{\rm x}) \leq 0.55$, and $0.36 \leq \log(x_{50})$ (kpc) ≤ 0.49. (The $c_{\rm x}$ and x_{50} limits are indicated in Fig. 3, and this selection is similar in [12]–[3.4] and slightly narrower in $M_{3.4\mu{\rm m}}$ than the star-forming sample depicted in Fig. 1.) The Milky Way's stellar mass and specific SFR have been estimated as roughly $M_* = 5 \times 10^{10}$ $M_\odot$ and SSFR $= 3 \times 10^{-11}$ yr^{-1} (Bland-Hawthorn & Gerhard, 2016), placing it within this bin (see Fig. 5.1). Thus, this sample consists of structurally average star-forming disc galaxies broadly similar in stellar mass and SFR to the Milky Way. Following Licquia et al. (2015), we refer to these as 'Milky Way analogues', but with the important advantages that this sample is also known to be structurally typical and is selected in a way that is insensitive to inclination and dust attenuation. With it, we can quantify how commonly-used optical SDSS metrics respond to inclination and dust for a sample of galaxies that are known to be intrinsically very similar to each other.

Fig. 5.4 shows our main results. In panel a, we see that the face-on members of our sample (bluer points) clearly fall within the star-forming 'blue cloud'. The more highly

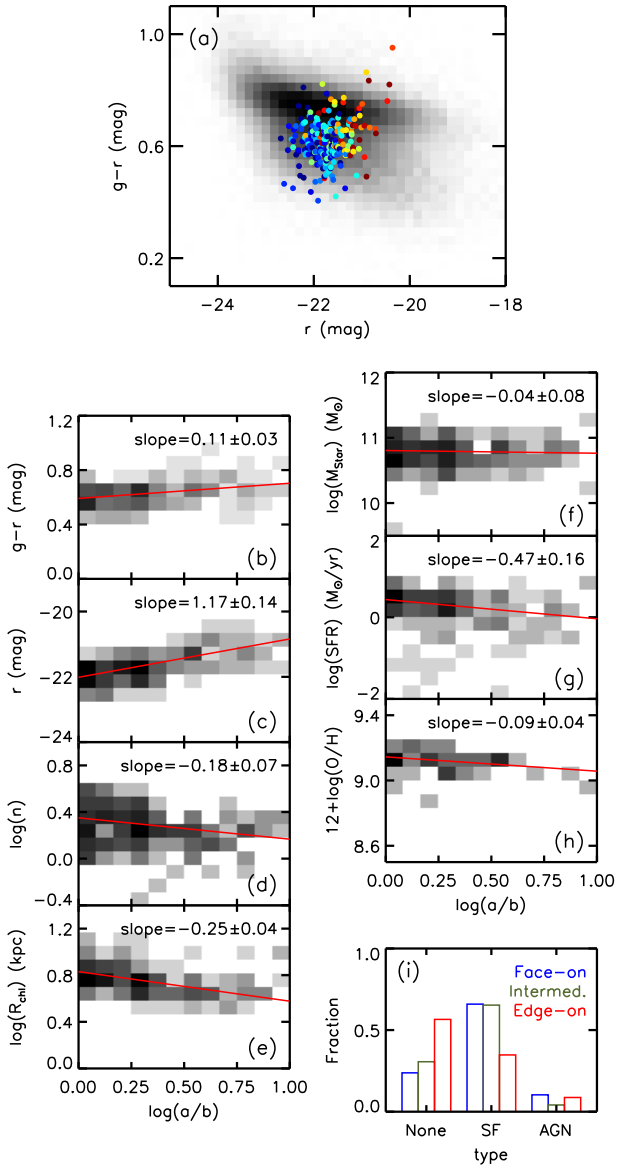

Figure 5.4: Panel a: Colour-magnitude diagram for the parent sample (grey histogram) and our sample of star-forming Milky Way analogue disc galaxies (overplotted points). Bluer colours show face-on galaxies and redder colours show edge-on galaxies. Panels b-e: Top to bottom, the distribution of our sample's g–r colours, r-band absolute magnitudes, Sérsic indices n, and circular half-light radii $R_{\rm chl}$ as a function of $\log(a/b)$. Panels f-i: Top to bottom, the distribution of our sample's SDSS estimates of stellar mass, optically-derived star formation rate, and metallicity as a function of $\log(a/b)$, and distribution of spectral classification for subsamples with low, moderate, and high inclination.

inclined members (redder points) become both redder and fainter, in some cases overlapping with the 'red sequence' of galaxies usually interpreted as quiescent. This variation in absolute magnitude and colour with axis ratio is quantified in panels b and c. Panels d and e confirm that SDSS optical structural measurements strongly depend on axis ratio, as foreshadowed in Figs. 5.1 and 5.2, and now verified and sharpened for a sample selected to have the same intrinsic light profiles. In panels f–i we show optical SDSS spectral line-derived galaxy properties: stellar mass, dust-corrected SFR, and metallicity from Kauffmann et al. (2003a), Tremonti et al. (2004), and Brinchmann et al. (2004), and spectral classification from Bolton et al. (2012). Stellar mass is not significantly affected by dust, as expected (Bell & de Jong 2001; Maller et al. 2009). In contrast, spectral line-based SFRs – meant to include dust corrections – emission-line derived metallicities, and spectral classifications all clearly vary with inclination for this sample of intrinsically similar galaxies. Optically-derived and 'dust-corrected' SFRs and spectral classifications are particularly strongly affected: SFRs for edge-on members of this sample appear to be only 1/3 of the SFRs of their face-on intrinsically similar counterparts, and edge-ons are only half as likely to be classified as star forming according to their emission line diagnostics.

To provide a visual illustration of the impacts of dust and inclination on this subsample, we show optical sdss gri-band (left column) and NIR UKIDDS K-band (right column) images of four representative galaxies in Fig. 5.5. These galaxies are chosen to lie along the best-fit trend of Sérsic index with axis ratio for this sample. The optical images appear to become less centrally concentrated and substantially redder as the galaxies move towards edge-on; the prominent bulges visible in the low-inclination members of the subsample are notably absent in their dust-reddened high-inclination counterparts. Importantly, the K-band images show distinct central brightness concentrations for all four galaxies. This difference is quantified using the structural measurements for these galaxies; those galaxies with obscured central regions in the optical show significantly lower Sérsic indices, while the IR-measured c_x shows no systematic trend with inclination.

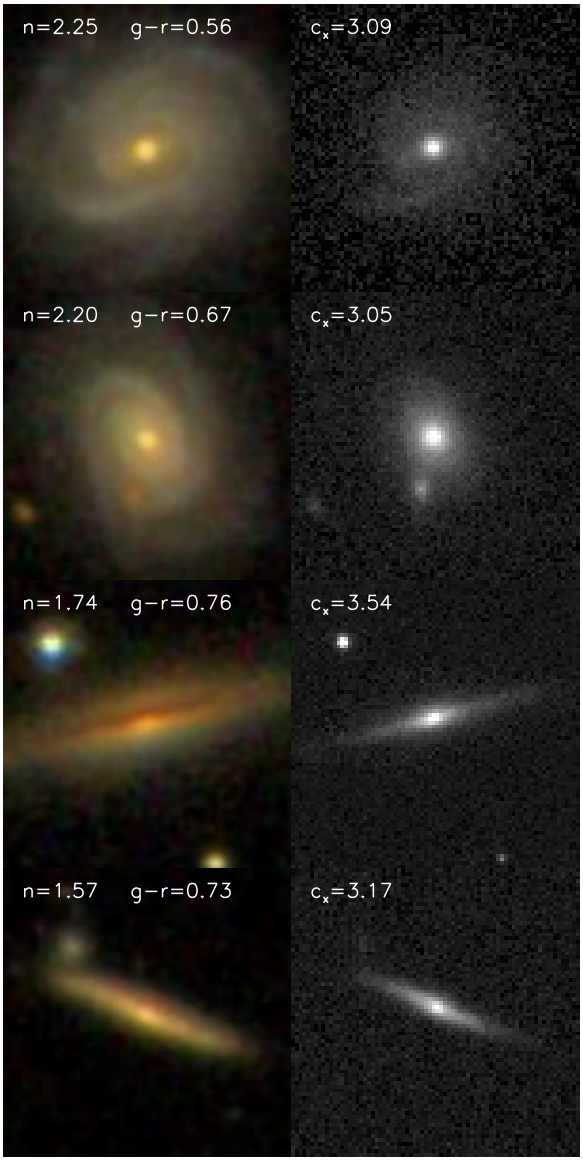

Figure 5.5: Optical sdss gri-band (left) and NIR UKIDDS K-band (right) images and measured optical colors and structural parameters for example representative galaxies from our sample.

The sample explored in Figs. 5.4 and 5.5 is selected to consist of intrinsically similar galaxies, with similar stellar masses, SFRs, sizes and concentrations, save for their viewing angles. And yet, *optical SDSS measurements of galaxy properties would conclude that the more edge-on members of this population are systematically dimmer, redder, less centrally concentrated, smaller, less actively star-forming, and lower metallicity than their face-on counterparts.* Optical observations of galaxy luminosities, light distributions, and spectral lines are all affected; it is clear that one cannot isolate samples of intrinsically similar galaxies for study without inclination-independent and IR-based selection tools.

5.5 Conclusions and outlook

In this chapter, we use inclination-independent infrared metrics to select samples of intrinsically similar star forming disc galaxies and quiescent galaxies. We show that traditional structural measurements suffer from severe inclination biases, showing variations from edge-on to face-on comparable to the spread of parameters within each population.

We present an alternative method for measuring structural parameters (the linear brightness profile) which is inclination independent by construction. When used with dust-penetrated NIR imagery, this technique gives inclination-independent measures of galaxy size and structure.

We then use our inclination-independent techniques to select a sample of star-forming disc galaxies with very similar intrinsic masses, SFRs, sizes and concentrations that are expected to be broadly similar to the Milky Way. While SDSS optical estimates of stellar mass are robust to inclination and dust effects, *measures of optical luminosity, colour, light profile shape, galaxy size, spectral classification, optically-derived 'dust-corrected' SFR and emission line metallicity all depend strongly on inclination and dust attenuation.*

These systematic errors in SDSS structural and spectral measurements may impact a wide range of studies. Samples selected by SFR or colour – green valley galaxies, red discs, starbursts – may all be affected by dust in an inclination-dependent fashion. The census

and properties of bulges in disc-dominated galaxies will be affected. Our work highlights the importance of IR imagery in understanding these effects, an important consideration given the upcoming launch of the James Webb Space Telescope. We will explore some of these issues in future papers, and release a dust-independent size and concentration catalog to allow others to quantify the effects of inclination and dust on their analyses.

CHAPTER VI

Conclusions & Outlook

6.1 Conclusions

Over the course of this thesis, we have investigated the effects of dust in a number of different ways. Carefully investigating a variety of photometric concerns, we have constructed, tested, and investigated the properties and distribution of a set of infrared-based inclination-independent measurements of galaxy stellar mass, star formation rate, size, and central concentration. Combined with the large sample sizes made possible by modern surveys, these measures allow us for the first time to isolate, across a wide range of parameter space, usefully sized samples of galaxies that are truly intrinsically similar in these four important physical properties simultaneously.

Applying the inclination test to galaxy luminosities in these samples, we have quantified the dependence of dust attenuation on intrinsic galaxy properties, again for the first time in all four dimensions simultaneously. Taking what we have learned, we have constructed a relative attenuation model based on physical scaling relations that can reproduce the patterns we see in our attenuation data, and using it we find we can *explain* these patterns in terms of simple physical properties and processes.

We have also applied the inclination test to other galaxy properties, quantifying the inclination and dust dependence of a variety of traditional optical-based galaxy property measurements. Along the way we have also refined our understanding of the inclination test

and other measurements and techniques.

The things we have learned from these investigations fall into three rough categories. First, insights into the nature and application of various measurements and methodologies. Second, insights into the nature of dust attenuation, specifically as a function of intrinsic galaxy properties. And third, insights into the effects of dust and inclination on various optical galaxy property measurements *other* than luminosity.

6.1.1 Methodological insights

One notable lesson to take away from our work is the importance of understanding the detailed properties of, and differences between, various photometric methods. Even seemingly minor differences (e.g. the difference between Petrosian and model-fit magnitudes, or isophotal versus model-fit axis ratios) can prove to have unexpectedly significant effects, as illustrated in §2.2 and §2.4.2. Similarly, there are a number of relatively subtle aspects of the implementation of our linear profile and linear structural measurement techniques that were necessary to produce unbiased measurements that are robust to the effects of the various practical limitations of photometric analysis. (For example, mis-estimation of sky levels has strong effects on the recovered measurements, and this procedure was the subject of much iteration and tweaking.) It is unlikely that we would have been able to produce the results we did if we had not been so careful in the selection of our parameters.

We also note that the necessity of selecting the most appropriately measured parameters can be a significant limitation. In particular, the use of the WISE gmags results in a major reduction in potential sample size, as most of the WISE catalog does not have this measurement type. Given the demonstration provided by our work of the usefulness of the WISE catalog's all-sky long-wavelength coverage to galaxy studies, the implementation of some form of robust extended source magnitude measurements for a larger fraction of the catalog would be very valuable.

A particular point of concern regarding choice of input measurements are the significant

effects of different measurements of axis ratio on the results of the inclination test that we observed in chapter 2. As the results of the inclination test are conventionally expressed as the slope of the relationship between the axis ratio and the parameter of interest, different axis ratio measurements that do not report the same ranges of axis ratio within a sample will yield different results for the same exact sample of galaxies. Given that axis ratio measurements can be affected in non-trivial ways by the presence of a bulge, seeing/PSF corrections (or lack thereof), choice of fit/model used, etc, *and* that these effects can vary with galaxy properties, this is a major potential source of uncertainty in interpreting the results of inclination tests and comparing different studies. For now we continue to use this particular parameterization in the interests of retaining commonality with previous work, but we have concluded that it would be better to redefine the results of the inclination test to avoid this issue. We would suggest instead that, after fitting to the parameter-axis ratio distribution, the slope then be scaled by the run in axis ratios present within that sample. This addresses this main issue and ensures that the same sample of galaxies will return the same result regardless of axis ratio measurement used; it also remedies the unphysically large slopes that can be returned for samples with intrinsically narrow axis ratio distributions, as well as arguably being closer to the conceptual root of the inclination test as the results are then literally the difference between the face-on and edge-on views regardless of the run in axis ratio.

A commonly overlooked aspect of the inclination test method is that the intercept of its fits between the parameter and axis ratio can also hold information, in addition to the commonly-focused-on slope. The intercept represents the face-on value of the property in question; the physical interpretation of this will vary depending on what property one is inclination testing and on the structure of the analysis, but it has the potential to add an additional dimension to the results. For our analysis, for example, we found that the distributions of face-on color offered insight into the face-on dust attenuation, which is otherwise inaccessible to this type of analysis. The intercept may not always offer useful insight, but

it is important to be aware of the possibility.

Our work has also stressed the importance of remembering that the definition of the inclination test is as the *difference* between the face-on and edge-on views of galaxies. This fact is easy to lose track of, but it can have important consequences as we saw in chapter 4. The face-on and edge-on views may not scale in the same way, and thus it is risky to automatically assume that variation in the *relative difference* of the measured parameter (that is, variation in the results of the inclination test) with dust content or other galaxy parameters is necessarily identical to the *total* variation in the measured parameter. In our case we saw that due to this effect the variation in the relative attenuation is not a direct function of dust density – even though the *total* dust attenuation continues to increase in both face-on and edge-on views with increasing dust density, the *relative* attenuation that the inclination test measures saturates. This does not invalidate the usefulness of the inclination test method, but it is necessary to keep this effect in mind.

6.1.2 Dust attenuation as a function of galaxy properties

We find that relative dust attenuation (defined as the difference in optical–NIR color between face-on and edge-on views) varies significantly with all four of stellar mass, specific star formation rate, size, and concentration. The relative attenuation varies the most strongly with star formation rate, being almost negligible for quiescent galaxies but quite large for the most intensely star-forming disks. For those star-forming disks, relative attenuation increases with increasing mass for low and intermediate mass galaxies, but decreases again for the most massive galaxies. For star-forming and intermediate galaxies, at a given mass and specific star formation rate the relative attenuation varies with galaxy size and concentration in a complex manner. In the most massive bins the relative attenuation is strongest for the largest and least concentrated galaxies, while for the less massive bins it is strongest for intermediate size and concentration galaxies, or in some cases even for the smallest and most concentrated galaxies. This overall pattern of variation (and particularly the variation

with structure) has not been seen before, as this is the first study to measure the relative attenuation in terms of these four parameters simultaneously.

As well, we observe that the face-on color, as measured by the intercept of the inclination test fit, also depends strongly on these parameters. The color is a function of both mass and star formation rate, becoming steadily redder with increasing mass at a given star formation rate, and also becoming steadily redder with decreasing star formation at a given mass. For galaxies of a given mass and star formation rate, the face-on color is not significantly dependent on concentration, but is a very strong function of size, with smaller galaxies being much redder than larger ones. Again, these patterns have not been seen before, particularly the dependence of color on size for galaxies that are *known* to have the same mass and star formation rate.

It is possible to construct a simple scaling-relation based model whose predictions match the patterns observed in the data to a startlingly good degree. This model operates off the simple assumption that optical depth is proportional to dust density, which is proportional to gas density and metallicity, which can be predicted from star formation rate and mass, and combines that with a relatively simple radiative transfer model to convert optical depth into face-on and relative attenuation. Yet, despite the simplicity of the assumptions, this model appears to capture all of the relevant physics necessary to reproduce the variation we see in the data.

Using this model we find that we can explain the observed patterns of variation in the relative attenuation and face-on color data in terms of simple physical properties. The first important point is that optical depth depends solely on dust surface density, and so varies both with dust content (which depends on star formation rate and mass) *and* with size (which converts a given dust *quantity* to a dust *density*). The second point is that the relative attenuation does not vary directly with optical depth, but rather is a complex non-monotonic function of both optical depth and geometry. The edge-on attenuation increases very quickly with increasing dust density at lower optical depths, but once the galaxy

becomes very strongly optically thick the edge-on attenuation only increases slowly with increasing optical depth. Thus, at high optical depths the *relative* attenuation saturates and no longer increases, as the edge-on and face-on attenuations increase at roughly the same rate. The relative attenuation then decreases for many of these highest optical depth galaxies due to geometric effects. The massive and concentrated galaxies that have the highest optical depths also tend to have large bulges, and the attenuation of bulge light is less affected by inclination than the disk attenuation, thereby reducing the difference between the face-on and edge-on attenuation for these galaxies. Thus, most of the patterns we observe in relative attenuation are due to variation in the normalization of dust content and bulge prominence affecting to what degree we observe this saturation and turnover behavior. The relative simplicity of the observed patterns in face-on color (which mostly just tracks the optical depth) is then due to not being subject to these additional complicating steps.

Knowledge of the variation in dust attenuation and face-on color with all four of the parameters of mass, star formation rate, size, and concentration simultaneously is new; we don't know yet where this will lead, but it represents filling in a gap in our knowledge in this field.

Understanding the actual cause of the downturn in relative attenuation at high luminosities/masses aids in interpreting past inclination test results in this area. For example, Masters et al. (2010) observe this effect in observations of SDSS colors, and speculate that it may be due to intrinsically lower dust levels caused by lower *recent* star formation rates. Our work suggests that this is an unnecessary complication and that the downturn can simply be explained in terms of the mechanics of the method, with obvious implications for the presumed actual dust densities.

The fact that such seemingly complex patterns can be explained by such simple scaling relations is very encouraging. First, it demonstrates the value of the inclination independent metrics, as they allow us to actually select intrinsically similar galaxies in order to see these simple effects. And second, this reinforces the value of these sorts of simple scaling relation

based models; that as long as one can avoid biases and flawed measurements, it is possible to understand the universe to a surprising degree of accuracy using quite simple analyses.

6.1.3 Dust and inclination effects on other measurements

Applying the inclination test to traditional structural measurements, we find that optical structural measurements such as Sérsic index, regular concentration, and half-light radius all suffer from significant dust and inclination dependences and are therefore often not particularly reliable. Notably, we find that this can even be the case for quiescent galaxies which should contain little or no dust; this calls into question the reliability of these methods in an algorithmic sense, as it appears that they do not always handle changing projection of light distributions correctly even in ideal cases.

We also find that a variety of other optical non-structural galaxy property measurements suffer from inclination dependence as well. Optical stellar masses are relatively unaffected, but star formation rates, metallicities, and line-based spectral classifications are all significantly affected. Notably, these star formation rates were supposed to be dust-corrected; this correction appears to have been insufficient.

The fact that all but one of the metrics we studied are affected by dust and inclination, and the obvious degree to which they are affected, suggests that these sorts of biases are likely both common and significant. As we have barely even scratched the surface of the measurements we can test using the inclination test method, there are likely other issues waiting to be uncovered.

The ease with which these biases are observed also reinforces the value of the simple inclination test method simply as a diagnostic tool, even when inclination biases are not the focus of the research. While one may have difficulties making rigorous measurements of the exact degree of inclination bias without access to inclination-independent galaxy property measurements for classification, one can still apply the inclination test to any measurement that is *believed* to represent an intrinsic property measurement. Any variation in such a

measurement with inclination can then act as a signal that something may be amiss with the measurement technique.

6.2 Outlook

There are a variety of directions that one could take in future research based on the work we have already done. Some of these are natural and immediate outgrowths of of our current work, while others are farther afield.

The ability to probe face-on attenuation by exploiting the intercept of inclination test fits offers a new method of testing SED fitting-based star formation rates and dust corrections. As the two techniques are very different in input and methodology, they can serve as valuable cross-checks on each other.

Expanding on our work in chapter 5, there are many other optical measurements one could test for dust and inclination biases using the inclination test method and our inclination-independent galaxy property measurements. Additionally, the analysis in chapter 5 focused on relatively limited samples of galaxies; we showed that the measurements in question suffered from dust and inclination biases, but we have not completed the parallel with our previous analysis by examining the question of how those biases vary with galaxy properties. In essence, the opportunities to 'inclination test all the things' have not even remotely been exhausted, and there are likely many profitable lines of inquiry to be explored.

One could also seek to repeat our general analysis at higher redshifts. While it is difficult to make structural measurements of such distant galaxies, one could still carry out analyses similar to those in chapter 2 as long as one could find the right inclination-independent measurements. As galaxies are known to generally be dustier and more actively star-forming at higher redshifts (e.g. Madau et al. 1996) one might expect the patterns we discuss in chapter 4 to be more prominent and/or shift in location; it would be interesting to see whether the universe matches this expectation.

Given our difficulties with finding appropriate photometry and inclination measurements,

one might also wish to pivot from studying the effects of inclination biases and focus on constructing robust extended source photometry or infrared inclination measurements. This is farther afield from our previous focus, but our work has highlighted the need for such measurements. Ultimately we are unlikely to carry this out, though along similar lines there is also likely still scope for further tweaking and improving our linear profile and linear structural measurement techniques.

There is also no reason that the linear brightness profile technique cannot be applied to optical images as well as infrared ones. In this case they would obviously not be useful for constructing inclination-independent structural measurements; rather, one could compare them to infrared linear brightness profiles to create a sort of spatially-resolved variant on the inclination test – the change in the linear brightness profile relative to the invariant infrared version as a function of inclination. This would allow for the study of spatially-resolved phenomena such as color gradients, localization of star formation, etc.

Currently our work involves only optical and NIR to MIR measurements, but it may be interesting to also attempt to incorporate longer wavelength measurements into our analyses. These could allow for studies of the variations of other physical properties, such as dust or gas masses. Given our conclusions about the dependence of relative attenuation on dust and gas density, it would be interesting to see to what degree direct measurements of these quantities match our models.

Finally, we may wish to refine our models by developing our own radiative transfer simulations rather than relying on those of Tuffs et al. (2004). The models of Tuffs et al. are well executed, but they have a number of limitations for the uses to which we put them. Significantly, they do not allow for any variation in morphology, and yet differences in bulge prominence are an important aspect of our model. Similarly, they are intended for disk galaxies only, and so our use of them for ellipticals is necessarily ad-hoc. It would also be useful to be able to measure simulated linear brightness profiles, particularly if we undertake the spatially-resolved inclination test investigation described above, but this would

require direct access to the simulations themselves rather than just the results presented in their paper. Likewise, with direct access we could use these models to predict the effects of dust and inclination on structural measurements such as Sérsic index, half-light radius, etc. We have already done some work with synthetic galaxy images in chapter 3, and although they did not end up figuring in any of the work presented in this thesis we have also already created more sophisticated radiative transfer simulations as part of our initial investigations of the properties of the linear brightness profile method. This work could relatively straightforwardly be expanded in order to provide our own fully customizable suite of radiative transfer simulations for use with our models.

6.3 Wrap-up

In chapter 1 of this thesis, we proposed four questions that we wished to address with our work. Namely, we wished to investigate the construction of inclination-independent measurements and any insights they may offer regarding traditional measurements, to measure the dependence of dust attenuation on intrinsic galaxy properties, to attempt to explain these dependencies in terms of their controlling physical processes, and to investigate the dust and inclination dependence of various traditional galaxy property measurements. While we cannot claim to have the final word on dust attenuation and properties, we can propose answers to these questions.

- Construction of inclination-independent galaxy property measurements requires the use of infrared observations and careful consideration of photometric and geometric limitations. Our work highlights the significant effects that even seemingly small differences in technique can cause.

- Dust attenuation increases strongly with star formation activity, and varies with mass, size, and concentration in complex ways. Simple scaling relation-based attenuation models can reproduce these patterns surprisingly well.

- These patterns may be explained by the direct dependence of dust optical depth on dust density (determined by gas density and metallicity), coupled with geometric effects and the strongly non-linear variation of relative attenuation with optical depth. This non-monotonic variation is observed differently in different regions of parameter space owing to variations in structure and the normalization of dust content.

- Traditional structural measurements and other optically-measured galaxy properties do indeed suffer from inclination and dust dependence; notably, even in some cases where they 'shouldn't' (e.g. Sérsic index for dust-free quiescent galaxies, 'dust corrected' star formation rates), suggesting that these biases are likely common.

In sum, we have shown that the combination of the inclination test method and inclination-independent galaxy property measurements can provide a powerful set of tools for understanding dust properties and effects. We have demonstrated that many traditional measurements suffer from biases with dust and inclination, we have measured the variation in dust attenuation with the intrinsic galaxy properties of stellar mass, specific star formation rate, size, and concentration simultaneously for the first time, and we have shown that surprisingly simple models are capable of not only reproducing, but also of explaining in terms of a remarkably simple conceptual framework, the observed variation in the effects and properties of dust.

Acknowledgments

We wish to thank Roelof de Jong and Ned Taylor for valuable discussions, and Dustin Lang for making the *WISE* magnitudes of Lang et al. (2014a) available for testing before their publication.

This work was partially supported by NSF-AST 1514835. Support for this work was also partially provided by a Rackham Merit Fellowship grant.

This research has made use of NASA's Astrophysics Data System Bibliographic Services.

This dissertation makes use of data products from the Wide-field Infrared Survey Explorer, which is a joint project of the University of California, Los Angeles, and the Jet Propulsion Laboratory/California Institute of Technology, funded by the National Aeronautics and Space Administration.

UKIRT is owned by the University of Hawaii (UH) and operated by the UH Institute for Astronomy; operations are enabled through the cooperation of the East Asian Observatory. When the data reported here were acquired, UKIRT was operated by the Joint Astronomy Centre on behalf of the U.K. Science and Technology Facilities Council.

Funding for the Sloan Digital Sky Survey IV has been provided by the Alfred P. Sloan Foundation, the U.S. Department of Energy Office of Science, and the Participating Institutions. SDSS-IV acknowledges support and resources from the Center for High-Performance Computing at the University of Utah. The SDSS web site is www.sdss.org.

SDSS-IV is managed by the Astrophysical Research Consortium for the Participating Institutions of the SDSS Collaboration including the Brazilian Participation Group, the Carnegie Institution for Science, Carnegie Mellon University, the Chilean Participation Group, the French Participation Group, Harvard-Smithsonian Center for Astrophysics, Instituto de Astrofísica de Canarias, The Johns Hopkins University, Kavli Institute for the Physics and Mathematics of the Universe (IPMU)/University of Tokyo, Lawrence Berkeley National Laboratory, Leibniz Institut für Astrophysik Potsdam (AIP), Max-Planck-Institut für Astronomie (MPIA Heidelberg), Max-Planck-Institut für Astrophysik (MPA Garching), Max-Planck-Institut für Extraterrestrische Physik (MPE), National Astronomical Observatories of China, New Mexico State University, New York University, University of Notre Dame, Observatário Nacional/MCTI, Ohio State University, Pennsylvania State University, Shanghai Astronomical Observatory, United Kingdom Participation Group, Universidad Nacional Autónoma de México, University of Arizona, University of Colorado Boulder, University of Oxford, University of Portsmouth, University of Utah, University of Virginia, University of Washington, University of Wisconsin, Vanderbilt University, and Yale University.

APPENDIX

APPENDIX A

Attenuation data tables

Table A.1: Attenuation parameter γ measurements and uncertainties, u band.

			$M_{3.4\mu m}$			
[12]−[3.4]	(−24)−(−23)	(−23)−(−22)	(−22)−(−21)	(−21)−(−20)	(−20)−(−19)	(−19)−(−18)
(3.0)−(3.5)		−0.72±0.37				
(2.5)−(3.0)	−0.64±0.59	−0.15±0.16	0.123±0.068	0.066±0.073	0.13±0.12	
(2.0)−(2.5)	−0.38±0.24	−0.003±0.071	0.087±0.054	0.008±0.057	−0.032±0.074	
(1.5)−(2.0)	−0.78±0.47	−0.071±0.078	0.223±0.060	0.138±0.069	0.00±0.12	
(1.0)−(1.5)		0.113±0.087	0.230±0.064	0.389±0.085		
(0.5)−(1.0)		0.452±0.092	0.467±0.071	0.532±0.081	0.80±0.12	
(0.0)−(0.5)		0.745±0.080	0.926±0.066	1.007±0.076	0.79±0.19	
(−0.5)−(0.0)		0.973±0.086	1.168±0.063	1.236±0.069	1.060±0.090	0.64±0.15
(−1.0)−(−0.5)		1.385±0.095	1.574±0.067	1.647±0.067	1.42±0.11	1.15±0.33
(−1.5)−(−1.0)		1.46±0.18	1.81±0.13	1.72±0.11	1.33±0.23	

Table A.2: Attenuation parameter γ measurements and uncertainties, g band.

			$M_{3.4\mu m}$			
[12]−[3.4]	(−24)−(−23)	(−23)−(−22)	(−22)−(−21)	(−21)−(−20)	(−20)−(−19)	(−19)−(−18)
(3.0)−(3.5)		−0.38±0.17				
(2.5)−(3.0)	−0.41±0.23	−0.015±0.088	0.131±0.056	0.108±0.059	0.167±0.087	
(2.0)−(2.5)	−0.30±0.13	0.048±0.057	0.137±0.052	0.060±0.053	0.036±0.065	
(1.5)−(2.0)	−0.22±0.22	0.119±0.061	0.200±0.054	0.176±0.059	0.076±0.082	
(1.0)−(1.5)		0.275±0.063	0.298±0.056	0.398±0.065		
(0.5)−(1.0)		0.457±0.063	0.457±0.058	0.502±0.062	0.662±0.083	
(0.0)−(0.5)		0.630±0.063	0.775±0.057	0.790±0.062	0.62±0.12	
(−0.5)−(0.0)		0.762±0.063	0.919±0.055	0.974±0.059	0.890±0.071	0.58±0.12
(−1.0)−(−0.5)		1.005±0.070	1.144±0.056	1.212±0.059	1.093±0.081	1.06±0.24
(−1.5)−(−1.0)		1.04±0.13	1.244±0.088	1.238±0.086	0.93±0.17	

Table A.3: Attenuation parameter γ measurements and uncertainties, r band.

			$M_{3.4\mu m}$			
[12]−[3.4]	(−24)−(−23)	(−23)−(−22)	(−22)−(−21)	(−21)−(−20)	(−20)−(−19)	(−19)−(−18)
(3.0)−(3.5)		−0.347±0.17				
(2.5)−(3.0)	−0.66±0.24	0.026±0.03	0.131±0.055	0.098±0.057	0.136±0.080	
(2.0)−(2.5)	−0.32±0.14	0.054±0.056	0.141±0.052	0.072±0.052	0.035±0.062	
(1.5)−(2.0)	−0.22±0.23	0.143±0.059	0.178±0.053	0.162±0.056	0.083±0.075	
(1.0)−(1.5)		0.281±0.061	0.279±0.055	0.344±0.061		
(0.5)−(1.0)		0.438±0.058	0.423±0.056	0.439±0.058	0.577±0.075	
(0.0)−(0.5)		0.583±0.059	0.689±0.054	0.697±0.058	0.553±0.096	
(−0.5)−(0.0)		0.713±0.060	0.824±0.054	0.853±0.056	0.781±0.065	0.53±0.10
(−1.0)−(−0.5)		0.897±0.064	0.982±0.054	1.023±0.056	0.908±0.073	0.91±0.19
(−1.5)−(−1.0)		0.87±0.11	1.002±0.076	0.982±0.076	0.80±0.14	

Table A.4: Attenuation parameter γ measurements and uncertainties, i band.

			$M_{3.4\mu m}$			
[12]−[3.4]	(−24)−(−23)	(−23)−(−22)	(−22)−(−21)	(−21)−(−20)	(−20)−(−19)	(−19)−(−18)
(3.0)−(3.5)		−0.314±0.17				
(2.5)−(3.0)	−0.57±0.22	0.024±0.081	0.108±0.055	0.071±0.056	0.114±0.080	
(2.0)−(2.5)	−0.33±0.13	0.035±0.055	0.116±0.051	0.050±0.052	0.026±0.060	
(1.5)−(2.0)	−0.24±0.22	0.095±0.058	0.133±0.053	0.127±0.055	0.057±0.074	
(1.0)−(1.5)		0.210±0.059	0.216±0.054	0.269±0.060		
(0.5)−(1.0)		0.336±0.057	0.343±0.054	0.346±0.057	0.504±0.073	
(0.0)−(0.5)		0.449±0.057	0.568±0.053	0.581±0.057	0.480±0.085	
(−0.5)−(0.0)		0.539±0.058	0.681±0.053	0.736±0.056	0.712±0.062	0.489±0.097
(−1.0)−(−0.5)		0.694±0.063	0.793±0.054	0.872±0.055	0.803±0.070	0.85±0.18
(−1.5)−(−1.0)		0.594±0.097	0.802±0.072	0.804±0.071	0.67±0.13	

Table A.5: Attenuation parameter γ measurements and uncertainties, z band.

			$M_{3.4\mu m}$			
[12]−[3.4]	(−24)−(−23)	(−23)−(−22)	(−22)−(−21)	(−21)−(−20)	(−20)−(−19)	(−19)−(−18)
(3.0)−(3.5)		−0.31±0.17				
(2.5)−(3.0)	−0.60±0.25	−0.077±0.079	−0.016±0.055	−0.040±0.056	0.001±0.083	
(2.0)−(2.5)	−0.32±0.14	−0.069±0.056	−0.016±0.051	−0.070±0.052	−0.080±0.060	
(1.5)−(2.0)	−0.24±0.21	−0.046±0.058	−0.022±0.052	−0.024±0.055	−0.044±0.072	
(1.0)−(1.5)		0.047±0.058	0.046±0.054	0.087±0.059		
(0.5)−(1.0)		0.154±0.057	0.170±0.054	0.165±0.057	0.329±0.073	
(0.0)−(0.5)		0.293±0.057	0.378±0.053	0.400±0.056	0.366±0.080	
(−0.5)−(0.0)		0.399±0.059	0.539±0.053	0.597±0.055	0.599±0.061	0.398±0.094
(−1.0)−(−0.5)		0.602±0.062	0.663±0.054	0.740±0.055	0.678±0.066	0.71±0.16
(−1.5)−(−1.0)		0.438±0.098	0.674±0.071	0.650±0.066	0.54±0.12	

BIBLIOGRAPHY

BIBLIOGRAPHY

Abazajian, K., Adelman-McCarthy, J. K., Agüeros, M. A., et al. 2004, AJ, 128, 502

Abraham, R. G., Valdes, F., Yee, H. K. C., & van den Bergh, S. 1994, ApJ, 432, 75

Ahn, C. P., Alexandroff, R., Allende Prieto, C., et al. 2014, ApJS, 211, 17

Bell, E. F. 2003, ApJ, 586, 794

Bell, E. F., & de Jong, R. S. 2001, ApJ, 550, 212

Bell, E. F., Gordon, K. D., Kennicutt, Jr., R. C., & Zaritsky, D. 2002, ApJ, 565, 994

Bell, E. F., van der Wel, A., Papovich, C., et al. 2012, ApJ, 753, 167

Bergin, E. A., & Tafalla, M. 2007, ARA&A, 45, 339

Berlind, A. A., Quillen, A. C., Pogge, R. W., & Sellgren, K. 1997, AJ, 114, 107

Bland-Hawthorn, J., & Gerhard, O. 2016, ARA&A, 54, 529

Blanton, M. R., & Roweis, S. 2007, AJ, 133, 734

Blanton, M. R., Dalcanton, J., Eisenstein, D., et al. 2001, AJ, 121, 2358

Blanton, M. R., Schlegel, D. J., Strauss, M. A., et al. 2005, AJ, 129, 2562

Bolton, A. S., Schlegel, D. J., Aubourg, É., et al. 2012, AJ, 144, 144

Brinchmann, J., Charlot, S., White, S. D. M., et al. 2004, MNRAS, 351, 1151

Bruzual A., G., Magris, G., & Calvet, N. 1988, ApJ, 333, 673

Byun, Y. I., Freeman, K. C., & Kylafis, N. D. 1994, ApJ, 432, 114

Calzetti, D. 2001, New A Rev., 45, 601

—. 2013, Star Formation Rate Indicators, ed. J. Falcón-Barroso & J. H. Knapen, 419

Calzetti, D., Armus, L., Bohlin, R. C., et al. 2000, ApJ, 533, 682

Caplan, J., & Deharveng, L. 1986, A&A, 155, 297

Cardelli, J. A., Clayton, G. C., & Mathis, J. S. 1989, ApJ, 345, 245

Chang, Y.-Y., van der Wel, A., da Cunha, E., & Rix, H.-W. 2015, ApJS, 219, 8

Charlot, S., & Fall, S. M. 2000, ApJ, 539, 718

Cho, J., & Park, C. 2009, ApJ, 693, 1045

Cluver, M. E., Jarrett, T. H., Hopkins, A. M., et al. 2014, ApJ, 782, 90

Conroy, C. 2010, MNRAS, 404, 247

Cutri, R. M., Skrutskie, M. F., Van Dyk, S., et al. 2006, Explanatory Supplement to the 2MASS All Sky Data Release and Extended Mission Products

de Jong, R. S. 1996a, A&AS, 118, 557

—. 1996b, A&A, 313, 377

de Jong, R. S., & Lacey, C. 2000, ApJ, 545, 781

de Vaucouleurs, G. 1948, Annales d'Astrophysique, 11, 247

—. 1959, Handbuch der Physik, 53, 275

Devour, B. M., & Bell, E. F. 2016, MNRAS, 459, 2054

—. 2017, MNRAS, 468, L31

Disney, M., Davies, J., & Phillipps, S. 1989, MNRAS, 239, 939

Djorgovski, S., & Davis, M. 1987, ApJ, 313, 59

Doi, M., Fukugita, M., & Okamura, S. 1993, MNRAS, 264, 832

Dopita, M. A., Groves, B. A., Sutherland, R. S., & Kewley, L. J. 2003, ApJ, 583, 727

Dopita, M. A., Fischera, J., Sutherland, R. S., et al. 2006, ApJS, 167, 177

Draine, B. T., & Li, A. 2007, ApJ, 657, 810

Draine, B. T., Dale, D. A., Bendo, G., et al. 2007, ApJ, 663, 866

Driver, S. P., Popescu, C. C., Tuffs, R. J., et al. 2007, MNRAS, 379, 1022

Driver, S. P., Robotham, A. S. G., Kelvin, L., et al. 2012, MNRAS, 427, 3244

Eisenstein, D. J., Weinberg, D. H., Agol, E., et al. 2011, AJ, 142, 72

Emsellem, E., Cappellari, M., Krajnović, D., et al. 2011, MNRAS, 414, 888

Erb, D. K., Steidel, C. C., Shapley, A. E., et al. 2006, ApJ, 647, 128

Ferrara, A., Bianchi, S., Cimatti, A., & Giovanardi, C. 1999, ApJS, 123, 437

Finkelstein, S. L., Ryan, Jr., R. E., Papovich, C., et al. 2015, ApJ, 810, 71

Fioc, M., & Rocca-Volmerange, B. 1997, A&A, 326, 950

Fontanot, F., Somerville, R. S., Silva, L., Monaco, P., & Skibba, R. 2009, MNRAS, 392, 553

Franx, M., van Dokkum, P. G., Förster Schreiber, N. M., et al. 2008, ApJ, 688, 770

Gallazzi, A., & Bell, E. F. 2009, ApJS, 185, 253

Garrod, R. T., Widicus Weaver, S. L., & Herbst, E. 2008, ApJ, 682, 283

Giovanelli, R., Haynes, M. P., Salzer, J. J., et al. 1994, AJ, 107, 2036

—. 1995, AJ, 110, 1059

Gould, R. J., & Salpeter, E. E. 1963, ApJ, 138, 393

Holmberg, E. 1958, Meddelanden fran Lunds Astronomiska Observatorium Serie II, 136, 1

—. 1975, Magnitudes, Colors, Surface Brightness, Intensity Distributions Absolute Luminosities, and Diameters of Galaxies, ed. A. Sandage, M. Sandage, & J. Kristian (the University of Chicago Press), 123

Holmberg, E. B., Lauberts, A., Schuster, H.-E., & West, R. M. 1974, A&AS, 18, 463

Holwerda, B. W., Gonzalez, R. A., Allen, R. J., & van der Kruit, P. C. 2005, AJ, 129, 1396

Holwerda, B. W., Draine, B., Gordon, K. D., et al. 2007, AJ, 134, 2226

Hopkins, P. F., & Conroy, C. 2017, ApJ, 835, 154

Hubble, E. P. 1926, ApJ, 64, doi:10.1086/143018

Huchra, J., Davis, M., Latham, D., & Tonry, J. 1983, ApJS, 52, 89

Huizinga, J. E., & van Albada, T. S. 1992, MNRAS, 254, 677

Jogee, S., Miller, S. H., Penner, K., et al. 2009, ApJ, 697, 1971

Jonsson, P., Cox, T. J., Primack, J. R., & Somerville, R. S. 2006, ApJ, 637, 255

Katz, N., Furman, I., Biham, O., Pirronello, V., & Vidali, G. 1999, ApJ, 522, 305

Kauffmann, G., Heckman, T. M., White, S. D. M., et al. 2003a, MNRAS, 341, 33

—. 2003b, MNRAS, 341, 54

Keel, W. C., Manning, A. M., Holwerda, B. W., Lintott, C. J., & Schawinski, K. 2014, AJ, 147, 44

Kennicutt, Jr., R. C. 1989, ApJ, 344, 685

—. 1998, ApJ, 498, 541

Klessen, R. S., Glover, S. C. O., & Clark, P. C. 2012, MNRAS, 421, 3217

Lang, D., Hogg, D. W., & Schlegel, D. J. 2014a, AJ, Submitted, arXiv:1410.7397

Lang, P., Wuyts, S., Somerville, R. S., et al. 2014b, ApJ, 788, 11

Lawrence, A., Warren, S. J., Almaini, O., et al. 2007, MNRAS, 379, 1599

Li, A., & Draine, B. T. 2001, ApJ, 554, 778

Licquia, T. C., Newman, J. A., & Brinchmann, J. 2015, ApJ, 809, 96

Liu, G., Calzetti, D., Hong, S., et al. 2013, ApJ, 778, L41

Madau, P., Ferguson, H. C., Dickinson, M. E., et al. 1996, MNRAS, 283, 1388

Maller, A. H., Berlind, A. A., Blanton, M. R., & Hogg, D. W. 2009, ApJ, 691, 394

Mao, S., Mo, H. J., & White, S. D. M. 1998, MNRAS, 297, L71

Masters, K. L., Nichol, R., Bamford, S., et al. 2010, MNRAS, 404, 792

Meidt, S. E., Schinnerer, E., Knapen, J. H., et al. 2012, ApJ, 744, 17

Meidt, S. E., Schinnerer, E., van de Ven, G., et al. 2014, ApJ, 788, 144

Ménard, B., Scranton, R., Fukugita, M., & Richards, G. 2010, MNRAS, 405, 1025

Möllenhoff, C., Popescu, C. C., & Tuffs, R. J. 2006, A&A, 456, 941

Morgan, W. W. 1958, PASP, 70, 364

Muzzin, A., Marchesini, D., Stefanon, M., et al. 2013, ApJ, 777, 18

Nilson, P. 1973, Uppsala general catalogue of galaxies

Noeske, K. G., Weiner, B. J., Faber, S. M., et al. 2007, ApJ, 660, L43

Oke, J. B., & Gunn, J. E. 1983, ApJ, 266, 713

Papovich, C., & Bell, E. F. 2002, ApJ, 579, L1

Pastrav, B. A., Popescu, C. C., Tuffs, R. J., & Sansom, A. E. 2013a, A&A, 553, A80

—. 2013b, A&A, 557, A137

Perets, H. B., Lederhendler, A., Biham, O., et al. 2007, ApJ, 661, L163

Popescu, C. C., Misiriotis, A., Kylafis, N. D., Tuffs, R. J., & Fischera, J. 2000, A&A, 362, 138

Reid, I. N., Brewer, C., Brucato, R. J., et al. 1991, PASP, 103, 661

Rosa-González, D., Terlevich, E., & Terlevich, R. 2002, MNRAS, 332, 283

Salim, S., Rich, R. M., Charlot, S., et al. 2007, ApJS, 173, 267

Schechtman-Rook, A., Bershady, M. A., & Wood, K. 2012, ApJ, 746, 70

Schneider, R., Omukai, K., Limongi, M., et al. 2012, MNRAS, 423, L60

Sérsic, J. L. 1963, Boletin de la Asociacion Argentina de Astronomia La Plata Argentina, 6, 41

Shen, S., Mo, H. J., White, S. D. M., et al. 2003, MNRAS, 343, 978

Simard, L., Mendel, J. T., Patton, D. R., Ellison, S. L., & McConnachie, A. W. 2011, ApJS, 196, 11

Skrutskie, M. F., Cutri, R. M., Stiening, R., et al. 2006, AJ, 131, 1163

Soifer, B. T., & Neugebauer, G. 1991, AJ, 101, 354

Steinacker, J., Baes, M., & Gordon, K. D. 2013, ARA&A, 51, 63

Strateva, I., Ivezić, Ž., Knapp, G. R., et al. 2001, AJ, 122, 1861

Strauss, M. A., Weinberg, D. H., Lupton, R. H., et al. 2002, AJ, 124, 1810

Temim, T., Dwek, E., Tchernyshyov, K., et al. 2015, ApJ, 799, 158

Tremblay, B., & Merritt, D. 1996, AJ, 111, 2243

Tremonti, C. A., Heckman, T. M., Kauffmann, G., et al. 2004, ApJ, 613, 898

Tuffs, R. J., Popescu, C. C., Völk, H. J., Kylafis, N. D., & Dopita, M. A. 2004, A&A, 419, 821

Tully, R. B., & Fisher, J. R. 1977, A&A, 54, 661

Tully, R. B., Pierce, M. J., Huang, J.-S., et al. 1998, AJ, 115, 2264

Valentijn, E. A. 1990, Nature, 346, 153

—. 1994, MNRAS, 266, 614

van den Bosch, F. C., Burkert, A., & Swaters, R. A. 2001, MNRAS, 326, 1205

van der Wel, A., Bell, E. F., van den Bosch, F. C., Gallazzi, A., & Rix, H.-W. 2009a, ApJ, 698, 1232

van der Wel, A., Rix, H.-W., Holden, B. P., Bell, E. F., & Robaina, A. R. 2009b, ApJ, 706, L120

van der Wel, A., Franx, M., van Dokkum, P. G., et al. 2014a, ApJ, 788, 28

van der Wel, A., Chang, Y.-Y., Bell, E. F., et al. 2014b, ApJ, 792, L6

Vincent, R. A., & Ryden, B. S. 2005, ApJ, 623, 137

Vorontsov-Vel'Yaminov, B. A., & Arkhipova, V. P. 1962, in Morphological catalogue of galaxies., 1 (1962)

Vulcani, B., Bamford, S. P., Häußler, B., et al. 2014, MNRAS, 441, 1340

Wen, X.-Q., Wu, H., Zhu, Y.-N., et al. 2014, MNRAS, 438, 97

White, III, R. E., Keel, W. C., & Conselice, C. J. 2000, ApJ, 542, 761

Whittet, D. C. B., ed. 2003, Dust in the galactic environment

Wild, V., Charlot, S., Brinchmann, J., et al. 2011, MNRAS, 417, 1760

Witt, A. N., & Gordon, K. D. 2000, ApJ, 528, 799

Wright, E. L., Eisenhardt, P. R. M., Mainzer, A. K., et al. 2010, AJ, 140, 1868

Wuyts, S., Förster Schreiber, N. M., van der Wel, A., et al. 2011, ApJ, 742, 96